Role of Extracellular Microenvironment on Lung Cancer Cell Metabolism

by

Nuriye Solcan

A Dissertation Submitted to the
Graduate School of Sciences and Engineering
in Partial Fulfillment of the Requirements for
the Degree of

Master of Science

in

Molecular Biology and Genetics

August 11, 2023

Role of Extracellular Microenvironment on Lung Cancer Cell Metabolism

Koç University

Graduate School of Sciences and Engineering

This is to certify that I have examined this copy of a master's thesis by

Nuriye Solcan

and have found that it is complete and satisfactory in all respects,
and that any and all revisions required by the final
examining committee have been made.

Committee Members:

_____

Assist. Prof. Ece Öztürk (Advisor)

_____

Assoc. Prof. Umut Şahin

_____

Prof. Tuğba Bağcı Önder

Date: August 11, 2023

I dedicate this thesis to the extraordinary tapestry of life, woven from the very fabric of star stuff.

ABSTRACT

Role of Extracellular Microenvironment on Lung Cancer Cell Metabolism

Nuriye Solcan

Master of Science in Molecular Biology and Genetics

August 11, 2023

Lung cancer is the second most prevalent type of cancer with the highest mortality rate among all cancer types. Despite significant progress in cancer drug development and therapeutic strategies targeting cancer metabolism, a lack of understanding about the intricate complexities of the tumor microenvironment continues to hinder effective treatment approaches. This study aims to tackle these challenges by using advanced three-dimensional (3D) *in vitro* cancer models to explore the role of interactions between cancer cells and their microenvironment in regulation of cancer metabolism. Due to limitations in conventional two-dimensional (2D) cultures, this work focused on creating two distinct hydrogel models representing healthy lung tissue and tumor conditions. These models were developed by combining decellularized native lung extracellular matrix with inert or tumor-mimetic biomaterials, aligning with the research objectives.

In the first phase of the study, an in-depth analysis of gene expression profiles in lung tumor cells was conducted, comparing metabolic and tumorigenic regulators between 2D culture and the novel 3D healthy lung-mimetic model. The results showed that the 3D healthy-mimetic environment influenced the expression of epithelial-mesenchymal transition (EMT) markers in tumor cells in response to changing glucose levels. The microenvironment also played a significant role in regulating the stemness of tumor cells and affected the expression of metabolic markers, providing valuable insights into cellular behavior and metabolism.

The second phase of the research explored the impact of elevated sulfation, mimicking the aberrant glycosaminoglycan increase within the tumor microenvironment, under varying glucose levels on tumor cell behavior. The investigation provided deeper insights into the complex interplay between sulfation, glucose availability, and cellular responses. Increased sulfation in the tumor-mimicking environment significantly affected cell proliferation and metabolic activity, while the effect of glucose levels varied depending on the microenvironmental conditions. The interplay between glucose levels and the expression of EMT markers was also observed, with high glucose in the tumor-

mimetic environment leading to significant upregulation of mesenchymal markers in tumor cells. The study highlighted the complexity of metabolic regulation in the tumor microenvironment.

The last phase of the study focused on investigating the role of the PIK3CA gene as a key cellular signaling regulator in the observed phenomena. Comprehensive analysis of PIK3CA's effect provided valuable insights into the processes influencing cellular responses in the novel hydrogel models under different microenvironmental conditions. The study revealed a significant role of PIK3CA in regulating cell proliferation in tumor-mimetic environments, with glucose levels modulating this effect, validated with PIK3CA knock-down cells. High glucose exposure partially compensated for the effects of PIK3CA knockdown, influencing EMT marker expression, stemness markers, and various metabolic pathways in tumor cells. The complex interplay between glucose metabolism, extracellular microenvironment and PIK3CA signaling was evident, offering potential therapeutic targets for PIK3CA-associated cancers.

In conclusion, this comprehensive research underscores the importance of sophisticated 3D *in vitro* cancer models to accurately simulate the tumor microenvironment and investigate cellular behavior. The findings provide valuable insights into cancer cell metabolism, the impact of microenvironmental factors, and potential therapeutic targets, advancing lung cancer treatment strategies.

ÖZETÇE

Akciğer Kanseri Hücre Metabolizması Üzerinde Hücre Dışı Mikroortamın Rolü

Role of Extracellular Microenvironment on Lung Cancer Cell Metabolism

Nuriye Solcan

Moleküler Biyoloji ve Genetik, Yüksek Lisans

11 Ağustos, 2023

Akciğer kanseri, tüm kanser türleri arasında ölüm oranı en yüksek ikinci kanser türüdür. Kanser ilacı geliştirme ve kanser metabolizmasını hedef alan terapötik stratejilerdeki önemli ilerlemeye rağmen, tümör mikroçevresinin karmaşık karmaşıklığı hakkındaki anlayış eksikliği, etkili tedavi yaklaşımlarını engellemeye devam etmektedir. Bu çalışma, kanser hücreleri ve mikroçevreleri arasındaki etkileşimlerin kanser metabolizmasının düzenlenmesindeki rolünü keşfetmek için gelişmiş üç boyutlu (3B) *in vitro* kanser modellerini kullanarak bu zorlukların üstesinden gelmeyi amaçlamaktadır. Geleneksel iki boyutlu (2B) kültürlerdeki sınırlamalar nedeniyle bu çalışma, sağlıklı akciğer dokusunu ve tümör koşullarını temsil eden iki farklı hidrojel modeli oluşturmaya odaklandı. Bu modeller, hücresizleştirilmiş doğal akciğer hücre dışı matrisini inert veya tümör taklidi biyomalzemelerle birleştirerek, araştırma hedefleriyle uyumlu olarak geliştirilmiştir.

Çalışmanın ilk aşamasında, 2B kültür ile yeni 3B sağlıklı akciğer mimetik modeli arasındaki metabolik ve tümörijenik düzenleyicileri karşılaştırarak, akciğer tümör hücrelerinde gen ekspresyon profillerinin derinlemesine bir analizi yapıldı. Sonuçlar, 3B sağlıklı mimetik ortamın, değişen glikoz seviyelerine yanıt olarak tümör hücrelerinde epitelyal-mezenkimal geçiş (EMT) belirteçlerinin ifadesini etkilediğini gösterdi. Mikroçevre, tümör hücrelerinin köklüğünü düzenlemede önemli bir rol oynadı ve metabolik belirteçlerin ifadesini etkileyerek hücresel davranış ve metabolizmaya ilişkin değerli bilgiler sağladı.

Araştırmanın ikinci aşaması, tümör mikroçevresindeki anormal glikozaminoglikan artışını, değişen glikoz seviyeleri altında tümör hücresi davranışı üzerinde taklit ederek yüksek sülfasyonun etkisini araştırdı. Araştırma, sülfasyon, glikoz mevcudiyeti ve hücresel tepkiler arasındaki karmaşık etkileşim hakkında daha derin bilgiler sağladı. Tümörü taklit eden ortamda artan sülfasyon, hücre çoğalmasını ve metabolik aktiviteyi önemli ölçüde etkilerken, glikoz seviyelerinin etkisi mikroçevre koşullarına bağlı olarak değişmiştir. Glikoz seviyeleri ile EMT belirteçlerinin ekspresyonu arasındaki etkileşim

de gözlendi; tümör-mimetik ortamda yüksek glikoz, tümör hücrelerinde mezenkimal belirteçlerin önemli ölçüde yukarı regülasyonuna yol açtı. Çalışma, tümör mikro ortamındaki metabolik düzenlemenin karmaşıklığını vurguladı.

Çalışmanın son aşaması, PIK3CA geninin gözlemlenen olaylarda önemli bir hücresel sinyal düzenleyici olarak rolünü araştırmaya odaklandı. PIK3CA'nın etkisinin kapsamlı analizi, farklı mikro-ortamsal koşullar altında yeni hidrojel modellerinde hücresel tepkileri etkileyen süreçler hakkında değerli bilgiler sağlamıştır. Çalışma, PIK3CA'nın, tümör taklidi ortamlarında hücre proliferasyonunu düzenlemede önemli bir rol oynadığını ortaya koydu ve bu etkiyi modüle eden glikoz seviyeleri, PIK3CA yıkım hücreleri ile doğrulandı. Yüksek glikoza maruz kalma, PIK3CA yıkımının etkilerini kısmen telafi ederek, EMT işaretleyici ifadesini, sap işaretçilerini ve tümör hücrelerinde çeşitli metabolik yolları etkiledi. Glikoz metabolizması, hücre dışı mikro ortam ve PIK3CA sinyali arasındaki karmaşık etkileşim, PIK3CA ile ilişkili kanserler için potansiyel terapötik hedefler sunarak açıktı.

Sonuç olarak, bu kapsamlı araştırma, tümör mikro ortamını doğru bir şekilde simüle etmek ve hücresel davranışı araştırmak için gelişmiş 3D *in vitro* kanser modellerinin önemini vurgulamaktadır. Bulgular, kanser hücresi metabolizması, mikroçevresel faktörlerin etkisi ve akciğer kanseri tedavi stratejilerini ilerleten potansiyel terapötik hedefler hakkında değerli bilgiler sağlar.

ACKNOWLEDGEMENTS

First, I would like to express my sincere gratitude to Dr. Ece Öztürk for her invaluable guidance, support, and mentorship throughout this research project. Her expertise, insightful feedback, and continuous encouragement were instrumental in shaping the direction and success of this study.

I am also thankful to my colleagues and fellow researchers in the ECOM Lab for their stimulating discussions and feedback during the course of this study. I want to extend my appreciation to Alican Kuşoğlu, Deniz Örnek, Sena Özkan, and Sevgi Sarıca for their assistance and support.

I would like to express my deepest gratitude to my family, particularly my mother, Fatma; my sisters, Selma and Hatice; as well as my nephews, Ahmed and Ali; and my nieces, Zeynep, Elif, and Esra. Their presence, encouragement, and understanding have been priceless, and I am truly thankful for their love and support.

I am grateful to my partner, Ataberk, for being my rock throughout this journey, just as he has been during every other moment in life. I deeply appreciate his consistent willingness to lend a listening ear whenever I've faced challenges. I also appreciate his invaluable guidance through insightful perspectives and suggestions, despite my occasional (!) stubbornness. His belief in my abilities and constant motivation has pushed me to overcome challenges and achieve my goals. I am glad to have met him (special thanks to my precious friends Sanem and Barış) and have shared precious moments with him during our five-year relationship.

I would also like to express my heartfelt gratitude to my friends Alper, Barış, and Sanem. Despite the limited opportunities to meet in person, their presence is reassuring and comforting. They exemplify what true friendship means, offering constant support that I deeply cherish. Their cheerful existence in my life raises the bar for friendship to incredible heights, and I cannot imagine my life without them. I hope that we will be in the same city during the next phase of my life.

Finally, I want to take a moment to thank myself. Throughout my academic life, I encountered a lot of difficulties, including my research and personal life. Even though I was not successful in every one of them, I have dedicated tremendous energy and countless hours of hard work to face and handle them. I am proud of the personal growth and skills I have developed throughout this journey. I am grateful for my own resilience and dedication to pursuing knowledge and making a meaningful contribution to my field.

In conclusion, I am profoundly grateful to everyone who has played a role in my research journey and personal life. Your support, guidance, and love have been invaluable to me. As I embark on new chapters and challenges, I carry with me the lessons learned and the connections forged during this remarkable journey. I am excited about the opportunities that lie ahead and look forward to continuing to learn, grow, and make a meaningful impact in my field with your ongoing support.

TABLE OF CONTENTS

ABSTRACT iv

ÖZETÇE vi

ACKNOWLEDGEMENTS viii

TABLE OF CONTENTS x

LIST OF TABLES xiv

LIST OF FIGURES xv

ABBREVIATIONS xviii

Chapter 1: INTRODUCTION 1

1.1 Lung Cancer 1

1.1.1 Non-Small Cell Lung Cancer (NSCLC) 1

1.1.2 Small Cell Lung Cancer (SCLC) 1

1.2 The Extracellular Matrix of Lung 2

1.2.1 Glycosaminoglycans (GAGs), Proteoglycans (PGs), and Heparan Sulfate Proteoglycans (HSPGs) 2

1.3 Tumor Microenvironment 3

1.4 Cancer Cell Metabolism 5

1.4.1 Intrinsic Alterations in Cancer Cell Metabolism 6

1.4.2 Extrinsic Modulators of Cancer Cell Metabolism 7

1.5 3D Cultures as a Tool to Mimic the Tumor Microenvironment 10

1.5.1 Alginate as a Biomaterial in 3D Cultures: Composition and Structural Properties 11

1.5.2 Decellularized ECM in 3D Cultures 11

1.6 Scope of the Study 12

Chapter 2: MATERIALS AND METHODS 14

2.1 Modification of Alginate 14

2.2 Decellularization and Digestion of Bovine Lung Tissue 14

2.3 Mechanical Characterization of AlgLung and AlgSLung Hydrogels 14
2.4 Cell Culture and Cell Encapsulation in Hydrogels 15
2.5 Plasmid Construction and Lentiviral Production 15
2.6 shPIK3CA A549 Cell Line Generation 16
2.7 Quantification of DNA Content 16
2.8 Quantification of ATP Level 17
2.9 Immunofluorescence and Image Analysis 17
2.10 RNA Isolation and cDNA Synthesis 17
2.11 qRT-PCR 18
2.12 Metabolic Assays (Glycolysis and Mitochondrial Stress Test) 19
2.13 Statistical Analysis 20
Chapter 3: RESULTS 21
3.1 Interpenetrating Network Formation of Decellularized Bovine Lung Matrix with Alginate or Alginate Sulfate 21
3.2 Effect of Glucose Concentration on A549 Cell Proliferation and Cell Metabolism 23
3.3 Comparing Gene Expression Profiles of A549 Cancer Cells in 2D and Healthy-mimetic 3D Environments 24
3.4 Growth of A549 Cells in Healthy and Tumor-mimetic Environments 28
3.5 Morphological Analysis of A549 Cells in Healthy and Tumor-mimetic Environments 31
3.6 Gene Expression Profiles of A549 Cells in Healthy and Tumor-mimetic Environments 32
3.7 Bioenergetic Variability of A549 Cells across Diverse Environmental Conditions 36
3.7.1 Metabolic Responses of A549 Cells: Exploring the Impact of Glucose Levels and Environmental Settings on Glycolysis, Glycolytic Capacity, and Glycolytic Reserve Characteristics 36

3.7.2 Respiratory Profiles of A549 Cells: Investigating the Influence of Glucose Levels and Environmental Settings on Basal Respiration, ATP Production, and Maximal Respiration Characteristics 39

3.8 Growth of shPIK3CA A549 cells in Tumor-mimetic Environments 41

3.9 Morphological Analysis of shPIK3CA A549 Cells in Tumor-mimetic Environments 43

3.10 Gene Expression Profiles of shPIK3CA A549 Cells in Tumor-mimetic Environments 45

3.11 Bioenergetic Variability of shPIK3CA A549 Cells in Tumor-mimetic Environments 48

Chapter 4: DISCUSSION 50

4.1 Overcoming Limitations of 2D Cultures: Advancing Towards 3D Models in Lung Cancer 50

4.2 Comparing A549 Cell Behavior in 2D and 3D Healthy-Mimetic Models: Effects of Glucose Levels on Cell Proliferation and Expression of EMT, Stemness, and Metabolic Markers 52

4.2.1 Variations in EMT, Stemness, and Metabolic Markers in A549 Cells: A Comparison Between Typical 2D System and AlgLung Hydrogel with Varying Glucose Concentrations 52

4.3 Exploring A549 Cell Behavior in 3D Tumor-Mimetic Hydrogel Models with Varying Glucose Levels 55

4.3.1 Effects of Glucose Levels and Tumor-Microenvironment on A549 Cell Proliferation and Clump Formation 57

4.3.2 Influence of Glucose and Tumor-Microenvironment on EMT Marker Expression in A549 Cells 58

4.3.3 Influence of Glucose and Tumor-Microenvironment on Stemness Marker Expression in A549 Cells 59

4.3.4 Influence of Glucose and Tumor-Microenvironment on Metabolic Marker Expression in A549 Cells 59

4.3.5 Influence of Glucose and Tumor-Microenvironment on Bioenergetic Characteristics of A549 Cells 61

4.4 Exploring the Role of PIK3CA and Glucose Variations on A549 Cell Behavior in Tumor-Mimetic Hydrogel Models 63

4.4.1 Unraveling the Role of PIK3CA and Glucose Levels in A549 Cell Growth and Morphology within 3D Tumor-Mimetic Hydrogels 64

4.4.2 Exploring the Impact of PIK3CA and Glucose Levels on Gene Expression Profiles of A549 Cells in Tumor-Mimetic Hydrogels 65

4.4.3 The Impact of PIK3CA and Glucose Levels on Glycolytic and Mitochondrial Bioenergetics in A549 Cells 68

Chapter 5: CONCLUSION 70

BIBLIOGRAPHY 72

LIST OF TABLES

Table 2-1: Primers used for qRT-PCR. 18
Table 2-2: Parameters for quantitative RT-PCR. 19
Table 2-3: Compound preparation of glycolysis and mitochondrial stress test. 19

LIST OF FIGURES

Figure 1-1: Matrix changes in cancer. From “The Matrix in Cancer,” by Thomas R. Cox, 2021. Copyright 2021 by Springer Nature Limited. Adapted with permission. 4

Figure 1-2: Factors influencing the metabolic profile of the tumor (Created with BioRender.com). 8

Figure 3-1: Schematic illustration of (A) the production of decellularized bovine lung extracellular matrix (dLung) hydrogels and (B) the encapsulation process of A549 cells in healthy and tumor-mimetic hydrogels (Created with BioRender.com). 21

Figure 3-2: Mechanical assessment of AlgLung and AlgSLung gels (a) storage modulus (G’) and (b) loss modulus (G’’). 22

Figure 3-3: DNA quantification of A549 cells on 2D culture under low (5mM) or high (25mM) glucose conditions for 72h. 23

Figure 3-4: Metabolic activity of A549 cells on 2D culture under low (5mM) or high (25mM) glucose conditions for 72h. 24

Figure 3-5: mRNA expression profiles of EMT markers in A549 cells on 2D or 3D culture under low (5mM) or high (25mM) glucose conditions. 24

Figure 3-6: mRNA expression profiles of stemness markers in A549 cells on 2D or 3D culture under low (5mM) or high (25mM) glucose conditions. 26

Figure 3-7: mRNA expression profiles of metabolic markers in A549 cells on 2D or 3D culture under low (5mM) or high (25mM) glucose conditions. 27

Figure 3-8: Bright-field images of A549 cells cultured in different hydrogels under low (5 mM) and high (25 mM) glucose conditions at various time intervals. (Scale bar: 70 μm) 28

Figure 3-9: DNA quantification of A549 cells cultured in different hydrogels under low (5 mM) and high (25 mM) glucose conditions. 29

Figure 3-10: Metabolic activity of A549 cells cultured in different hydrogels under low (5 mM) and high (25 mM) glucose conditions. 30

Figure 3-11: Immunofluorescence images of A549 cells cultured in different hydrogels under low (5 mM) and high (25 mM) glucose conditions. (Phalloidin: Red; DAPI: Blue; Scale bar:50 μm) 31

Figure 3-12: Clump area analysis of A549 cells cultured in different hydrogels under low (5 mM) and high (25 mM) glucose conditions. 32

Figure 3-13: mRNA expression profiles of EMT markers in A549 cells cultured in different hydrogels under low (5 mM) and high (25 mM) glucose conditions. 33
Figure 3-14: mRNA expression profiles of stemness markers in A549 cells cultured in different hydrogels under low (5 mM) and high (25 mM) glucose conditions. 34
Figure 3-15: mRNA expression profiles of metabolic markers in A549 cells cultured in different hydrogels under low (5 mM) and high (25 mM) glucose conditions. 35
Figure 3-16: Real-time assessment of glycolysis, glycolytic capacity, and glycolytic reserve characteristics in A549 cells under various environmental conditions using Seahorse XF Glycolysis Stress Test. 37
Figure 3-17: Real-time assessment of basal respiration, ATP production, and maximal respiration characteristics in A549 cells under various environmental conditions using Seahorse XF Cell Mito Stress Test. 39
Figure 3-18: PIK3CA mRNA expression level of A549 and shPIK3CA A549 cells 41
Figure 3-19: Bright-field images of shPIK3CA A549 cells cultured in AlgSLung hydrogels under low (5 mM) and high (25 mM) glucose conditions at various time intervals. (Scale bar (Day0, 14, and 21): 70 μm, Scale bar (Day 7): 100 μm) 42
Figure 3-20: DNA quantification of A549 and shPIK3CA A549 cells cultured in AlgSLung hydrogels under low (5 mM) and high (25 mM) glucose conditions. 42
Figure 3-21: ATP level quantification of A549 and shPIK3CA A549 cells cultured in AlgSLung hydrogels under low (5 mM) and high (25 mM) glucose conditions. 43
Figure 3-22: Immunofluorescence images of shPIK3CA A549 cells cultured in AlgSLung hydrogels under low (5 mM) and high (25 mM) glucose conditions at day 21. (Phalloidin: Red; DAPI: Blue; Scale bar:50 μm) 44
Figure 3-23: Clump area analysis of A549 and shPIK3CA A549 cells cultured in AlgSLung hydrogels under low (5 mM) and high (25 mM) glucose conditions at day 21. 44
Figure 3-24: mRNA expression profiles of EMT markers in A549 and shPIK3CA A549 cells cultured in AlgSLung hydrogels under low (5 mM) and high (25 mM) glucose conditions. 45
Figure 3-25: mRNA expression profiles of stemness markers in A549 and shPIK3CA A549 cells cultured in AlgSLung hydrogels under low (5 mM) and high (25 mM) glucose conditions. 46

Figure 3-26: mRNA expression profiles of metabolic markers in A549 and shPIK3CA A549 cells cultured in AlgSLung hydrogels under low (5 mM) and high (25 mM) glucose conditions..... 47

Figure 3-27: Real-time assessment of glycolysis, glycolytic capacity, and glycolytic reserve characteristics in A549 and shPIK3CA A549 cells under various environmental conditions using Seahorse XF Glycolysis Stress Test. 48

Figure 3-28: Real-time assessment of basal respiration, ATP production, and maximal respiration characteristics in A549 and shPIK3CA A549 cells under various environmental conditions using Seahorse XF Cell Mito Stress Test..... 49

ABBREVIATIONS

2D	Two Dimensional
3D	Three Dimensional
2-DG	2-Deoxy-D-Glucose
ADCY5	Adenylate Cyclase 5
ADH1C	Alcohol Dehydrogenase 1C
Alg	Alginate
AlgS	Alginate Sulfate
AlgLung	Alginate-Decellularized Lung Hydrogel
AlgSLung	Alginate Sulfate-Decellularized Lung Hydrogel
ANOVA	Analysis of Variance
CDH1	Cadherin 1
CDH2	Cadherin 2
DAPI	4',6-Diamidino-2-Phenylindole
dLung	Decellularized Bovine Lung Extracellular Matrix
DMEM	Dulbecco's Modified Eagle's Medium
ECAR	Extracellular Acidification Rate
ECM	Extracellular matrix
EMT	Epithelial to Mesenchymal Transition
FBS	Fetal Bovine Serum
FCCP	Carbonyl cyanide-4 (trifluoromethoxy) phenylhydrazone
FXYD2	FXYD Domain Containing Ion Transport Regulator 2
FN1	Fibronectin 1
GAG	Glycosaminoglycan
GAPDH	glyceraldehyde-3-phosphate dehydrogenase
GCGR	Glucagon Receptor
HMGCS2	3-hydroxy-3-methylglutaryl-CoA synthase 2
HS	Heparan Sulfate
HSGAGs	Heparin/Heparan Sulfate Glycosaminoglycans
HSPG	Heparan Sulfate Proteoglycan
IGFL2	Insulin Growth Factor-Like Family Member 2
IGFBP2	Insulin Like Growth Factor Binding Protein 2
IGFBP5	Insulin Like Growth Factor Binding Protein 5

KLF4	Kruppel-Like Factor 4
NSCLC	Non-Small Cell Lung Cancer
OCR	Oxygen Consumption Rate
PCK1	Phosphoenolpyruvate Carboxykinase 1
PG	Proteoglycan
PIK3CA	Phosphoinositide 3-Kinase Alpha
POU5F1	Octamer-Binding Transcription Factor 3
P/S	Penicillin-Streptomycin
Rot/AA	Rotenone/Antimycin A
RT-q-PCR	Reverse Transcription Quantitative Polymerase Chain Reaction
sGAG	Sulphated Glycosaminoglycan
SNAI1	Snail Family Transcriptional Repressor 1
SOCS3	Suppressor of Cytokine Signaling 3
SOX2	SRY-Box Transcription Factor 2
TME	Tumor Microenvironment
VIM	Vimentin

Chapter 1: **INTRODUCTION**

1.1 Lung Cancer

Lung cancer has 2.21 billion occurrences worldwide, making it the second most frequent type of cancer, according to the World Health Organization (WHO, 2022). In addition, with 1.8 million fatalities annually, lung cancer has the greatest mortality rate of all cancer forms (Sun et al., 2007). Although smoking is the primary cause of most lung cancers, 25% of lung cancer diagnoses globally are unrelated to smoking (Gridelli et al., 2015). In addition to chemical carcinogens such as tobacco, arsenic, asbestos, nickel, polycarbonate, and chromium, other environmental factors, such as radiation, can also contribute to the development of lung cancer. There are two major types of lung cancer which are non-small cell lung cancer (NSCLC) and small cell lung cancer (SCLC) (Giaccone, 2005).

1.1.1 Non-Small Cell Lung Cancer (NSCLC)

NSCLC accounts for between 80% and 85% of all lung cancer cases. It subdivides into adenocarcinoma, squamous cell carcinoma (SCC), and large cell carcinoma (LCC) (Gridelli et al., 2015). Adenocarcinoma has the highest occurrence rate, with 40% among the other two types of NSCLC. Typically, lung adenocarcinoma arises from the mucosal glands. It is the most prevalent form of lung cancer in smokers and nonsmokers (Sun et al., 2007). Non-small cell lung cancer (NSCLC) metastases are typically found in the brain, bone, liver, adrenal glands, contralateral lung, and distal lymph nodes. Metastases in other organs are uncommon (Niu et al., 2016).

1.1.2 Small Cell Lung Cancer (SCLC)

Small-cell lung cancer (SCLC) accounts for approximately 15% of all lung cancers. It has a high proliferative rate, a strong tendency towards early metastasis, and a poor prognosis. SCLC is strongly linked to exposure to tobacco carcinogens (Rudin et al., 2021). Primary SCLC tumors have a tendency to be centrally located and frequently manifest as bulky masses. Similar to NSCLC, the most frequent sites of SCLC metastasis include the contralateral lung, brain, liver, adrenal glands, and bone (Han et al., 2019).

1.2 The Extracellular Matrix of Lung

The extracellular matrix (ECM), which is the noncellular component found in all tissues and organs, provides the cells with critical physical scaffolding. Furthermore, ECM initiates essential biochemical and biomechanical cues for tissue morphogenesis, differentiation, and homeostasis (Frantz et al., 2010). In addition to being a reservoir for growth factors and cytokines, ECM also provides structural integrity, such as stiffness, and performs a variety of other functions. The functions of ECM differ between different tissues. Lung ECM is mainly composed of fibrous proteins such as collagen and elastin, glycoproteins, glycosaminoglycans (GAGs), and proteoglycans (PGs) in a dynamic and complex arrangement (Burgstaller et al., 2017).

1.2.1 Glycosaminoglycans (GAGs), Proteoglycans (PGs), and Heparan Sulfate Proteoglycans (HSPGs)

Glycosaminoglycans are long linear polysaccharides made up of repeated disaccharide units. The repeating two-sugar unit consists of an amino sugar and a uronic sugar (Potter, 2008)**.** Based on the disaccharide central structures, GAGs are divided into four categories. One of the class heparin/heparan sulfate glycosaminoglycans (HSGAGs) is synthesized in the Golgi apparatus, where protein centers from the rough endoplasmic reticulum are modified by glycosyltransferases with O-linked glycosylation to form proteoglycans (Sarrazin et al., 2011). Sulfation motifs of HS chains in HSGAGs are crucial for interactions of HS with growth factors, cytokines, and proteins (Malavaki et al., 2011). Consequently, the sulfation pattern of these domains could impact their biological functions.

Proteoglycans are a class of glycoproteins where core protein domains are covalently linked to glycosaminoglycans (GAGs) (Walimbe & Panitch, 2020). Heparan sulfate proteoglycans (HSPGs) are one of the major types of glycoproteins containing one or more covalently attached HSGAGs in their structure (Esko et al., 2009). HSPGs are recognized as one of the most significant elements of the ECM, performing essential roles in ECM assembly and function in both healthy tissue and disease contexts. The abundance of sulfated groups in HSPGs facilitates their interactions with diverse ECM components and ligands, among them growth factors, enzymes, cytokines, and chemokines (Kirn-Safran et al., 2009). HSPGs primarily serve as co-receptors for growth

factors, thereby enhancing the activation of their receptors. Moreover, HSPGs are also capable of functioning as receptors and can activate receptors in neighboring cells (Billings & Pacifici, 2015). They regulate a wide variety of processes, including cell proliferation, apoptosis, cell adhesion, motility, inflammation, and tumorigenesis (Hassan et al., 2021; Walimbe & Panitch, 2020). Changes in the expression and structural characteristics of HSPGs have been linked to significant TME remodeling. They can perform a dual role in this context, contributing to tumor growth as structural support, and by actively regulating cell-matrix interactions, cell-cell interactions, and cell signaling (Barbouri et al., 2014; Hull et al., 2017). They can contribute to the development of drug resistance and impact the angiogenesis of tumor stroma. Alterations in the structure or activity of HSPGs have been identified in a variety of cancers (Reticker-Flynn & Bhatia, 2015; Theocharis & Karamanos, 2019). Different types of HSPGs constitute a significant component of lung ECM, and they can be severally altered in different lung diseases (Burgstaller et al., 2017). Syndecans (types 1, 2, and 4) and Glypicans (types 3 and 4) are the main types of HSPGs that are dysregulated in lung cancer ECM (Götte & Kovalszky, 2018).

1.3 Tumor Microenvironment

A tumor is a heterogeneous collection of infiltrating and resident host cells, secreted factors, and extracellular matrix, in addition to a group of cancer cells. Immune cells, tumor stromal cells, blood vessels, and altered ECM are defining characteristics of the tumor microenvironment (TME), which varies depending on the type of tumor (Anderson & Simon, 2020). An early dynamic and mutual relationship between cancer cells and components of the TME promotes cancer cell survival, local invasion, and metastasis. The most well-known example of this concept is the coordination of an angiogenesis-supporting program by the TME, allowing cancer cells to survive in hypoxic and acidic microenvironments; as a result, oxygen and nutrient availability can be restored, and metabolic waste can also be eliminated (Z.-L. Liu et al., 2023).

According to the article by Hanahan and Weinberg, tumor progression depends not only on cell-autonomous alterations in tumor cells but also on microenvironmental modifications like modifications in ECM (Hanahan & Weinberg, 2011). An altered ECM is also a crucial aspect of the dysregulated microenvironment of lung cancer. As depicted in Figure 1.1, during tumor growth, progression, and metastasis, the TME undergoes

numerous matrix modifications. These modifications could include alterations in the biochemical properties and composition of the ECM, which lead to changes in the local sequestration of growth factors, cytokines, and inorganic molecules. Similar to alterations in the biochemical characteristics of the ECM, alterations in post-translational modification of the ECM, such as hydroxylation and enzymatic crosslinking, result in alterations in the biophysical properties of the matrix, including molecular density, stiffness, and tension, which activate mechanosensing pathways within tumor cells. Moreover, changes in the distribution of matrix components affect the density of the ECM, leading to modifications in its structure, organization, and porosity. This, combined with abnormal degradation and turnover of the matrix, significantly affects the adhesion and interaction of ligands available to cells in the TME.

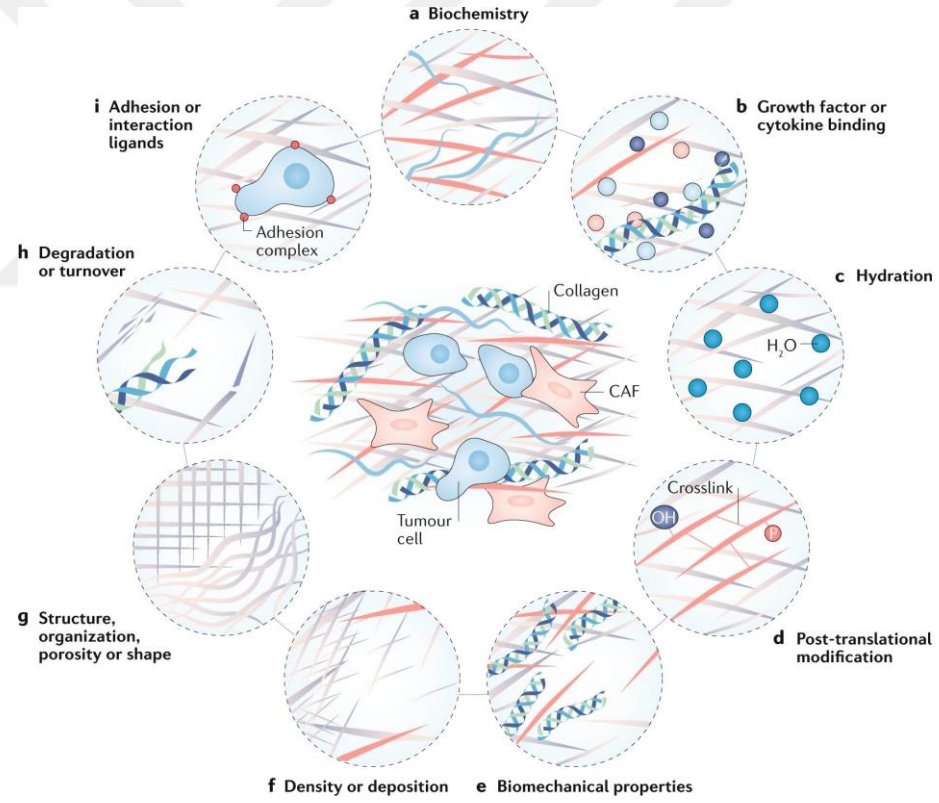

Figure 1-1: Matrix changes in cancer. From “The Matrix in Cancer,” by Thomas R. Cox, 2021. Copyright 2021 by Springer Nature Limited. Adapted with permission.

In lung cancer, there is an increase in fibrillar collagen deposition and an alteration in collagen structure, which are indicative of a fibrotic response. For example, SCLCs

contain high levels of fibronectin, laminin, collagen IV, and tenascin-C (Burgstaller et al., 2017). In the same way, increased expression of type VI collagen in NSCLCs creates an inflammatory and pro-invasive environment that helps lung cancer spread by turning on several intrinsic pathways, such as the focal adhesion kinase and Erk signaling pathways (Voiles et al., 2014).

Laminin is another ECM component that is dysregulated in lung cancer. A poor prognosis is associated with the dysregulation of multiple laminin isoforms in the TME and serum of NSCLC cancer patients (An et al., 2012; Teng et al., 2016). The functional impacts of laminin dysregulation depend on laminin degradation along with laminin receptor inactivation.

sGAGs can participate in fibroblast growth factor (FGF), vascular endothelial growth factor (VEGF), hepatocyte growth factor (HGF), transforming growth factor (TGF), platelet-derived growth factor (PDGF), integrin, interleukin (IL), and WNT signaling (Fuster & Esko, 2005). All these signaling pathways are previously shown for their involvement in the initiation or progression of tumors. An aberrant increase in sGAG content of TME is shown in many cancer types, including lung cancer (Reticker-Flynn & Bhatia, 2015; Vallen et al., 2014). In the majority of cases, the increased expression of sGAGs and the degree of sulfation lead to RTK overstimulation in lung cancer.

Finally, as indicated earlier, lung ECM contains various HSPGs, which can be altered in different lung diseases, including lung cancer. Syndecans (SDC1, SDC2, and SDC4) and Glypicans (GPC3 and GPC4) are the main types of HSPGs that are dysregulated in lung cancer ECM (Götte & Kovalszky, 2018). While the expression of syndecan type 1 (SDC1) declines in NSCLCs, the expression of syndecan type 2 (SDC2) rises (Kind et al., 2019; Mytilinaiou et al., 2017). Like syndecans, the glypicans (GPCs) are cell surface HSPGs. Glypicans have diverse functions in lung cancer. They can regulate cell proliferation, survival, and differentiation, as well as cell migration and angiogenesis, by modifying the activity of numerous signal transduction pathways such as Wnt, FGF, and IGF (Filmus & Capurro, 2014; Theocharis et al., 2010). Both GPC3 and GPC5 have decreased expression in NSCLC (De Pasquale & Pavone, 2020a; Knelson et al., 2014).

1.4 Cancer Cell Metabolism

In the early twenty-first century, a landmark paper by Douglas Hanahan and Robert A. Weinberg proposed that there were six hallmarks of cancer that were, in fact,

fundamental characteristics of a variety of cancer types. Multiple studies on various types of cancer cells have verified these hallmarks. In 2011, they also published a follow-up article stating that, over time, additional studies demonstrated the emergence of additional hallmarks. These emerging hallmarks are deregulating cellular metabolism and avoiding immune destruction (Pavlova & Thompson, 2016).

The main idea behind deregulating metabolic activity is so that tumor cells can use these modifications to fulfill their unique needs and increase their survival. Altered cell metabolism provides three basic needs for cancer cells. These are rapid ATP synthesis to maintain energy status within cells, increased macromolecule biosynthesis, and tightened maintenance of appropriate cellular redox status (Deberardinis & Chandel, 2016). These three basic needs are also observed in rapidly growing, healthy cells (Vander Heiden et al., 2009). On the other hand, in the case of cancer cells, these modifications must be adapted to the challenging and dynamic microenvironment of tumor cells, where the concentrations of essential nutrients like glucose, glutamine, and oxygen vary spatially and temporally. To satisfy these requirements, cancer cells acquire metabolic alterations in all four main classes of macromolecules, which are carbohydrates, proteins, lipids, and nucleic acids (J. Zhu & Thompson, 2019).

The most known metabolic alteration within cancer cells is the Warburg effect or aerobic glycolysis (Warburg, 1956a). Otto Warburg first noted in 1956 that cancer cells exhibit elevated glucose uptake and lactic acid production. Even under normal oxygen conditions, cancer cells appear to prefer aerobic glycolysis over oxidative phosphorylation, as stated in the paper. Warburg initially believed that cancer cells had impaired respiration because of dysfunctional mitochondria (Warburg, 1956b). However, it was subsequently reported by several research groups that cancer cells did not sacrifice oxidative phosphorylation for enhanced lactate production (Newsholme et al., 1985; Weinhouse, 1956). The Warburg effect remains valid for the vast majority of cancer cell types; nevertheless, despite numerous hypotheses regarding the benefits of aerobic glycolysis, its exact reasons and physiological values remain obscure.

1.4.1 Intrinsic Alterations in Cancer Cell Metabolism

Multiple intrinsic and extrinsic molecular mechanisms play a role in altering the central cellular metabolism of cancer cells and supporting the three fundamental requirements of cancer cells (J. Zhu & Thompson, 2019). Mutations in oncogenes and

tumor suppressor genes result in modifications to various intracellular signaling pathways that impact tumor cell metabolism and redesign it for improved survival and growth. The genetic alterations that influence the metabolism of cancer cells can vary depending on the type of cancer; however, there are certain pathways that are altered in most cancers.

The PI3K signaling pathway is one of the most frequently changed signaling pathways in cancer (Fruman et al., 2017; Hemmings & Restuccia, 2012). This pathway can be activated by different mutations. It can be activated via mutations in tumor suppressor genes like *PTEN*. Moreover, it can be activated due to mutations in the PI3K complex components or aberrant signaling from receptor tyrosine kinases (RTKs) (Cairns et al., 2011). After aberrant activation of the PI3K signaling pathway, it has profound effects on tumor growth and metabolism. AKT1 is the most thoroughly researched effector downstream of PI3K. AKT1 is a key regulator of the glycolytic phenotype of tumors, as it stimulates ATP production through multiple mechanisms and ensures that tumor cells have the bioenergetic capacity required to respond to growth signals (Manning & Cantley, 2007). AKT1 can enhance the expression and translocation of glucose transporters, as well as phosphorylate critical glycolytic enzymes like hexokinases (Sahlberg et al., 2017). By phosphorylating and inhibiting its negative regulator, AKT1 substantially enhances mTOR-mediated signaling. mTOR is a crucial metabolic coordinator that links growth signals to nutrient availability. In response to nutrient availability and energy conditions, activated mTOR induces protein and lipid biosynthesis and cell growth (Harachi et al., 2018; Sangüesa et al., 2019). It is frequently activated during tumorigenesis. Activation of mTOR stimulates mRNA translation and ribosome biogenesis, which induces indirect metabolic alterations by activating transcription factors such as hypoxia-inducible factor 1 (HIF1) even during normoxic conditions (Bond, 2016; DeBerardinis et al., 2008). In conclusion, the PI3K-AKT-mTOR network harbors many extensively studied oncogenes and tumor suppressors, and the abnormal activation of this pathway is one of the most common alterations observed in various cancers (De Berardinis & Chandel, 2016; DeBerardinis et al., 2008).

1.4.2 Extrinsic Modulators of Cancer Cell Metabolism

Besides intrinsic molecular mechanisms, there are extrinsic molecular mechanisms that significantly impact the metabolism of cancer cells (Lyssiotis & Kimmelman, 2017). Multiple studies have demonstrated that the characteristics of TME, such as the

stiffness and composition of ECM, can exert profound effects on cancer cells (Burgstaller et al., 2017; Nazemi & Rainero, 2020). Mechanotransduction is the process by which cells detect and respond to mechanical stimuli from their microenvironment, like the stiffness and elasticity of their ECM (Humphrey et al., 2014). Changes in mechanotransduction can affect several different processes such as proliferation, differentiation, migration, and metabolism in cancer cells (Chin et al., 2016). For example, when cancer cells detect an increase in ECM stiffness, mechanotransduction pathways are activated, resulting in the upregulation of multiple signaling cascades that regulate metabolic reprogramming, including the activation of the PI3K-Akt-mTOR pathway (Romani et al., 2021). This activation promotes enhanced nutrient uptake and glycolysis in cancer cells, as mentioned earlier.

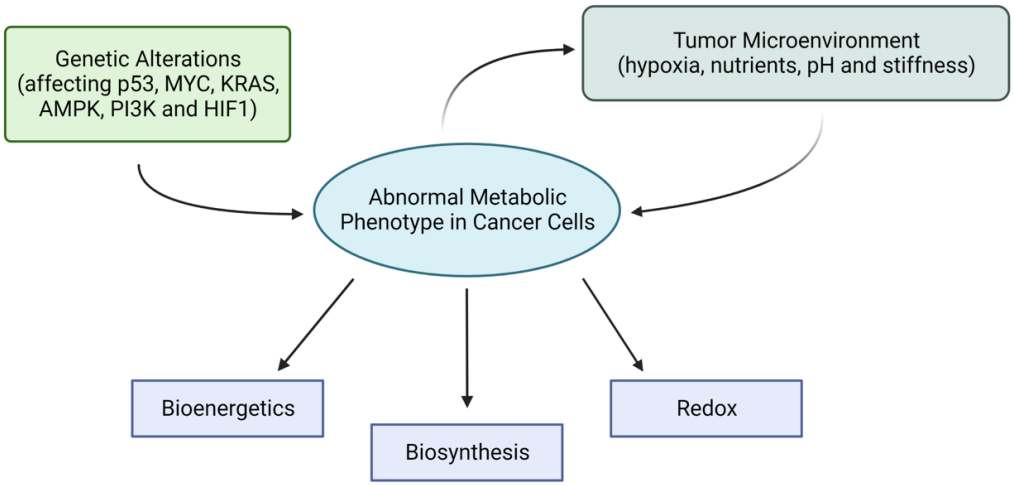

Figure 1-2: Factors influencing the metabolic profile of the tumor (Created with BioRender.com).

The stiffness of the ECM serves a crucial role in modulating the behavior of cancer cells, including their metabolism (Ge et al., 2021a). In healthy tissues, the stiffness of ECM provides a dynamic microenvironment in order to modulate cellular processes. On the other hand, the stiffness of ECM in tumor tissue changes because of alterations and modifications in ECM composition and structure. Multiple studies have shown that an increase in ECM stiffness can promote metabolic reprogramming in cancer cells, resulting in more aggressive behaviors (Acerbi et al., 2015; Jiang et al., 2022). The Warburg effect is a well-known effect of ECM stiffness on the metabolism of cancer cells.

Similar to the metabolic profile observed in the Warburg effect, cancer cells grown on rigid ECM frequently exhibit increased glycolysis and decreased oxidative phosphorylation (Ge et al., 2021b). This metabolic shift permits cancer cells to satisfy their energy needs and maintain rapid proliferation under conditions of low oxygen availability. Furthermore, it has been shown that ECM stiffness activates essential metabolic signaling pathways, such as the Hippo and YAP/TAZ pathways, which have important roles in cancer progression and metabolism (Cai et al., 2021; H. Li et al., 2022).

In addition to that, alterations in the composition and structure of the ECM have several roles in modulating the behavior of cancer cells, including their metabolism. For example, the presence of sGAG side chains on HSPGs within the ECM has crucial roles in terms of regulating the metabolism of cancer cells. These sGAG side chains serve as a supporting structure for growth factors and cytokines so that they can regulate the accessibility of growth factors to neighboring cells (Kirn-Safran et al., 2009; Malavaki et al., 2011). In addition, the coordination of receptor dimerization by HSPGs on the cell surface facilitates the binding of growth factors to their receptors. Initiated by these growth factors, this process activates downstream signaling pathways (Presta et al., 2005). Fibroblast growth factor (FGF), vascular endothelial growth factor (VEGF), WNT signaling, and integrin are notable growth factors involved in these interactions (Ornitz & Itoh, 2015; Vallen et al., 2014). Consequently, alterations in the ECM, specifically alterations in the level of sGAG side chains, can have a profound effect on the regulation of cancer cell metabolism.

Finally, as illustrated in Figure 1-2, both intrinsic genetic mutations and extrinsic modulators from TME determine the metabolic characteristics of tumor cells. The loss of tumor suppressors like p53 or the activation of oncoproteins such as KRAS and PI3K frequently activates oncogenic signaling pathways. These alterations in the activation of oncogenic signaling pathways result in modifications in cellular metabolism to meet the energy requirements of rapid cell division. TME, with its aberrant conditions such as increased stiffness, hypoxia, and nutrient deprivation, also has a significant impact on cancer cell metabolism. In response to these challenging conditions, cancer cells exhibit a number of adaptations, including deregulation of their cellular metabolism. Overall, these genetic mutations and modifications in ECM optimize deregulated metabolism in order to adapt to stressful conditions in TME. These metabolic adaptations result in

increased ATP levels, enhanced biosynthetic capacity, and the maintenance of balanced redox status.

1.5 3D Cultures as a Tool to Mimic the Tumor Microenvironment

Not only does the complexity of cancer depend on its altered genetics and cellular structure, but also on the complexity of its environment. Solid tumors display distinct alterations in their ECM compared to the ECM found in their healthy tissue counterparts (Henke et al., 2019). Throughout tumor development, the TME undergoes various modifications. These alterations can serve multiple functions, including promoting tumor growth, stimulating tumor metastasis, and inhibiting the host's immune system (Arneth, 2020; Rianna et al., 2018). The specifics and necessity of the modifications depend on the type and location of the tumor (Chaudhuri et al., 2014). In lung tumors, for instance, there is extensive stiff stroma due to highly crosslinked collagen and elevated levels of fibronectin, tenascin C, and hyaluronan; besides, proteoglycan types and levels, particularly heparan sulfate proteoglycan, differ in healthy lungs (Burgstaller & Oehrle, 2017). Given the complexity of the TME, providing tumor cells with an environment that accurately replicates the composition and intricacy of the TME becomes imperative to attain more precise outcomes in scientific research. The fundamental character of 2D cultures is incapable of providing this level of complexity, and some results obtained from 2D cultures can be misleading, especially in drug studies (Alemany-Ribes & Semino, 2014; Jensen & Teng, 2020). There are several studies that demonstrate the significance and necessity of the 3D culture in order to replicate the native tumor microenvironment as compared to flat, 2D cultures (Muguruma et al., 2020; Souza et al., 2018). Adding to that, when designing 3D cultures, it is important to consider both the form of the tumor to be investigated and its original location.

There are numerous techniques available for designing 3D cultures. One of the techniques that can be applied to create 3D cultures is hydrogel formation (Caliari & Burdick, 2016; Merivaara et al., 2022). Different polymers and polysaccharides can serve as the primary building blocks of these hydrogels (Andersen et al., 2015; Tibbitt & Anseth, 2009). Polymers and polysaccharides with different functions can be advantageous when simulating varied environmental conditions (Alemany-Ribes & Semino, 2014). The primary benefit of hydrogels is that they can be readily manipulated to create the desired 3D microenvironments for various types of tumors.

1.5.1 Alginate as a Biomaterial in 3D Cultures: Composition and Structural Properties

Alginate (Alg) is a biocompatible polysaccharide with anionic properties that makes it highly suitable for a wide variety of biomedical applications thanks to its inert nature with cells. Alg consists of repeating monomeric units of -L-guluronic acid (G) blocks and 1,4-linked -D-mannuronic acid (M) epimers with free functional hydroxyl (-OH) and carboxyl (-COOH) groups. The interaction between free carboxylate (COO-) groups of alginate monomers and divalent cations such as Ca^{2+}, Mg^{2+}, and Ba^{2+} results in hydrogel formation, also known as ionic gelation (Ahmad Raus et al., 2021; K. Y. Lee & Mooney, 2012). Different divalent ions have distinct crosslinking affinities, which can be desirable when casting hydrogels for various biomedical applications (Sahoo & Biswal, 2021).

Multiple compounds, such as sulfate or acetic acid, can be used to modify alginate (Rosiak et al., 2021). On this basis, the biophysical properties of the modified alginates, such as stiffness and viscoelasticity, can be altered in comparison to those of the original alginates. Thanks to the adaptability of the biophysical properties of alginate, numerous 3D tumor microenvironments can be engineered (Charbonier et al., 2021b; Rosiak et al., 2021). Besides, modifying the stiffness of alginate hydrogels is as simple as adjusting the quantity of divalent ions used in their production. Alginate sulfate is one of the modified forms of alginate that functions as an analog of sGAGs (Arlov et al., 2021; Arlov & Skjåk-Bræk, 2017; Nikitovic et al., 2008; Öztürk et al., 2020). The ability of alginate to undergo modification by sulfation permits the development of alginate hydrogels with consistent sulfation levels but varying stiffness levels.

1.5.2 Decellularized ECM in 3D Cultures

The extracellular matrix is an extremely complex structure comprised of tissue-specific components. The persistent interaction between cells and their microenvironment has a profound effect on the properties of the ECM and the function of cells (Frantz et al., 2010; Kim et al., 2011). Both mechanical and biochemical alterations in the ECM are influenced by the cells embedded within it, resulting in dynamic reciprocity, a bidirectional cell-matrix interaction (Humphrey et al., 2014). This interaction is essential for the regulation of tissue-specific physiological and pathological processes. Recent studies have demonstrated that tissue rigidity governs a variety of cellular processes, such

as differentiation, proliferation, apoptosis, and drug resistance (Stowers et al., 2019; C. Wang et al., 2021; Wei et al., 2022; X. Zhu et al., 2022). Recognizing the significance of the ECM in modulating cellular behavior, tissue engineering has been trying to develop models that faithfully replicate the ECM's native properties. Tissue and organ decellularization, which involves removing cellular content while preserving the native tissue matrices, is an increasingly popular method for this purpose (Fernández-Pérez & Ahearne, 2019; Petersen et al., 2012). These decellularized matrices can subsequently be reconstituted into hydrogels, allowing for cell embedding.

Lung tissue engineering also aims to develop *in vitro* human models that mimic the native lung microenvironment using synthetic or natural materials (Huh et al., 2010). The use of decellularized matrices by removing cells from lung tissue to preserve its specific ECM content and complexity is a promising approach to modeling diseases related to lung tissue. Numerous studies have previously shown the successful decellularization of rat, pig, and human lung tissue (Balestrini et al., 2015; O'Neill et al., 2013; Sengyoku et al., 2018; X. Zhu et al., 2022). Lung ECM is composed of biomolecules such as collagen, elastin, sGAGs, laminin, and fibronectin (Burgstaller et al., 2017). Under disease conditions, these biomolecules serve a crucial role in determining the mechanical properties of the ECM. Hence, it is vital to precisely replicate these complex environments in order to develop accurate disease models.

1.6 Scope of the Study

The primary objective of this study is to understand how lung tumor cell behavior is influenced by increased sulfation in the tumor microenvironment (TME) along with varying glucose levels. Specifically, we will investigate the effects on cell growth, morphology, and metabolism, and explore the role of the PIK3CA gene in these cellular changes.

To accomplish a more accurate and precise *in vitro* model, we will develop double network hydrogels that consist of either alginate or alginate sulfate in combination with decellularized bovine lung extracellular matrix (ECM). These hydrogel models will mimic the conditions of the TME (increased sGAGs level) and healthy tissue environment. To gain insights into the differences between our engineered 3D model and conventional 2D cell culture, we will compare tumor cell behavior in the 2D environment with that in our healthy-mimetic hydrogel model. By doing so, we can identify how gene

expression profiles and cellular behavior vary in the more representative model. The investigation will focus on observing how tumor cells respond to increased sulfation in the TME and varying glucose levels, particularly in terms of cell growth, morphology, and metabolism. Furthermore, we will specifically examine the role of the PIK3CA gene, a key regulator of cellular signaling, to better understand the molecular mechanisms underlying the observed cellular changes in the hydrogel models under different microenvironmental conditions.

Overall, this study aims to provide comprehensive insights into the behavior of lung tumor cells within 3D hydrogel models that resemble the tumor microenvironment and healthy tissue with varying glucose levels. The research will shed light on how altered microenvironmental factors, such as increased sulfation and glucose levels, affect cancer cell behavior and the involvement of the PIK3CA gene in these processes.

Chapter 2:**MATERIALS AND METHODS**

2.1 Modification of Alginate

For the sulfation of Alg, 99% chlorosulfonic acid ($HClSO_3$) (Sigma) was diluted to a final concentration of 2% in formamide (Sigma) with a total volume of 20 mL. The solution mix was added drop by drop while agitating 500 mg of Alg. The reaction was conducted at 60 °C for 2.5 hours on a stirrer. Alginate sulfate was precipitated with ice-cold acetone by centrifugation at 5000 RPM for 10 minutes. Precipitated AlgS was redissolved in ultrapure water to dialyze in 12 kDa molecular weight cut-off (MWCO) dialysis tubing (Sigma) against 100 mM NaCl for 48 hours and ultrapure water for 72 hours. Finally, the AlgS solution was lyophilized and stored at -20°C.

2.2 Decellularization and Digestion of Bovine Lung Tissue

The decellularization process of bovine lung tissue was performed as described previously (Kuşoğlu et al., 2022). In short, pieces of bovine lung tissue were incubated for 1 minute in a 2% iodine solution. The tissue pieces were then washed twice in sterile dH_2O. After that, the tissue in sterile dH_2O was flash-frozen in liquid nitrogen for 2 minutes and thawed at 37 °C for 10 minutes. This step was repeated five times. The tissue was then treated for 1 hour at 37 °C with 10 U/mL DNase in 10 mM $MgCl_2$ buffer. The tissue fragments were then rinsed with sterile dH_2O for 72 hours while gently rotating. Finally, the tissue was lyophilized and cryo-milled into a fine powder form.

To solubilize lyophilized decellularized lung (dLung), the powder was digested at room temperature for 48 hours with 1 mg/ml pepsin solution (Sigma) at a final concentration of 15 mg/ml. Finally, it was neutralized and lyophilized in preparation for hydrogel synthesis.

2.3 Mechanical Characterization of AlgLung and AlgSLung Hydrogels

Hydrogels were mechanically characterized via a TA Instruments Discovery HR-2 rheometer. Hydrogels were placed on the lower plate, which had been pre-cooled to 4°C, and the 20 mm parallel plate was lowered until the resulting separation measured 1 mm. To prevent hydrogels from drying out during testing, mineral oil (Sigma) was applied to

their exteriors. The storage and loss moduli were measured via oscillatory rheology at a constant frequency (1 Hz) and amplitude (1% strain) for 2 hours. At least three measurements were conducted for each hydrogel.

2.4 Cell Culture and Cell Encapsulation in Hydrogels

Human Lung Adenocarcinoma Cell Line A549 (CCL-185) was purchased from American Type Culture Collection (ATCC). Both A549 (CCL-185) and shPIK3CA A549 cells were grown in Dulbecco's Modified Eagle Medium Low Glucose (Biowest-L0066) containing 10% (v/v) fetal bovine serum (Biowest) and 1% (v/v) penicillin-streptomycin (Biowest). All cells were maintained in the 5% CO_2 incubator at 37°C. For high glucose conditions, the cells were cultured in Dulbecco's Modified Eagle Medium High Glucose (Biowest-L0103) supplemented with 10% (v/v) FBS (Biowest) and 1% (v/v) P/S (Biowest). In 2D experiments, cells were treated with a high concentration of glucose for either 48 hours or 72 hours, then subjected to additional experiments.

In 3D experiments, sodium alginate (Novamatrix) or its sulfated form called alginate sulfate was combined with decellularized bovine lung extracellular matrix to produce a healthy-mimicking (AlgLung) or tumor-mimicking (AlgSLung) hydrogel. Prior to use, Alg and AlgS solutions were filtered through a 0.2 μm pore size filter. Hydrogels containing Alg or AlgS were crosslinked with $CaCl_2$ solution. To achieve the same stiffness environment in healthy and tumor-mimetic hydrogels, various $CaCl_2$ solution concentrations were employed. The final Ca^{2+} concentration in healthy-mimicking hydrogels was 6 mM, while it was 40 mM in tumor-mimicking hydrogels. The final concentration of Alg or AlgS solution was 1%, and that of dLung was 15 mg/ml. After encapsulating, cells were grown in either DMEM with Low Glucose or High Glucose containing 10% (v/v) FBS, 1% (v/v) P/S, and 2 mM $CaCl_2$ for 3 weeks.

2.5 Plasmid Construction and Lentiviral Production

The short hairpin-mediated RNA inhibitor (shRNA) encoding PI3KCA (NM_0062) was obtained from Vector Builder, whose plasmid ID numbers were VB9000619992CNJ, VB9000619992GSY, and VB90000558929. Viral particles were produced by applying the second-generation lentiviral system. The psPAX2 packaging plasmid and the PCMVVSVG envelope plasmid were used for the production.

HEK293T cells were transfected for lentiviral production using Lipofectamine 3000 transfection reagent (Invitrogen). Lentiviral plasmid DNA, psPAX2 packaging plasmid, and PCMV-VSVG envelope plasmid are used in a 4:3:1 ratio. The medium was replaced 6 hours after transfection. The viral supernatant was collected and filtered through a 0.45 μm syringe filter 2 days after transfection. It was centrifuged at 800 G for 10 minutes at room temperature. After centrifugation, the viral supernatant was combined with PEG8000 at a ratio of 3:1. The solution mix was incubated at 4°C for 1 day on a shaker. The next day, it was centrifuged at 1600 G for 1 hour at 4°C. Pellet was resuspended with PBS in a 1:10 ratio of the original volume. It was stored at -80°C until use.

2.6 shPIK3CA A549 Cell Line Generation

The day prior to transduction, A549 cells were seeded in 6-well plates at 20% confluency. On the transduction day, the medium was changed to DMEM F12, including 10% FBS only. The cells were incubated for 4 hours in this medium. A549 cells were transduced with viral particles and 10 μg/mL of protamine sulfate (Sigma) at MOI of 5. The following day, the transduction efficiency was assessed using GFP fluorescence as a metric. The viral supernatant was maintained until 80% of the total population fluoresced with GFP. Afterward, they were treated with 1.5 μg/mL of puromycin (Sigma). The selection process persisted until puromycin completely eradicated the entire population of the control group, which had not received viral particles.

2.7 Quantification of DNA Content

The digestion and quantification of DNA were done after collecting all samples at the desired time points. Before storing hydrogels at -80°C, they were rinsed three times for 5 minutes in a 150×10^{-3} M NaCl and 5×10^{-3} M $CaCl_2$ solution (wash buffer). After collecting all hydrogels, they were digested with 125 μg/mL papain in 10×10^{-3} M EDTA, 100×10^{-3} M sodium phosphate, and 10×10^{-3} M L-cysteine at pH 6.3 and 60°C overnight. The DNA content of the digested samples was measured using the Quant-IT PicoGreen assay (Invitrogen) according to the manufacturer's instructions. Each experimental group was provided with at least three hydrogels.

2.8 Quantification of ATP Level

Cell-Titer Glo 3D was used to quantify ATP levels within samples. The manufacturer's instructions were followed. In short, the CTG 3D solution was thawed at 4°C and balanced to room temperature. The samples were also brought to room temperature for equilibration. The hydrogels in the CTG 3D solution were shaken for 10 minutes at room temperature on a shaker, followed by 30 minutes of incubation at room temperature. Finally, luminescence was recorded. Each experimental group was provided with at least three hydrogels.

2.9 Immunofluorescence and Image Analysis

Hydrogels were fixed with freshly prepared 4% formaldehyde (Sigma) and 0.1% Triton-X (Sigma) in wash buffer for 1 hour at 4°C. The hydrogels were then washed twice for 5 minutes with wash buffer solution. After that, the hydrogels were incubated for 45 minutes at room temperature with Alexa Fluor 488 Phalloidin. The nucleus was visualized using 1 µg/mL of DAPI solution. The hydrogels were incubated for 15 minutes at room temperature before being washed. The samples were visualized using a Leica DMI/SP8 Laser Scanning Confocal Microscope. ImageJ software (National Institutes of Health, USA) was used for image analysis.

2.10 RNA Isolation and cDNA Synthesis

The hydrogels were collected on day 21, washed for 5 minutes with a wash buffer, and then flash-frozen in liquid nitrogen. The hydrogels were homogenized in Trizol (Invitrogen) with a tissue pestle and centrifuged at 12,000 g for 5 minutes at 4 °C. The supernatant was chloroform-phase separated and centrifuged at 12,000 g for 15 minutes at 4 °C to obtain the aqueous phase. The NucleoSpin RNA Kit (Macherey-Nagel AG) was used to isolate RNA according to the manufacturer's instructions, and the NanoDrop Spectrophotometer (Thermo Scientific) was used to measure the RNA concentration of the samples. The M-MLV Reverse Transcriptase Kit (Invitrogen) was used to synthesize cDNA.

2.11 qRT-PCR

Primer3 was used to design primers. The tool-generated sequence was compared with NCBI primer-BLAST to identify potential off-targets. Sentebiolab was the supplier of the primers. The primers utilized in this research are listed in Table 2.1. qPCR reactions were conducted with the SYBR Green PCR Master Kit (Qiagen), and the manufacturer's instructions were applied. Light Cycler 480 Instrument II (Roche) was used for the qPCR experiment. qRT-PCR parameters that were used in this study are displayed in Table 2.2.

Table 2-1: Primers used for qRT-PCR.

Gene	Forward Primer Sequence (5'-3')	Reverse Primer Sequence (5'-3')
ADCY5	CCGCCAACGCCATAGACTTC	GCCAGCACAAAGACTGAGATG
ADH1C	ACTTGTGGCTGACTTTATGGCTA	AGGACGGTACGGATACTCTTTC
CDH1	CTGCCAATCCCGATGAAATTG	TCCTTCATAGTCAAACACGAGC
CDH2	CAGAATCAGTGGCGGAGATC	CAGCAACAGTAAGGACAAACATC
CD44	CTCACTCAAGCTCTTTAACT	GAATATCTAGAAGGAGTGGA
FN1	CAGAGGCATAAGGTTCGGG	TTCAGACATTCGTTCCCACTC
FXYD2	GCCTGATCTTCGCTGGACTG	CTCATCTTCATTGATTTGCCTGC
GAPDH	CTGACTTCAACAGCGACACC	GTGGTCCAGGGGTCTTACTC
GCGR	TGTTTGCGTCCTTCGTGCT	CCACCGCTCCATCACTGAG
HMGCS2	CTTCTGTCCCACCACTCTGC	CCTCAGGAGACACACACTTTCG
IGFBP2	ACATCCCCAACTGTGACAAGC	GCCTCCTGCTGCTCATTGTAGA
IGFBP5	GTGCTGTGTACCTGCCCAAT	CATCCCGTACTTGTCCACGC
IGFL2	GGAAGTCATCGCTCCCGCT	ATGGCGTCATTGTAACAGCACTG
KLF4	TCTGTGACTGGATCTTCTAT	CTTCCTCTTCTTCTAACATC
PCK1	AACTGCTGGTTGGCTCTCAC	CCTGGCATTGAACGCTTTCTC
PIK3CA	CCATATCTCCAAAGTAGAAC	TAGAATGACGACTAGCAGTA
POU5F1	CACTAAGGAAGGAATTGG	GTGTGTCTATCTACTGTGTCC
SNAI1	GGAAGCCTAACTACAGCGAG	CAGAGTCCCAGATGAGCATTG
SOCS3	CGGAGACTTCGATTCGGGAC	CGGGAAACTTGCTGTGGGT
SOX2	CTTTTATGAGAGAGATCCTG	ACCGTACCACTAGAACTTT
VIM	ACCAGCTAACCAACGACAAAG	AAAGATTGCAGGGTGTTTTCG

Table 2-2: Parameters for quantitative RT-PCR.

Cycle Number	Stages	Temperature	Time
1	Initial Denaturation	95°C	5 min
45	Denaturation	95°C	30 s
	Annealing	55°C	30 s
	Elongation	72°C	30 s
1	Melting Curve	95°C	10 s
		65°C	1 min
		97°C	
1	Cooling	40°C	30 sec

2.12 Metabolic Assays (Glycolysis and Mitochondrial Stress Test)

Cells were cultured in low-glucose DMEM, including 10% FBS and 1% P/S with or without 100 µg/mL Alg or AlgS for 48 hours prior to the metabolism assays. The same protocol was applied to high-glucose samples. After the treatment, the manufacturer's instructions for either glycolysis or the mitochondrial stress test kit (Agilent) were followed. The compounds used in these assays are listed in Table 2.3. Extracellular acidification rate (ECAR) and oxygen consumption rate (OCR) values were taken using an Agilent Seahorse XFe24 Analyzer (Agilent Technologies). Mitochondrial respiration was assessed with OCR values taken via the Seahorse XF Cell Mito Stress Test. On the other hand, ECAR values taken via the Seahorse XF Glycolysis Stress Test were used for the glycolysis assessment of the samples. The obtained results were normalized to the cell count of each sample. There were at least three replicates for each condition.

Table 2-3: Compound preparation of glycolysis and mitochondrial stress test.

Assay	Port	Compound	Final Well Concentration	Port Volume	Port Concentration
Glycolysis Stress Test	A	Glucose	10 mM	75 µL	80 mM
	B	Oligomycin	1 µM	75 µL	9 µM
	C	2-DG	50 mM	75 µL	500 mM
Mitochondrial Stress Test	A	Oligomycin	1.5 µM	56 µL	15 µM
	B	FCCP	1 µM	62 µL	10 µM
	C	Rot/AA	0.5 µM	69 µL	5 µM

2.13 Statistical Analysis

The data that came from n=3 triplicates were presented as mean ± S.D. Statistical analyses were carried out with GraphPad Prism 8 Software. The statistical significance between groups was estimated by Student's t-test with Welch's correction, and p-values less than 0.05 were considered statistically significant. Prism's recommended classification for significance was followed. $p < 0.0001$ = extremely significant (****), $0.0001 < p < 0.001$ = extremely significant (***), $0.001 < p < 0.01$ = very significant (**), and $0.01 < p < 0.05$ = significant (*)

Chapter 3: **RESULTS**

3.1 Interpenetrating Network Formation of Decellularized Bovine Lung Matrix with Alginate or Alginate Sulfate

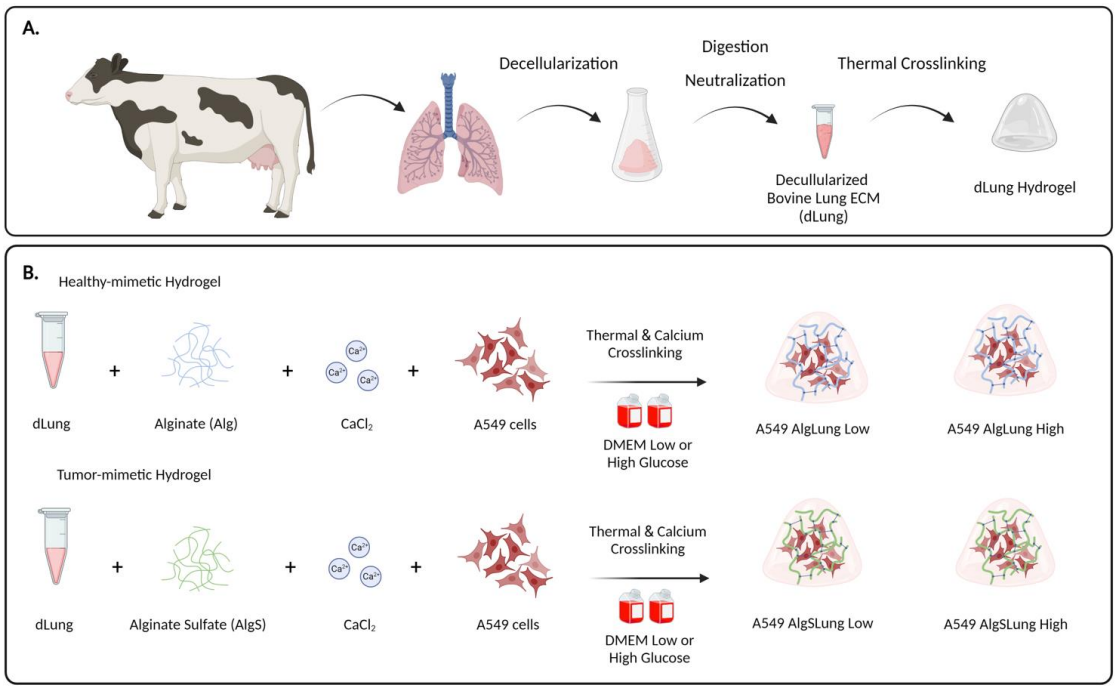

Figure 3-1: Schematic illustration of (A) the production of decellularized bovine lung extracellular matrix (dLung) hydrogels and (B) the encapsulation process of A549 cells in healthy and tumor-mimetic hydrogels (Created with BioRender.com).

In a prior study, we demonstrated that decellularized bovine lung extracellular matrix (dLung) is an optimal tool for modeling the native-like properties of healthy lung tissue with respect to organ-related cues (Kuşoğlu et al., 2022). In addition, numerous studies indicate that alginate (Alg) can serve as a bio-scaffold for three-dimensional *in vitro* models (Charbonier et al., 2021a; K. Y. Lee & Mooney, 2012). As indicated earlier, the inert and modifiable nature of Alg allows us to create a three-dimensional environment with the desired stiffness and modification without changing the biopolymer composition of hydrogels. Besides, several studies indicate that sulfated alginate (AlgS) acts as a sulfated glycosaminoglycan (sGAG)-mimetic (Nikitovic et al., 2008; Öztürk et al., 2016).

As shown in Figure 3-1A, bovine lung tissue was initially decellularized to eliminate cellular material and obtain an extracellular matrix. Following decellularization, the remaining bovine lung extracellular matrix (dLung) was digested

with the pepsin enzyme and brought to a neutral pH. The digestion procedure was required to solubilize lyophilized dLung. Consequently, dLung supplied the essential extracellular matrix required to mimic native lung composition in hydrogels. To investigate the extracellular microenvironment in lung cancer growth and metabolism, three-dimensional environments were generated by fabricating double-network hydrogels using dLung and Alg or AlgS. To mimic a healthy lung environment, Alg and dLung were utilized to produce hydrogels. These hydrogels were described as AlgLung. Besides that, AlgS and dLung were utilized to mimic the aberrantly sulfated tumor environment, and these hydrogels were named AlgSLung. Figure 3-1B depicts the encapsulation process of A549 cells in various environments.

To eliminate the effects of stiffness on tumor growth and metabolism, hydrogels with the same stiffness were produced. The stiffness of the hydrogels was calibrated by manipulating Ca^{2+} concentration during encapsulation. Oscillatory rheology was employed to evaluate the mechanical characteristics of the hydrogels. As presented in Figure 3-2, the storage modulus of hydrogel samples was greater than the loss modulus, indicating the gelation capabilities of the hydrogels. Furthermore, the storage modulus, which is directly proportional to Young's modulus, a measure of stiffness, did not differ significantly between the AlgLung and AlgSLung models. Despite having different compositions, their stiffness values were adjusted to the same value without altering the composition or concentration of their matrix.

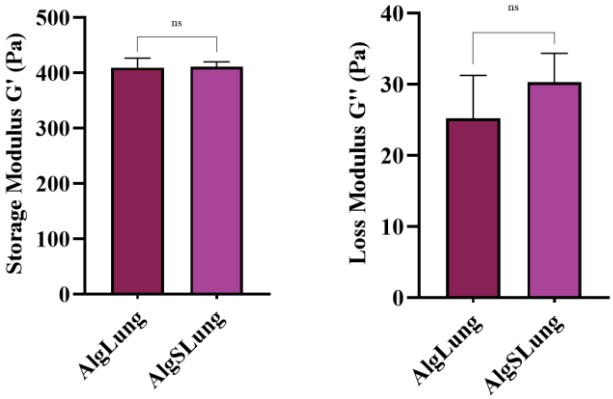

Figure 3-2: Mechanical assessment of AlgLung and AlgSLung gels (a) storage modulus (G’) and (b) loss modulus (G’’).

3.2 Effect of Glucose Concentration on A549 Cell Proliferation and Cell Metabolism

After successfully establishing a hydrogel model suitable for our investigation, our initial focus was on comparing the growth and metabolism of A549 cells cultured in the traditional 2D system with those in our healthy-mimicking model. We were interested in determining whether there was indeed a distinction between these two systems. Additionally, we sought to observe the behavior of A549 cells in a more physiologically relevant model, one that incorporates a complex ECM composition and appropriate stiffness. Furthermore, we aimed to incorporate two different glucose levels into our study. The first level, 5 mM, represents a normal blood sugar concentration, while the second level, 25 mM, simulates an elevated glucose level. The purpose was to investigate the impact of varying glucose concentrations on the growth and metabolism of A549 cells within our hydrogel models.

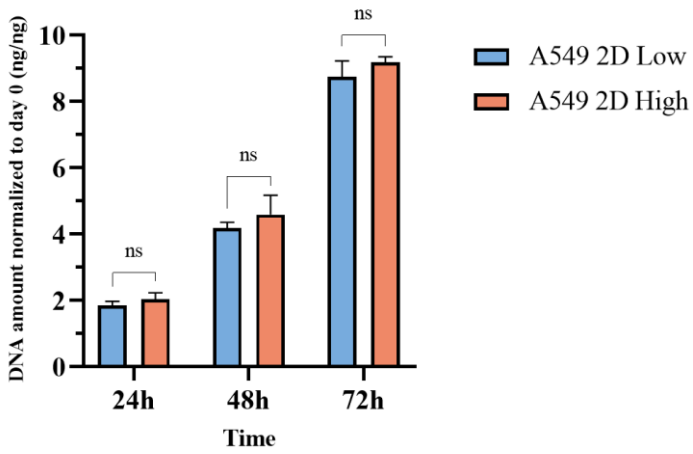

Figure 3-3: DNA quantification of A549 cells on 2D culture under low (5mM) or high (25mM) glucose conditions for 72h.

In several studies, we noticed that metabolism-based assays were utilized to assess cell proliferation. As our primary goal in this study was to explore alterations in A549 cell metabolism, we aimed to differentiate between proliferation and metabolic activity. We performed DNA quantification with Quant-iT picogreen assay to assess proliferation. Furthermore, we conducted assessment of metabolic activity with CellTiter Glo assay. Prior to encapsulating A549 cells in the healthy-mimetic hydrogel, we assessed the DNA content and ATP levels of A549 cells in a 2D environment while they were cultured under either low or high glucose levels for a duration of up to 72 hours. As exhibited in Figure

3-3, there was no significant difference between the samples in terms of cell proliferation. On the contrary, A549 cells treated with high glucose demonstrated significantly higher metabolic activity beginning on day 1 (Figure 3-4). This distinction became even more pronounced when A549 cells were exposed to high glucose for three days.

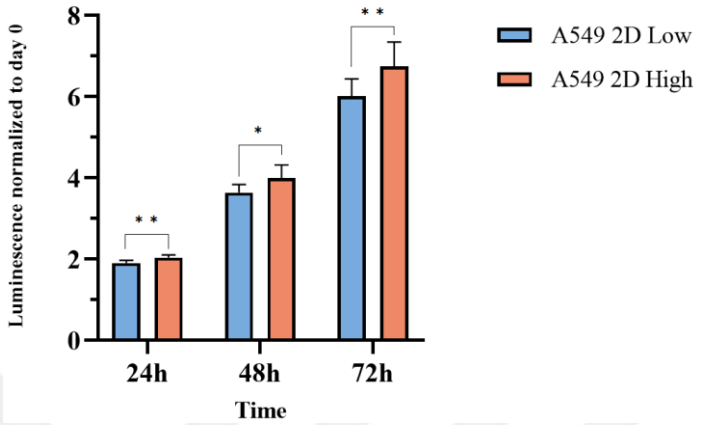

Figure 3-4: Metabolic activity of A549 cells on 2D culture under low (5mM) or high (25mM) glucose conditions for 72h.

3.3 Comparing Gene Expression Profiles of A549 Cancer Cells in 2D and Healthy-mimetic 3D Environments

After evaluating the effect of high glucose on cell proliferation via DNA quantification and overall cell metabolism via ATP quantification, we investigated how high glucose influences the gene expression level of EMT markers, stemness markers, and several metabolism markers in A549 cells cultured either on 2D or within a 3D healthy-mimicking environment.

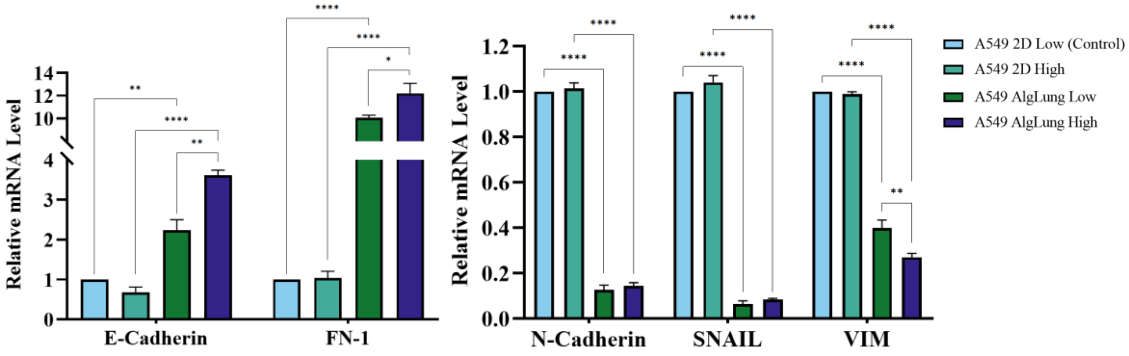

Figure 3-5: mRNA expression profiles of EMT markers in A549 cells on 2D or 3D culture under low (5mM) or high (25mM) glucose conditions.

As depicted in Figure 3-5, regardless of the glucose concentration, there were significant differences in the expression levels of all EMT markers between cells cultured in a 2D environment and those cultured in hydrogels that replicate healthy conditions (AlgLung). A549 cells that were grown in a healthy-mimic environment showed lower expression levels of N-Cadherin and Vimentin, which are mesenchymal markers, and SNAIL, which is an EMT regulator, than the cells that were grown in a 2D environment, regardless of whether they were treated with high or low glucose. Compared to the 2D control groups, the mRNA expression levels of the AlgLung groups were downregulated by more than 50%. On the other hand, E-Cadherin, a marker for epithelial cells, and FN-1, a marker for mesenchymal cells, were expressed more in AlgLung groups than in 2D cultured groups. The increase in FN-1 expression level in AlgLung was the same in both AlgLung Low and AlgLung High. Their expression level was approximately ten times higher than their counter groups which were 2D Low and 2D High. Finally, the increase in the expression level of E-Cadherin was higher in the AlgLung High versus 2D High groups when compared to the AlgLung Low versus 2D Low groups. Consequently, there was a significant difference regarding the expression levels of EMT markers in cells cultured in a healthy-mimetic environment as opposed to a conventional 2D environment.

When we examined the effect of glucose concentration on EMT marker expression level in A549 cells grown in a 2D environment, we found that glucose concentration had no effect. Regardless of whether the cells were grown in 2D Low or 2D High environments, their expression pattern was comparable. In AlgLung groups, however, we observed that the level of E-Cadherin expression was upregulated in the AlgLung High group in contrast to the AlgLung Low group. Similarly, there was a significant difference in the FN-1 expression level between the different glucose levels of the AlgLung groups, with the AlgLung High group exhibiting significantly higher FN-1 expression. In contrast to E-Cadherin and FN-1, the AlgLung High group had a substantially lower level of Vimentin expression. Finally, in AlgLung environments, there was no difference in the expression of N-Cadherin and SNAIL regardless of whether they were treated with high or low glucose levels.

When we compared the effect of healthy mimicking environments on the stemness behavior of A549 cells to typical 2D growth, we discovered that, apart from CD44, all other stemness markers were downregulated in healthy mimicking conditions, regardless

of their glucose concentration. Figure 3-6 depicts that the expression of CD44 decreased only in the AlgLung High condition and not in the AlgLung Low condition.

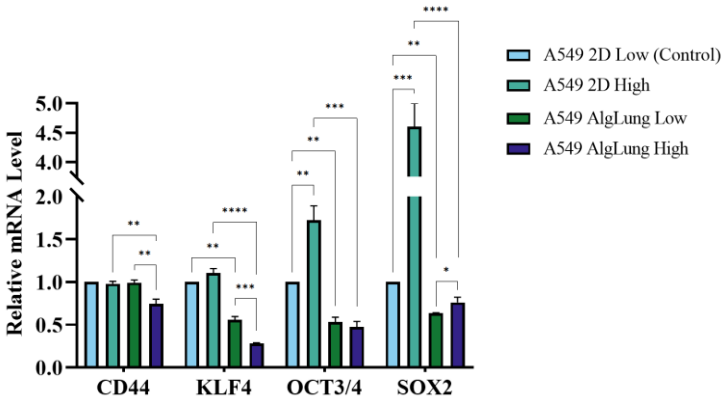

Figure 3-6: mRNA expression profiles of stemness markers in A549 cells on 2D or 3D culture under low (5mM) or high (25mM) glucose conditions.

The effect of glucose on the stemness markers of A549 cells varied depending on the marker. Changes in glucose concentration had no effect on the expression of CD44 and KLF4 in A549 cells grown in a 2D environment. In contrast, OCT3/4 and SOX2 were significantly upregulated when they were treated with elevated glucose under 2D conditions. For instance, the expression of SOX2 increased four times in a 2D high glucose environment compared to a 2D low glucose environment. Again, the effect of glucose on A549 cells grown under conditions mimicking healthy lungs differed by the marker. In a healthy-mimicking environment, CD44 and KLF4 markers were downregulated in response to a high glucose treatment. However, high glucose treatment caused an increase in SOX2 expression. OCT3/4 revealed no difference.

The effect of glucose and mimicking healthy lung microenvironment on the metabolic regulation of A549 cells was investigated by comparing their gene expression levels. Figure 3-7 displays the results of an examination of a number of distinct metabolic pathway markers. All markers differed significantly when A549 cells were grown in AlgLung hydrogels as opposed to 2D culture. ADCY5, FXYD2, and IGFBP5 mRNA expression levels were upregulated in both AlgLung Low and AlgLung High conditions. In contrast, the expression of IGFBP2, IGFL2, and SOCS3 markers decreased in both AlgLung Low and AlgLung High conditions. Despite the fact that the PCK1 marker was upregulated in the AlgLung Low condition compared to the 2D Low condition, it did not show any difference when the glucose concentration was increased.

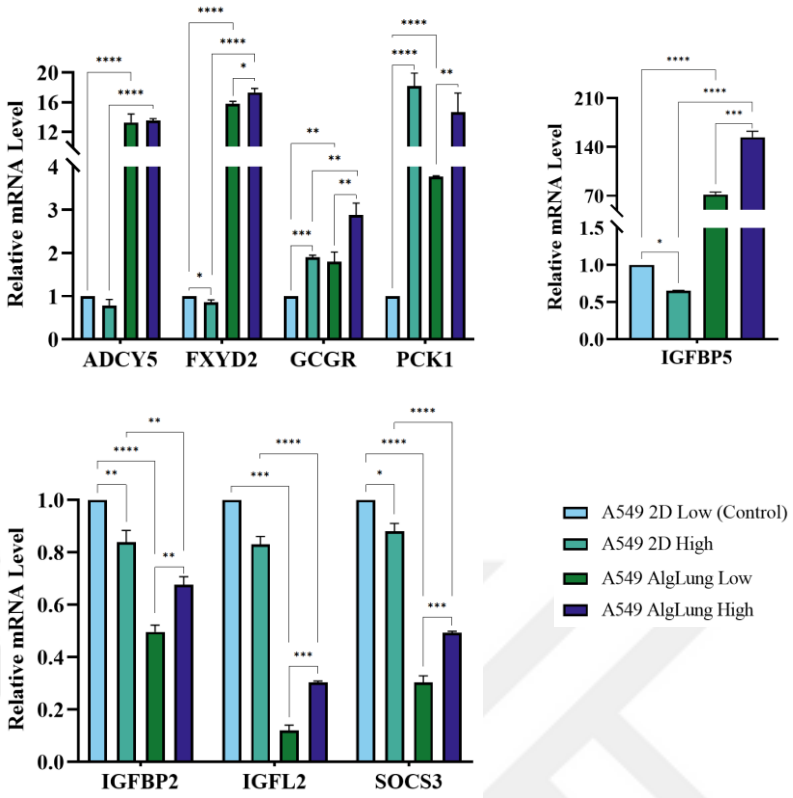

Figure 3-7: mRNA expression profiles of metabolic markers in A549 cells on 2D or 3D culture under low (5mM) or high (25mM) glucose conditions.

Except for the ADCY5 and IGFL2 markers, all other markers exhibited distinct expression patterns in 2D cultures treated with high glucose. FXYD2, IGFBP5, IGFBP2, and SOCS3 were downregulated in the 2D High condition, whereas GCGR and PCK1 were upregulated. The increase in PCK1 expression was approximately sixteen-fold greater than in the 2D Low condition. Other than the mRNA expression level of the ADCY5 marker, the expression of all other markers changed significantly when they were treated with high glucose in AlgLung. All of them were significantly upregulated in the AlgLung High condition compared to the AlgLung Low condition.

3.4 Growth of A549 Cells in Healthy and Tumor-mimetic Environments

After demonstrating that A549 cells behave differently in an environment that mimics a healthy lung as opposed to a conventional 2D environment, attention turned to investigating how these cancer cells behave in a tumor-mimicking environment and understanding the differences in their behavior compared to a healthy-mimicking environment. With the intention of achieving this goal, A549 cells were encapsulated in either AlgLung as a healthy lung-mimicking environment or AlgSLung as a tumor-mimicking, aberrantly sulfated environment. In addition to that, to investigate the effect of glucose levels on A549 cells in these two different environments, they were grown either in low glucose medium or high glucose medium. Following the three weeks of growth periods, the hydrogels were assessed for DNA content and metabolic activity.

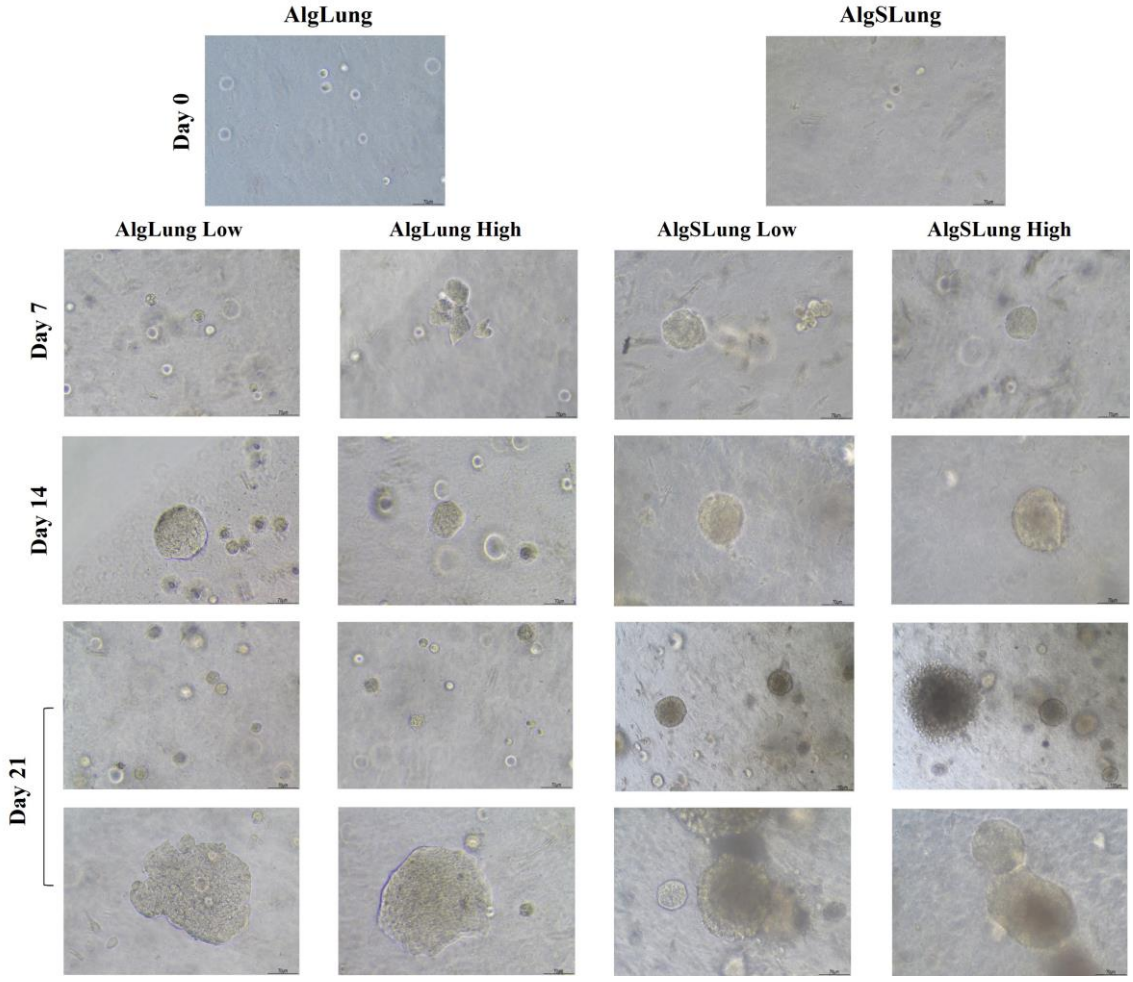

Figure 3-8: Bright-field images of A549 cells cultured in different hydrogels under low (5 mM) and high (25 mM) glucose conditions at various time intervals. (Scale bar: 70 μm)

As displayed in Figure 3-8, A549 cells exhibited distinct growth patterns when cultured in healthy-mimicking environments compared to tumor-mimicking ones. In the tumor-mimicking hydrogels, clump formation was observed starting from day 7, whereas in the healthy-mimicking hydrogels, it only began on day 14. Besides, a significant difference was noted in the number of clumps formed between AlgLung and AlgSLung gels. At the end of the three-week growth period, AlgLung hydrogels showed only a few clump formations, while AlgSLung hydrogels had a higher abundance of clumps. Regarding the impact of glucose concentration on clump formation, there were no visible differences between the low and high glucose conditions in both the AlgLung and AlgSLung gels. In addition to that, there was no visible difference in the overall morphological features of the clumps.

To further investigate the proliferation of A549 cells in AlgLung and AlgSLung hydrogels, DNA quantification was performed at the end of the three-week period. As revealed in Figure 3-9, the effect of sulfate on cell proliferation was notably significant, regardless of whether the glucose levels were low or high. Under high glucose conditions, cell growth was doubled in AlgSLung hydrogels compared to AlgLung, while under low glucose conditions the difference was approximately threefold. On the other hand, the effect of high glucose is only observed in AlgLung gels. There was a significant increase in cell proliferation upon increasing glucose concentration in AlgLung hydrogels. Conversely, there was no significant effect of changing glucose levels on cells when cultured in AlgSLung gels.

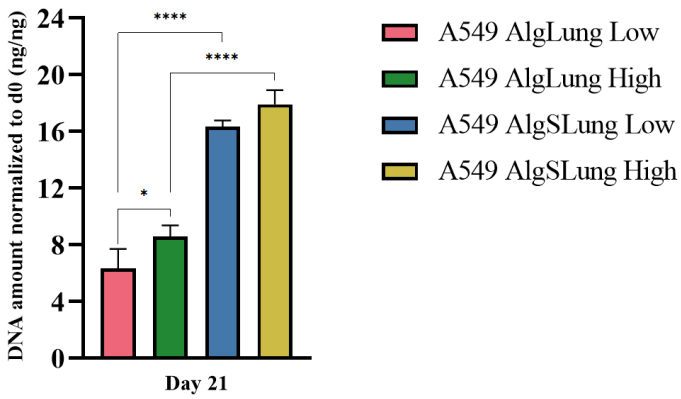

Figure 3-9: DNA quantification of A549 cells cultured in different hydrogels under low (5 mM) and high (25 mM) glucose conditions.

Finally, Cell-Titer Glo 3D assay was conducted at the end of the three-week culture period in order to quantify ATP levels. As displayed in Figure 3-10, notable differences in ATP levels were observed among the different 3D culture conditions. The effect of sulfation in the extracellular microenvironment on ATP levels was profound. When compared to healthy-mimetic, non-sulfated environments, ATP level was increased seven fold in AlgSLung hydrogels under low glucose conditions and nine fold under high glucose conditions. In contrast to cell growth pattern, this time, the effect of glucose increase on metabolic activity was distinct in cells grown in tumor-mimetic hydrogels rather than healthy-mimetic environments. There was a significant rise in the ATP levels of tumor cells in AlgSLung hydrogels under high glucose conditions compared to low glucose conditions.

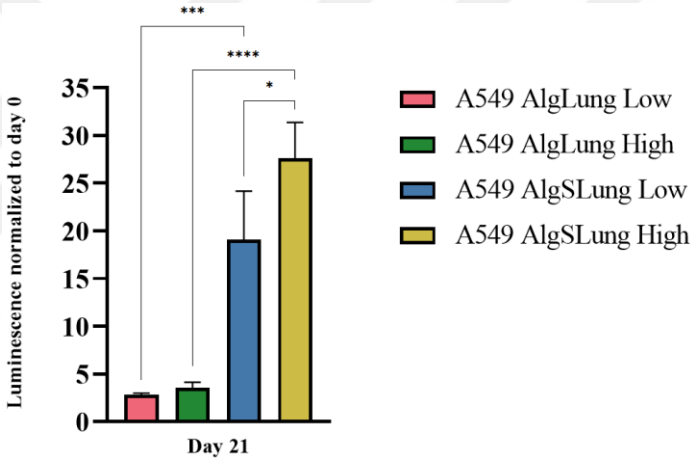

Figure 3-10: Metabolic activity of A549 cells cultured in different hydrogels under low (5 mM) and high (25 mM) glucose conditions.

3.5 Morphological Analysis of A549 Cells in Healthy and Tumor-mimetic Environments

To explore the impact of both healthy and tumorigenic environments on the growth and morphological characteristics of A549 cells, hydrogels were stained with Phalloidin to observe the actin cytoskeleton and DAPI to visualize the cell nuclei on day 21. As observed in Figure 3-11, the number of clumps formed in tumorigenic environments was higher than in the healthy-mimetic environments. Besides, the clump size was considerably higher in AlgSLung hydrogels under high glucose conditions.

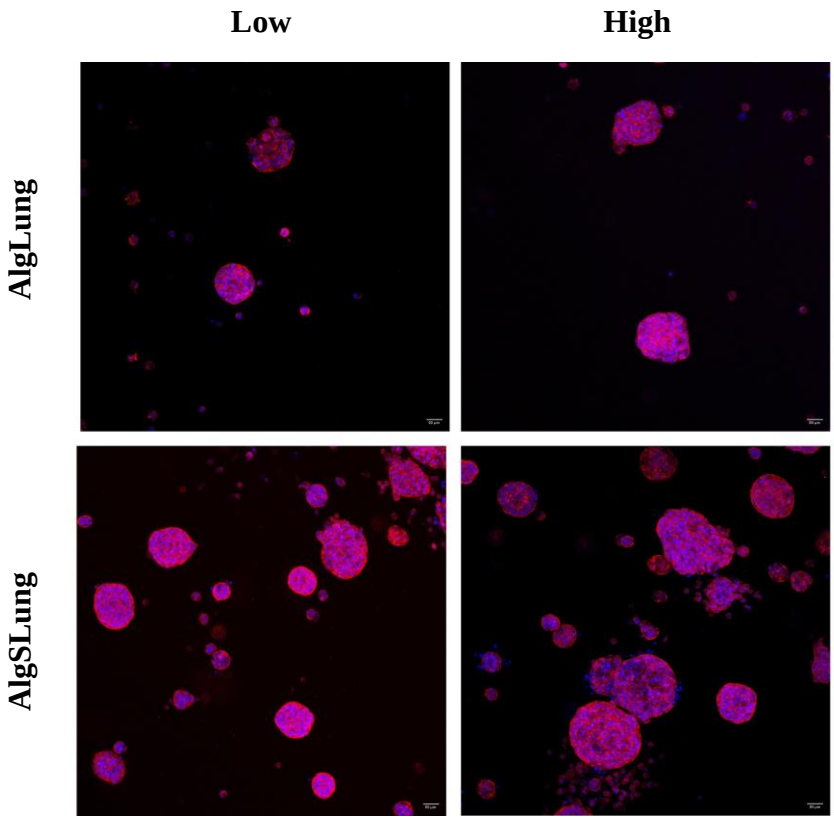

Figure 3-11: Immunofluorescence images of A549 cells cultured in different hydrogels under low (5 mM) and high (25 mM) glucose conditions. (Phalloidin: Red; DAPI: Blue; Scale bar: 50 μm)

To conduct a more in-depth investigation into the variations in clump size within these environments, clump analysis was performed. As shown in Figure 3-12, although tumorigenic gels exhibited a greater number of clump formation compared to healthy-mimetic gels, there was no significant difference in their average clump area. Conversely, the effect of high glucose on the clump area was significantly higher in AlgSLung gels.

There was no notable difference in the clump area in response to glucose increase in AlgLung hydrogels.

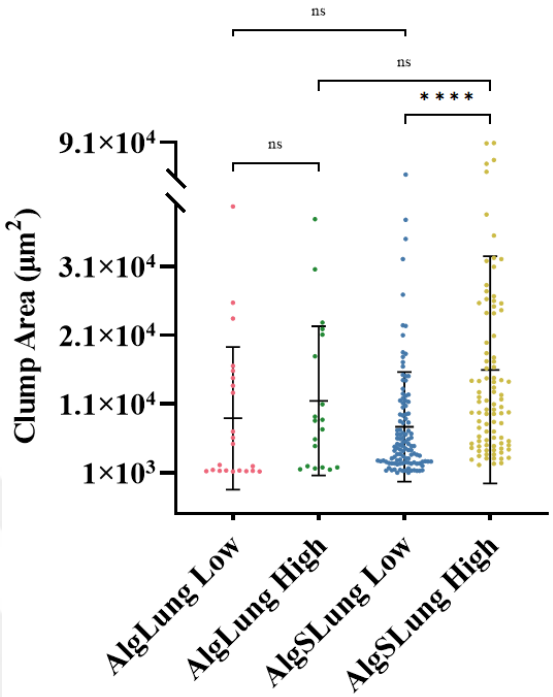

Figure 3-12: Clump area analysis of A549 cells cultured in different hydrogels under low (5 mM) and high (25 mM) glucose conditions.

3.6 Gene Expression Profiles of A549 Cells in Healthy and Tumor-mimetic Environments

Following our assessment of how A549 cells behave in healthy and tumor-mimetic environments with varying glucose levels, specifically focusing on cell growth and morphology, our next step was to investigate the impact of these conditions on the expression of several markers involved in cellular processes including EMT, stemness and metabolic regulation.

When examining the gene expression levels of different EMT markers, significant differences were observed between A549 cells grown in healthy and tumor-mimetic environments as displayed in Figure 3-13. In the AlgSLung hydrogels, the expression of E-Cadherin, N-Cadherin, and SNAIL increased regardless of glucose levels. However, the expression level of fibronectin (FN-1) remained unchanged in the tumor-mimetic environment independent of glucose levels. Additionally, vimentin (VIM) showed an upregulation in A549 cells encapsulated in AlgSLung hydrogels under high glucose

conditions, while it was downregulated in A549 cells grown in AlgSLung hydrogels under low glucose conditions.

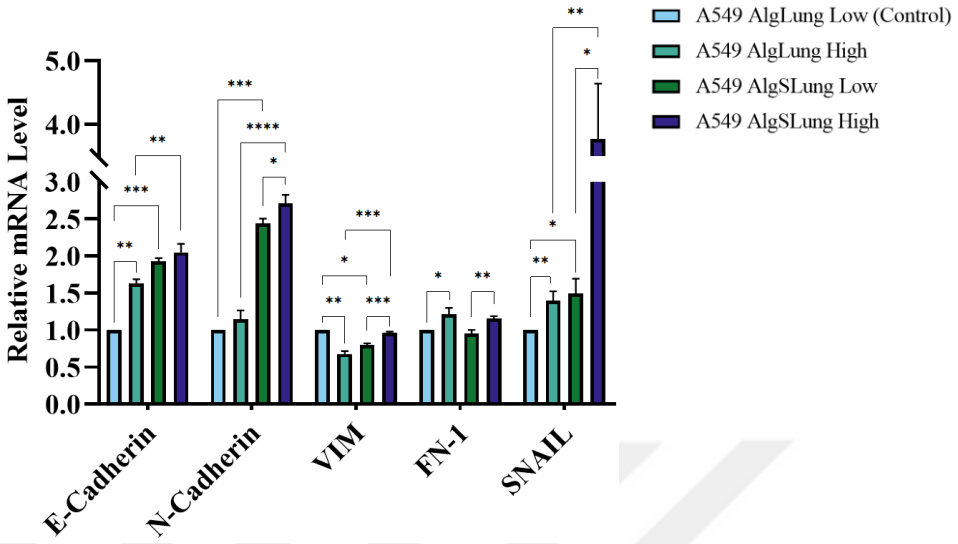

Figure 3-13: mRNA expression profiles of EMT markers in A549 cells cultured in different hydrogels under low (5 mM) and high (25 mM) glucose conditions.

The effect of glucose levels on EMT related marker expression exhibited a diverse pattern. For instance, the impact of high glucose on epithelial E-Cadherin was observed only in the healthy-mimetic environment, leading to a significant increase. Conversely, for the mesenchymal marker, N-Cadherin, a significant increase was observed in the tumor-mimetic environment in response to high glucose treatment. In the case of SNAIL and FN-1 markers, their expression was upregulated in both AlgLung and AlgSLung hydrogels following high glucose treatment. However, for VIM, there was an opposite effect observed in AlgLung and AlgSLung gels. Upon glucose treatment, VIM expression was downregulated in AlgLung gels but upregulated in AlgSLung gels.

The second set of markers examined was related to stemness (Figure 3-14). In tumor-mimetic environments, all stemness markers exhibited a significant increase in their expression levels across both low and high glucose levels. For instance, under low glucose conditions, the expression of OCT3/4 was upregulated more than 3 times in AlgSLung hydrogels compared to AlgLung, while under high glucose conditions, the increase was 4-fold. Notably, the expression of SOX2 showed an even more pronounced change, with a twelve-fold increase in tumor-mimetic environments under low glucose

and a nine-fold increase in high-glucose conditions compared to healthy-mimetic hydrogels.

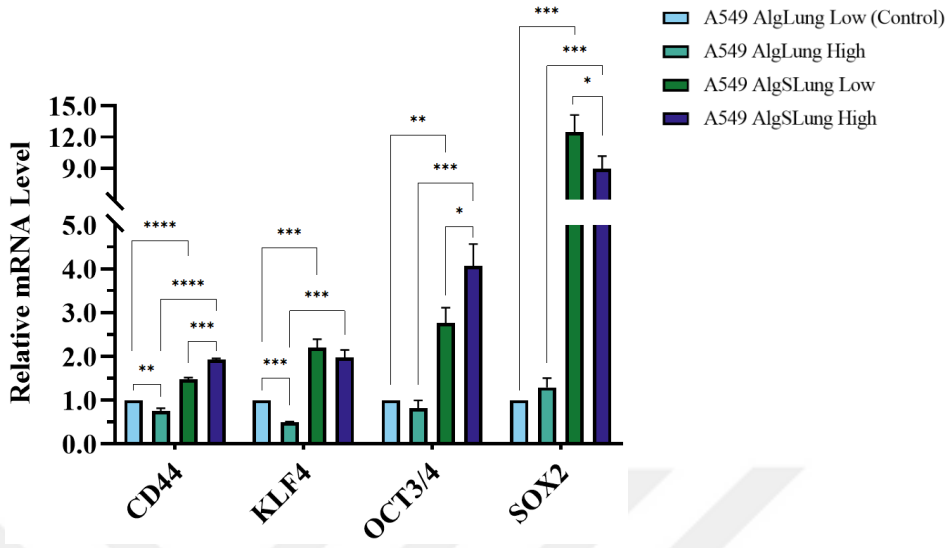

Figure 3-14: mRNA expression profiles of stemness markers in A549 cells cultured in different hydrogels under low (5 mM) and high (25 mM) glucose conditions.

When examining the effect of glucose on stemness marker expression in different 3D environments, we observed significant downregulation of CD44 and KLF4 markers in AlgLung gels in response to high glucose levels. Despite exposure to high glucose, the expression levels of OCT3/4 and SOX2 remained unchanged in these gels. In contrast, CD44 and OCT3/4 expression levels were significantly upregulated in AlgSLung hydrogels when cells were subjected to high glucose. In AlgSLung hydrogels, there was no significant difference in the expression of the KLF4 marker, whereas SOX2 was downregulated.

We also assessed the expression of different metabolic markers, as depicted in Figure 3-15. In tumor-mimetic environments, both at low and high glucose levels, ADCY5, ADH1C, FXYD2, HMGCS2, IGFL2, and SOCS3 markers were upregulated when compared to healthy-mimetic hydrogels. In AlgSLung hydrogels under high glucose conditions, for instance, the expression of the HMGCS2 increased dramatically, reaching up to fourteenfold higher levels. Conversely, IGFBP2 and PCK1 markers demonstrated downregulation in tumor-mimetic environments, regardless of glucose levels. IGFBP5 and GCGR expression levels only decreased in tumor-mimetic environments with high

glucose, while there was no difference between healthy and tumor-mimetic environments under low glucose conditions.

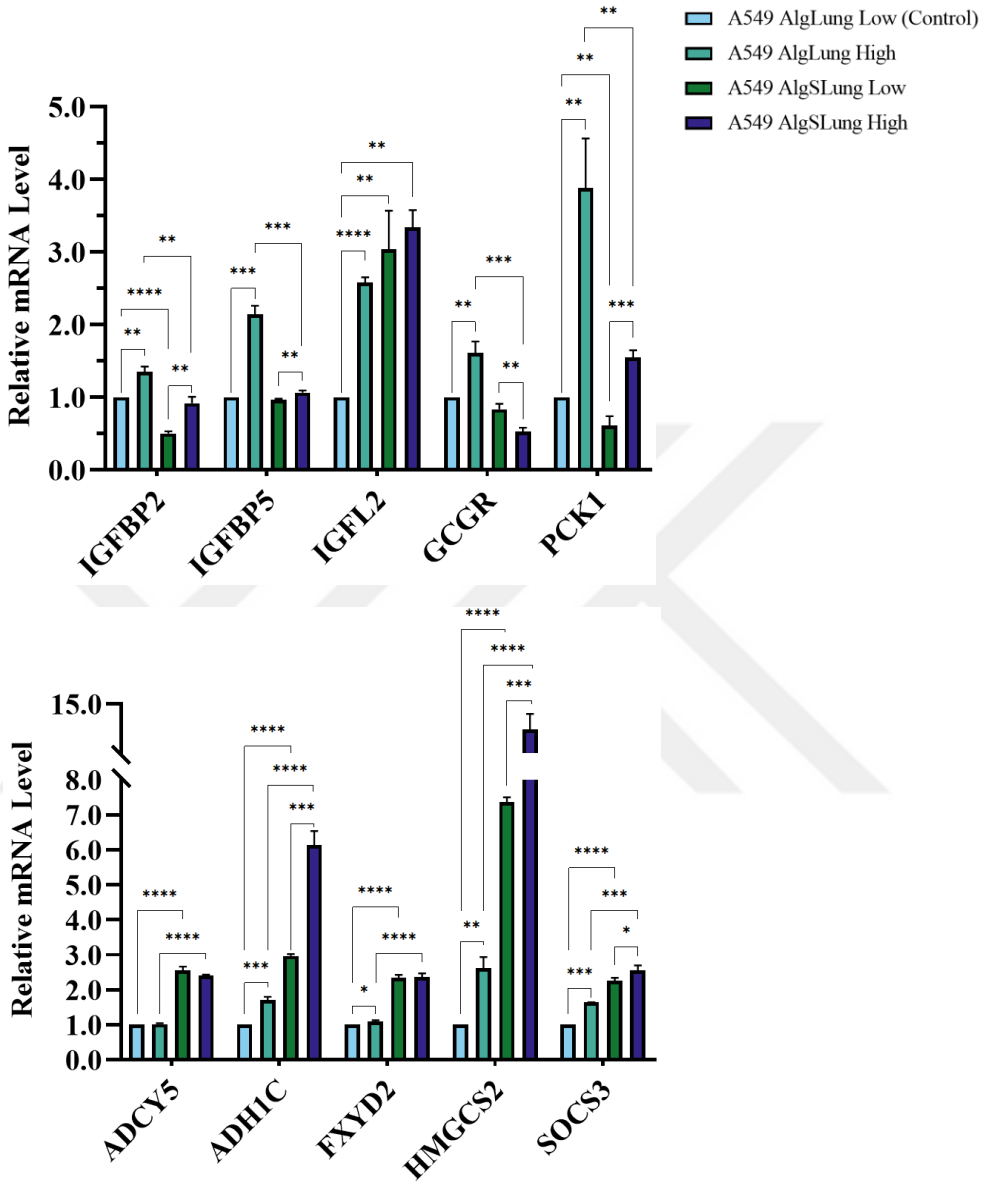

Figure 3-15: mRNA expression profiles of metabolic markers in A549 cells cultured in different hydrogels under low (5 mM) and high (25 mM) glucose conditions.

In conclusion, the investigation into the glucose effect on metabolic marker expression revealed distinct patterns in healthy and tumor-mimicking hydrogels. In AlgLung hydrogels, except for ADCY5, the expression of all metabolic markers increased upon glucose elevation. ADCY5, on the other hand, showed no difference in its expression level. In addition to that, the response to high glucose treatment was more

variable in AlgSLung gels. In tumor-mimetic hydrogels, there were no significant differences in the expression levels of ADCY5, FXYD2, and IGFL2 in response to high glucose levels. However, the expressions of IGFBP2, IGFBP5, PCK1, ADH1C, HMGCS2, and SOCS3 were upregulated. Only GCGR expression level was downregulated upon high glucose treatment of AlgSLung gels.

3.7 Bioenergetic Variability of A549 Cells across Diverse Environmental Conditions

Following the evaluation of changes in gene expression profiles of A549 cells encapsulated in both healthy and tumor-mimetic hydrogels, focusing on EMT, stemness, and metabolic markers, our primary objective was to examine the bioenergetic responses of cells upon alterations in their microenvironment. To achieve this, we utilized the Seahorse XF analyzer to measure the bioenergetic characteristics of A549 cells in real time. By monitoring the extracellular acidification rate (ECAR) and oxygen consumption rate (OCR) of the cells when subjected to certain inhibitors, we could calculate the distinct bioenergetic characteristics of cells under various conditions. For this purpose, A549 cells were cultured under different conditions. Firstly, they were cultivated in a standard 2D environment with either low or high glucose levels, enabling us to observe the impact of glucose levels on the cells' bioenergetic behavior. Secondly, A549 cells were grown with the addition of Alg at either low or high glucose levels. Finally, to simulate the increased sulfation in the tumor microenvironment, they were cultured with the addition of AlgS under either low or high glucose levels. To assess alterations in glycolysis, glycolytic capacity, and glycolytic reserve characteristics of the cells, we employed the Seahorse XF Glycolysis Stress Test. Additionally, the Seahorse XF Mitochondrial Stress Test was utilized to evaluate the basal respiration, ATP production, and maximal respiration of A549 cells in diverse environmental settings.

3.7.1 Metabolic Responses of A549 Cells: Exploring the Impact of Glucose Levels and Environmental Settings on Glycolysis, Glycolytic Capacity, and Glycolytic Reserve Characteristics

The effect of glucose on glycolysis varied depending on the microenvironmental composition as shown in Figure 3-16. On conventional 2D culture, a significant increase in glycolysis was observed in response to a higher glucose concentration. On the other

hand, when cells were presented with healthy-mimetic, inert (Alg) or tumor-mimetic, sulfated (AlgS) macromolecular cues, increase in glucose concentration led to a significant decrease in glycolysis indicated with ECAR values. The decrease was particularly pronounced for sulfated conditions when compared to healthy-mimetic conditions.

The effects of the environment at a given glucose concentration on glycolysis were diverse. Under conditions of low glucose, tumor cells treated with healthy-mimetic Alg displayed increased glycolysis than cells on conventional 2D environment. In contrast, under high glucose conditions, cells on 2D culture yielded significantly higher ECAR values compared to cells treated with Alg or AlgS. Under low glucose, glycolysis was unchanged whether cells were treated with healthy-mimetic or tumor-mimetic cues. However, under high glucose conditions, tumor-mimetic microenvironment led to a strong decrease in glycolysis compared to healthy-mimetic.

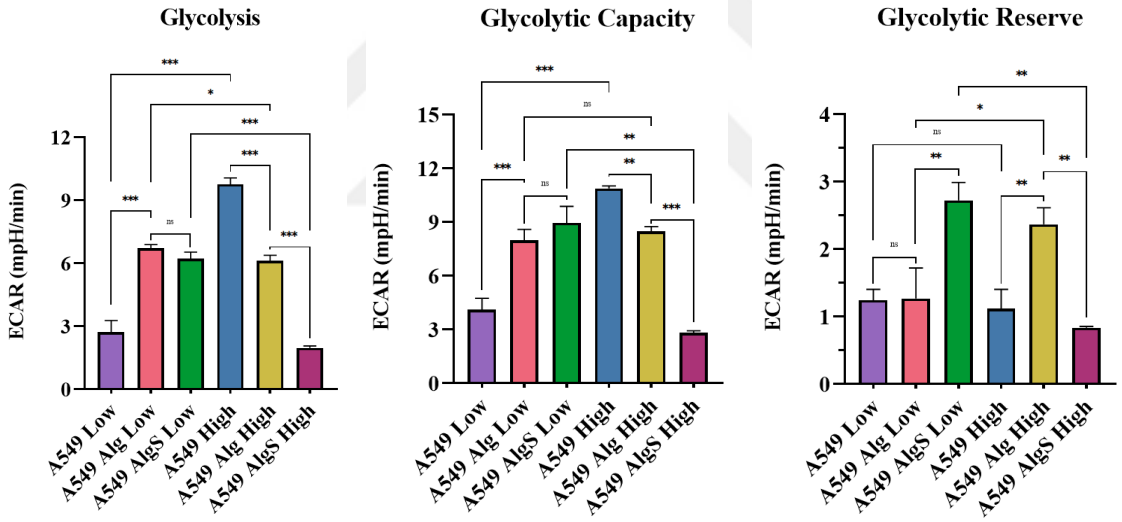

Figure 3-16: Real-time assessment of glycolysis, glycolytic capacity, and glycolytic reserve characteristics in A549 cells under various environmental conditions using Seahorse XF Glycolysis Stress Test.

The second characteristic evaluated from the glycolysis stress test was the cells' glycolytic capacity. Except for the cells in the healthy-mimicking environment, the effect of elevated glucose on the glycolytic capacity of A549 cells followed a similar pattern to that of glycolysis. In the conventional 2D environment, glycolytic capacity increased as glucose levels increased, whereas, in the tumor-mimicking environment, glycolytic capacity decreased. In contrast to glycolysis, in a healthy-mimicking environment, A549

cells exhibited no significant difference in their glycolytic capacity when exposed to high glucose.

The effect of environmental settings on glycolytic capacity was the same as glycolysis. In low glucose conditions, the cells in a healthy-mimetic environment exhibited greater glycolytic capacity than the ones in the standard 2D environment. Conversely, glycolytic capacity decreased in the presence of high glucose when A549 cells were grown in a healthy-mimicking environment rather than 2D environment. In addition to that, under low glucose conditions, the tumor-mimicking cues had no effect on the cells, and their glycolytic capacity was comparable to that of cells treated with healthy-mimetic cues. In contrast, A549 cells in the tumor-mimetic environment demonstrated less glycolytic capacity than those in the healthy-mimetic environment when exposed to elevated glucose levels.

Finally, the glycolytic reserve of A549 cells was determined based on the results of the glycolysis stress test. Figure 3-16 depicts how the effect of elevated glucose on the glycolytic reserve of A549 cells varied across environments. On 2D culture, no significant distinctions were observed. A549 cells cultured with healthy-mimetic cues increased in glycolytic reserve when exposed to elevated glucose levels, whereas A549 cells cultured with tumor-mimetic AlgS exhibited decrease in glycolytic reserve.

When investigating the effect of various environmental settings on glycolytic reserve, we discovered that, under low glucose conditions, there was no significant difference between the healthy-mimicking environment and 2D environment in terms of the cells' glycolytic reserve. However, this was not the case when glucose levels were elevated. In the presence of high glucose concentration, cells in the healthy-mimetic environment exhibited a greater glycolytic reserve than cells on 2D culture. Cells in the tumor-mimicking, sulfated environment had a higher glycolytic reserve than those in the healthy-mimicking environment when glucose levels were low. Interestingly, under high glucose levels, this result was reversed, and cells in the tumor-mimicking environment demonstrated a lower glycolytic capacity than cells in the healthy-mimicking environment.

3.7.2 Respiratory Profiles of A549 Cells: Investigating the Influence of Glucose Levels and Environmental Settings on Basal Respiration, ATP Production, and Maximal Respiration Characteristics

The impact of glucose concentration on basal respiration differed depending on environmental conditions as demonstrated in Figure 3-17. With elevated glucose levels in 2D culture, basal respiration was also increased. In healthy-mimicking environments, however, basal respiration decreased significantly in response to high glucose. In tumor-mimicking environments, there was no significant difference between low and high-glucose-level groups in terms of basal respiration.

A549 cells in a healthy-mimicking environment had higher basal respiration than those on 2D at low glucose level. In contrast, the basal respiration of cells in tumor-mimetic environments was significantly lower than that of cells in healthy-mimetic environments. This outcome was also observed in groups with elevated glucose levels. There was no significant difference in basal respiration between cells on 2D and cells treated with Alg under high glucose conditions.

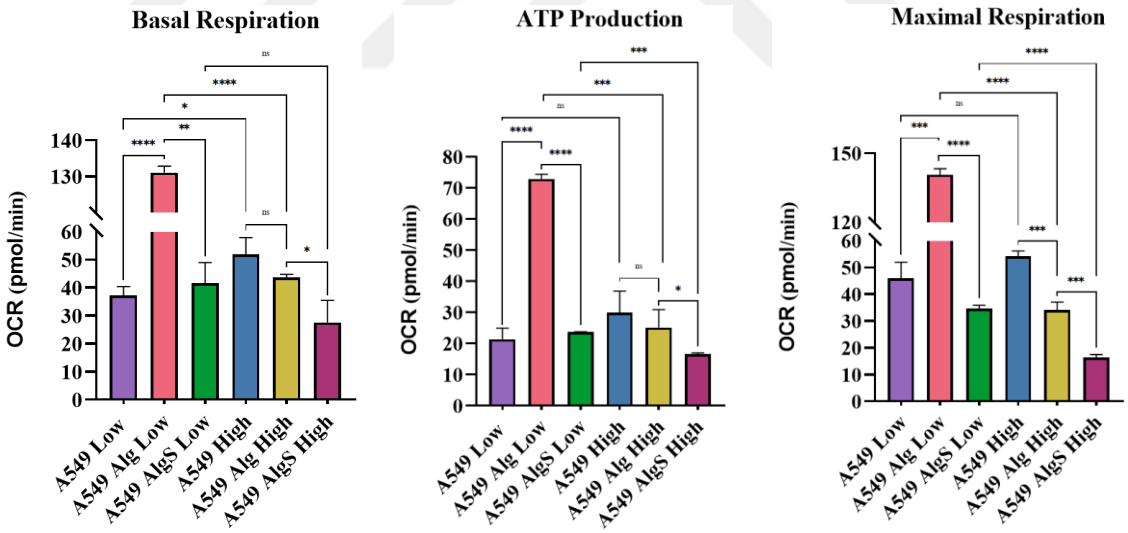

Figure 3-17: Real-time assessment of basal respiration, ATP production, and maximal respiration characteristics in A549 cells under various environmental conditions using Seahorse XF Cell Mito Stress Test.

ATP production in the mitochondria of cells was the second characteristic evaluated by the mitochondrial stress test. There was no significant difference in ATP production upon glucose increase in 2D conditions. However, in both Alg and AlgS environments,

the cells' ATP production decreased significantly when exposed to elevated glucose levels.

When we evaluated the influence of environmental cues on ATP production, we observed that ATP production was significantly increased under low glucose conditions with the addition of healthy-mimetic Alg cues when compared to cells on 2D. Under high glucose conditions, no such increase was observed between 2D and Alg groups. On the other hand, the ATP production of A549 cells treated with tumor-mimetic AlgS cues was significantly lower than the ones treated with Alg, regardless of glucose levels.

The maximal respiration of A549 cells in different settings was then compared. Similar to ATP production, the cells in Alg and AlgS environments showed a significant decrease in maximal respiration when treated with high glucose. Moreover, there was no difference in maximal respiration of cells cultured on 2D in response to increased glucose.

The effects of environmental conditions on maximal respiration under low glucose levels were consistent with those observed in ATP production. In the presence of healthy-mimetic cues, maximal respiration increased approximately three times compared to 2D under low glucose conditions. Conversely, cells in tumor-mimetic environment exhibited lower maximal respiration than those treated with healthy-mimetic cues under low glucose levels. Lastly, in the high glucose-treated groups, the cells in Alg environments displayed lower maximal respiration than those on 2D but higher maximal respiration than those in AlgS environment.

3.8 Growth of shPIK3CA A549 cells in Tumor-mimetic Environments

After studying the distinct behaviors of A549 cells in healthy and tumor-mimetic environments with varying glucose levels across various cellular processes, our next objective was to explore the role of PIK3CA. We aimed to investigate whether PIK3CA plays a key regulatory role in mediating the observed behavioral differences and how its knockdown influence A549 cells in the tumor-mimetic environment. To accomplish this, we utilized short-hairpin RNA interference (shRNA) technology to knock down the expression of PIK3CA in A549 cells, resulting in the creation of a new cell line called shPIK3CA A549. As depicted in Figure 3-16, the knockdown procedure resulted in a significant decrease in the mRNA expression level of PIK3CA in shPIK3CA A549 cells.

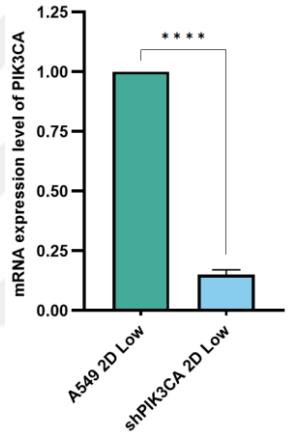

Figure 3-18: PIK3CA mRNA expression level of A549 and shPIK3CA A549 cells

Following the shPIK3CA A549 cell line generation, these cells were encapsulated in tumor-mimetic hydrogels and cultured under varying glucose levels. Following the three week culture period, the hydrogels were collected to quantify the DNA amount or ATP levels. As observed in Figure 3-19 and Figure 3-8, there was a significant difference in the timing of clump formation between shPIK3CA A549 cells and A549 cells. Clump formation in shPIK3CA A549 cells started on day 14, whereas A549 cells initiated clump formation on day 7. Moreover, in shPIK3CA A549 cells, there was no visible difference in clump number and size in AlgSLung hydrogels under low and high glucose conditions.

To further investigate the role of PIK3CA in regulation of cellular proliferation with varying glucose levels within tumor-mimetic microenvironments, DNA quantification was performed for shPIK3CA A549 cells grown in AlgSLung hydrogels. As demonstrated in Figure 3-20 while A549 cells did not exhibit significant changes in DNA

amount when subjected to high glucose, shPIK3CA A549 cells showed a significant increase in DNA amount thanks to high glucose treatment. The knockdown of PIK3CA alone did not affect the DNA amount in low glucose conditions. However, when combined with high glucose treatment, shPIK3CA A549 cells in AlgSLung hydrogels showed a significant increase in DNA amount.

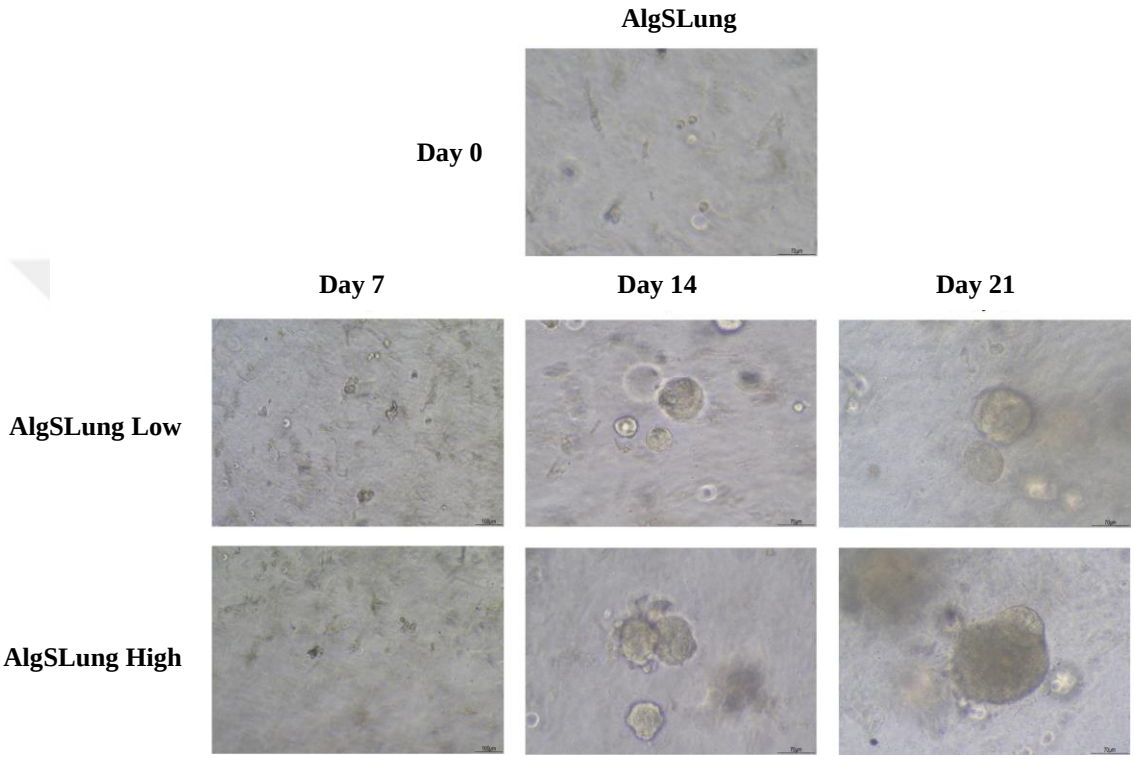

Figure 3-19: Bright-field images of shPIK3CA A549 cells cultured in AlgSLung hydrogels under low (5 mM) and high (25 mM) glucose conditions at various time intervals. (Scale bar (Day0, 14, and 21): 70 µm, Scale bar (Day 7): 100 µm)

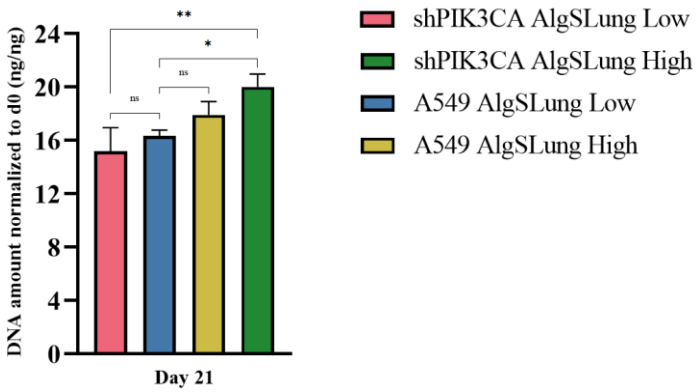

Figure 3-20: DNA quantification of A549 and shPIK3CA A549 cells cultured in AlgSLung hydrogels under low (5 mM) and high (25 mM) glucose conditions.

Finally, at the end of the three-week culture period, the Cell-Titer Glo 3D assay was performed to quantify the ATP levels. As displayed in Figure 3-21, similar to A549 cells, shPIK3CA A549 cells exhibited an increase in ATP levels when exposed to high glucose in tumor-mimetic environments. The ATP level in shPIK3CA cells in AlgSLung hydrogels under high glucose conditions was twice of those under low glucose. On the contrary, in low glucose environments, the knockdown of PIK3CA resulted in a notable reduction in ATP levels. While high glucose by itself did not completely restore the phenotype, it partially alleviated the decrease in ATP levels.

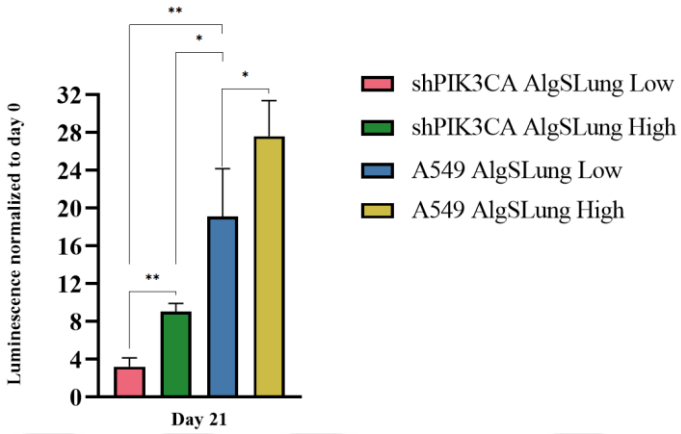

Figure 3-21: ATP level quantification of A549 and shPIK3CA A549 cells cultured in AlgSLung hydrogels under low (5 mM) and high (25 mM) glucose conditions.

3.9 Morphological Analysis of shPIK3CA A549 Cells in Tumor-mimetic Environments

To investigate the effects of PIK3CA knockdown on A549 cells and cell clusters, shPIK3CA A549 cells were embedded in tumor-mimicking hydrogels containing varying glucose levels. After 21 days, the hydrogels were treated with Phalloidin to examine the actin cytoskeleton and DAPI to visualize the cell nuclei. As observed in Figure 3-22, there was no visible difference in the number of clumps formed or clump size between the two glucose levels. This observation was further confirmed by the clump analysis in Figure 3-23. Unlike naïve A549 cells, where the clump area increased in response to high glucose levels in a tumorigenic environment, the shPIK3CA A549 cells did not exhibit any variation in their clump area when exposed to high glucose levels. Furthermore, the downregulation of PIK3CA did not have a noticeable impact on the clump area when the cells were cultured in a tumor-mimetic low glucose environment. However, when the

shPIK3CA A549 cells were grown in tumor-mimetic hydrogels with high glucose levels, they exhibited a larger clump area compared to A549 cells cultured in the tumor-mimetic low glucose environment. Consequently, the combined effect of PIK3CA knockdown and high glucose treatment resulted in a synergistic increase in the clump area, even though neither factor alone had a significant effect on its own.

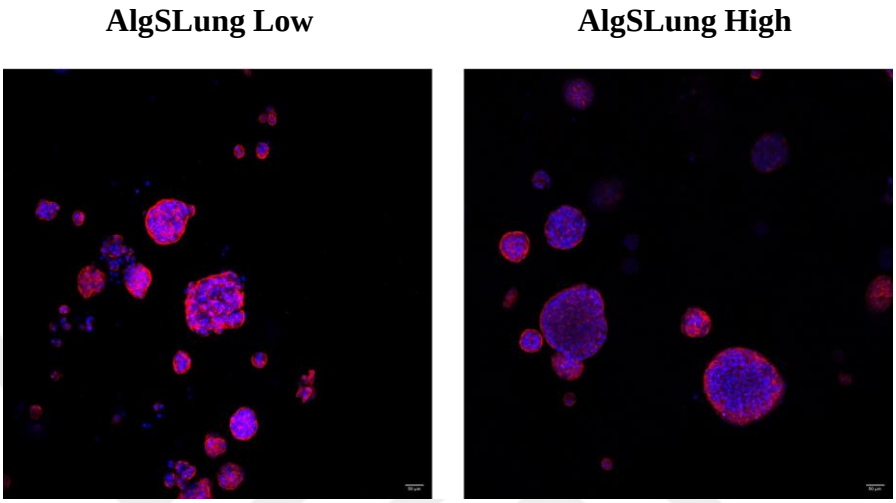

Figure 3-22: Immunofluorescence images of shPIK3CA A549 cells cultured in AlgSLung hydrogels under low (5 mM) and high (25 mM) glucose conditions at day 21. (Phalloidin: Red; DAPI: Blue; Scale bar: 50 µm)

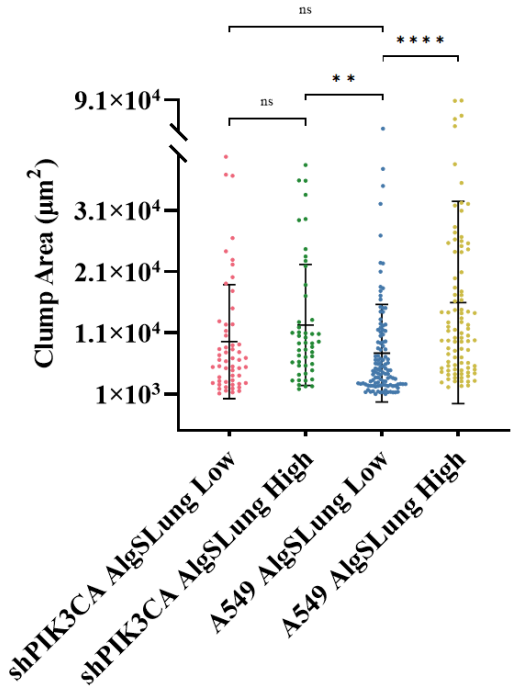

Figure 3-23: Clump area analysis of A549 and shPIK3CA A549 cells cultured in AlgSLung hydrogels under low (5 mM) and high (25 mM) glucose conditions at day 21.

3.10 Gene Expression Profiles of shPIK3CA A549 Cells in Tumor-mimetic Environments

After observing the distinct behavior of shPIK3CA A549 cells in tumor-mimetic environments with different glucose levels, with a particular focus on cell growth and morphology, the next phase of our study involved examining the effects of PIK3CA knockdown on gene expression. This investigation aimed to explore alterations in gene expression related to cellular processes including EMT, stemness, and metabolism.

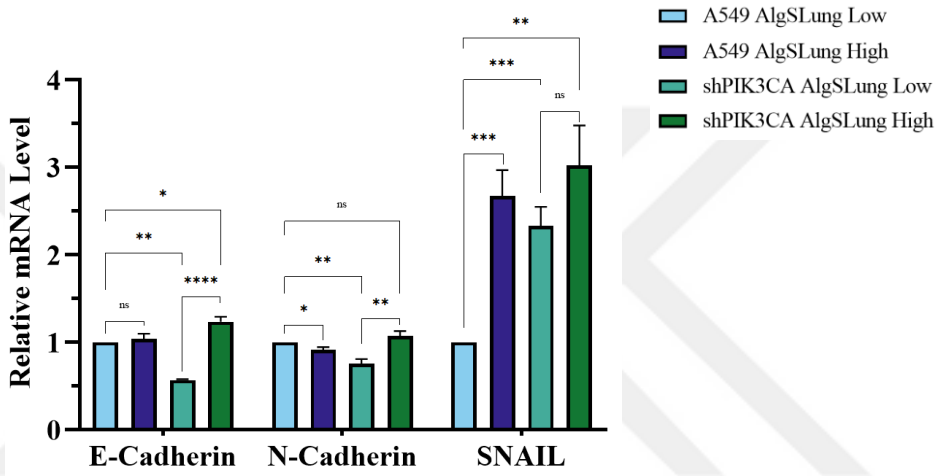

Figure 3-24: mRNA expression profiles of EMT markers in A549 and shPIK3CA A549 cells cultured in AlgSLung hydrogels under low (5 mM) and high (25 mM) glucose conditions.

As depicted in Figure 3-24, the impact of high glucose on naïve A549 cells differed from its effect on their knockdown counterparts. In A549 cells, the expression of E-Cadherin remained unaffected by elevated glucose levels. However, in shPIK3CA A549 cells, there was an increase in E-Cadherin expression when exposed to high glucose. Conversely, N-Cadherin showed a downregulation in A549 cells but an upregulation in shPIK3CA A549 cells when glucose levels were increased. Additionally, the expression of SNAIL differed between the two cell lines in response to an increase in glucose concentration. In A549 cells, SNAIL expression was upregulated, while in shPIK3CA A549 cells, it did not exhibit significant changes when exposed to higher glucose levels.

The effect of PIK3CA knockdown also showed varying results. Under low glucose conditions, except SNAIL, E-Cadherin and N-Cadherin expression were downregulated in response to PIK3CA knockdown. SNAIL expression, however, was upregulated in

shPIK3CA A549 cells. Interestingly, when shPIK3CA A549 cells were treated with high glucose, E-Cadherin expression was upregulated, and N-Cadherin expression was restored compared to A549 cells in tumor-mimetic low glucose environment.

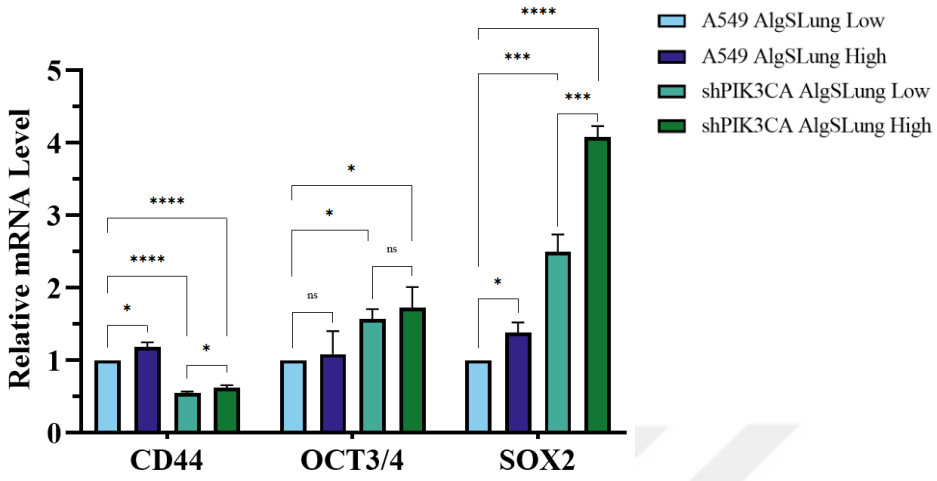

Figure 3-25: mRNA expression profiles of stemness markers in A549 and shPIK3CA A549 cells cultured in AlgSLung hydrogels under low (5 mM) and high (25 mM) glucose conditions.

The second set of markers examined in the study were related to stemness (Figure 3-25). Both CD44 and OCT3/4 exhibited similar changes in A549 and shPIK3CA A549 cells when they were subjected to high glucose treatment. While the expression of the CD44 marker increased in both cell lines, the OCT3/4 expression did not show significant changes in either cell line when exposed to elevated glucose levels. Furthermore, the analysis of SOX2 expression revealed that it was upregulated in both cell lines. Notably, the increase in SOX2 expression was more pronounced in shPIK3CA A549 cells compared to A549 cells. Interestingly, while PIK3CA knockdown increased the expression of OCT3/4 and SOX2, the expression of CD44 decreased in shPIK3CA A549 cells in tumor-mimetic hydrogels under low glucose conditions.

Finally, we investigated the function of PIK3CA in various metabolic pathways (Figure 3-26). The PIK3CA knockdown decreased the expression of several markers including SOCS3, HMGCS2, ADCY5, and FXYD2 in A549 cells. The downregulated PIK3CA also resulted in upregulation of two markers that were IGFBP5 and PCK1. PIK3CA downregulation did not change GCGR expression in A549 cells; however, when it was combined with high glucose levels, it resulted in upregulation of GCGR in A549 cells.

All markers responded similarly to high glucose treatment in A549 and shPIK3CA A549 cells, with the exception of ADCY5 and GCGR. SOCS3, HMGCS2, PCK1, and IGFBP5 were upregulated in both cell lines. In addition, FXYD2 expression did not significantly change in either cell line. Upon increased glucose levels, ADCY5 expression was downregulated in A549 cells but not in shPIK3CA A549 cells. In addition, the expression of GCGR reversed itself in two cell lines. GCGR was downregulated in high glucose treated A549 cells but upregulated in A549 knockdown cells.

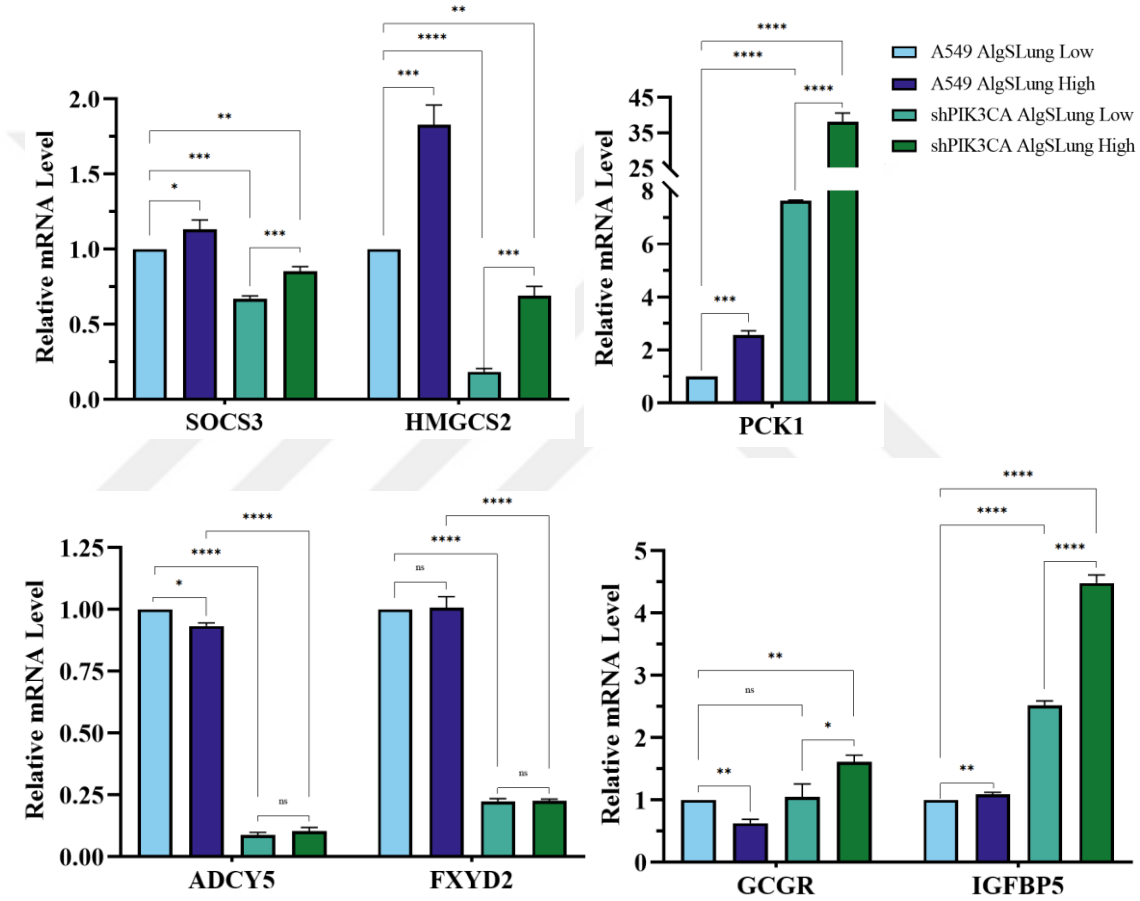

Figure 3-26: mRNA expression profiles of metabolic markers in A549 and shPIK3CA A549 cells cultured in AlgSLung hydrogels under low (5 mM) and high (25 mM) glucose conditions.

3.11 Bioenergetic Variability of shPIK3CA A549 Cells in Tumor-mimetic Environments

Following the evaluation of changes in gene expression profiles of A549 cells upon PIK3CA knockdown, focusing on EMT, stemness, and metabolic markers, our final objective was to examine how the bioenergetic properties of A549 cells differ in response to PIK3CA knockdown. We again performed two Seahorse tests which were glycolysis and mitochondrial stress test to analyze different bioenergetic characteristics of shPIK3CA A549 cells.

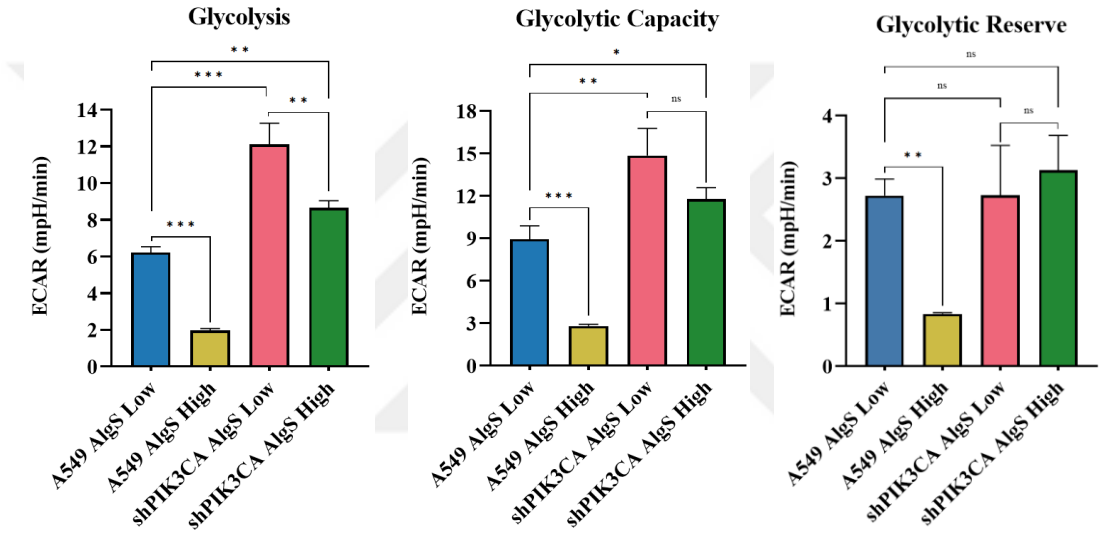

Figure 3-27: Real-time assessment of glycolysis, glycolytic capacity, and glycolytic reserve characteristics in A549 and shPIK3CA A549 cells under various environmental conditions using Seahorse XF Glycolysis Stress Test.

As shown in Figure 3-27, when PIK3CA was downregulated, glycolysis and glycolytic capacity of A549 cells increased. Glycolytic reserve, however, was unaffected by PIK3CA knockdown. The effect of elevated glucose on the two cell lines was also interesting. Both cell lines exhibited a significant decrease in glycolysis in response to high glucose. Conversely, glycolytic capacity and reserve did not change significantly in shPIK3CA A549 cells, but they decreased when A549 cells were exposed to high glucose.

In addition to assessing the glycolytic characteristics of shPIK3CA-A549 cells, we also wanted to investigate how mitochondrial-related bioenergetic characteristics of A549

cells changed upon PIK3CA knockdown. As displayed in Figure 3-28, when PIK3CA expression was downregulated in A549 cells, basal respiration, ATP production, and maximal respiration all increased as a response. Finally, we compared the high glucose response of A549 and shPIK3CA A549 cells. ATP production and maximal respiration decreased in both cell lines, but this decrease was more pronounced in A549 cells. Basal respiration, on the other hand, did not change significantly in A549 cells but decreased in shPIK3CA A549 cells in response to high glucose levels.

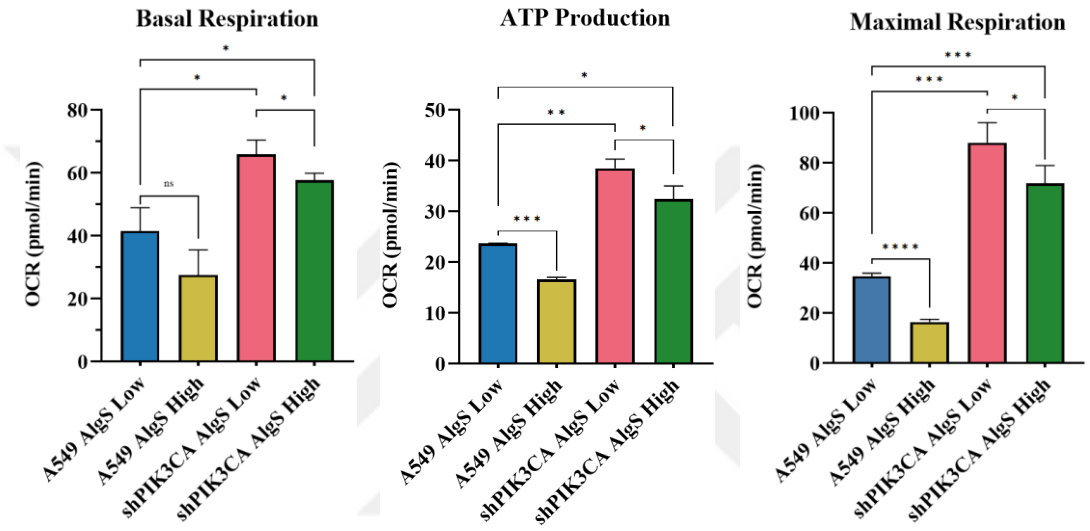

Figure 3-28: Real-time assessment of basal respiration, ATP production, and maximal respiration characteristics in A549 and shPIK3CA A549 cells under various environmental conditions using Seahorse XF Cell Mito Stress Test.

Chapter 4: **DISCUSSION**

Lung cancer is the second most frequent type of cancer and has the greatest mortality rate of all cancer types with 1.8 million fatalities annually (Sun et al., 2007). Therefore, it is crucial to develop a reliable preclinical models to investigate the intricacy of this cancer and cellular processes involved in its progression including aberrant metabolism.

Following the landmark paper by Douglas Hanahan and Robert A. Weinberg, which established the deregulation of metabolism in cancer cells, numerous studies have captured significant interest and revealed that various types of cancer exhibit distinct metabolic deregulation in their cellular mechanisms (Pavlova & Thompson, 2016; Pupo et al., 2019; L. Yu et al., 2017). The primary goal of deregulating metabolic activity is to allow cancer cells to utilize these modifications to meet their specific requirements and enhance their survival. This is crucial mainly since altered cell metabolism provides three fundamental requirements for cancer cells: rapid ATP synthesis to maintain energy status within cells, increased macromolecule biosynthesis, and better maintenance of an appropriate cellular redox status (Deberardinis & Chandel, 2016).

4.1 Overcoming Limitations of 2D Cultures: Advancing Towards 3D Models in Lung Cancer

Traditionally, cancer research has heavily relied on two-dimensional cultures (Alemany-Ribes & Semino, 2014). It is widely recognized that such cultures impose non-physiological constraints on cell growth since cells adhere to rigid and flat substrates, which results in the polarization of the cells and increases their surface area for nutrient exchange (Yamada & Cukierman, 2007). Thereby, this setup leads to excessive nutrition and oxygenation, making it impossible to replicate natural molecular gradients. The second disadvantage of 2D cultures is that natural ECM composition and configuration cannot be replicated because rigid surfaces lead to differences in the orientation and clustering of surface receptors (Ng & Brugge, 2009; Samuel et al., 2011). Consequently, cells do not receive proper signals as they would from the natural ECM configuration. This can be especially problematic in cancer research since cancer cells have heavily altered ECM and adaptations in their TME, which are the structural frameworks that support cancer cells in various cellular processes like angiogenesis, deregulated metabolism, and resistance to drug treatments (Loessner et al., 2010). For example,

metastatic cells, which are poorly adherent cell types, cannot form tight focal adhesions, and it is challenging to culture these cells by using conventional 2D cultures; as a result, this leads to limited outcomes in drug screening studies (Fontoura et al., 2020; Szot et al., 2011). In addition to this, 2D cultures can favor and trigger certain modifications in cancer cells that misrepresent the complex nature of the whole tumor (Kapałczyńska et al., 2018). In conclusion, to overcome experimental limitations and inconsistencies in 2D cultures, there is a need to develop models that mimic the actual TME complexity while maintaining reproducibility.

One of the techniques that can be applied to generate 3D cultures is hydrogel formation (Caliari & Burdick, 2016; Merivaara et al., 2022). In our pursuit of developing a more intricate and accurate lung cancer model, we sought to incorporate decellularized bovine lung hydrogels to provide lung tumor cells with a native tissue-like microenvironment, with distinct ECM composition and complexity. To achieve this, we conducted a thorough investigation of various decellularization processes in a prior study to ensure successful removal of cellular components while preserving ECM complexity and ability to generate hydrogels (Kuşoğlu et al., 2022). The freeze-thaw method emerged as the most effective approach, ensuring hydrogel generation without compromising ECM composition. While the incorporation of dLung provided us with essential ECM composition and structure, it was insufficient to replicate the exact mechanical properties of real lung tissue. To address this, we introduced alginate as a secondary material due to its inertness to cells and modifiable mechanical properties thanks to its nature (Figure 3-1). By adjusting the concentration of divalent ions, we were able to modulate the stiffness of the hydrogels to suit our lung cancer study. Furthermore, alginate offered versatility through easy modification with various chemical groups. Multiple studies have demonstrated that sulfated alginate mimics sGAGs (Arlov et al., 2021; Öztürk et al., 2016). We modified alginate with sulfate groups to generate a hydrogel model that mimics the increased sGAGs content in TME of cancer cells. Through rheological measurements, we effectively demonstrated that both of our hydrogel models, namely AlgLung (representing a healthy-mimetic) and AlgSLung (representing a tumor-mimetic), exhibited the same stiffness range as actual lung tissue (Figure 3-2). This crucial finding ensured that any observed differences were solely attributed to the effects of sulfation and not due to variations in stiffness between the two hydrogel models. By

eliminating the confounding factor of stiffness, we were able to focus on the specific impact of sulfation on the tumor microenvironment mimicry.

4.2 Comparing A549 Cell Behavior in 2D and 3D Healthy-Mimetic Models: Effects of Glucose Levels on Cell Proliferation and Expression of EMT, Stemness, and Metabolic Markers

After successfully establishing a hydrogel model suitable for our investigation, our initial focus was on comparing the growth and metabolism of A549 cells cultured in the traditional 2D system with those in our healthy-mimicking model with varying glucose levels. As expected, the metabolism-based assay, CellTiter Glo, yielded different results compared to the cell proliferation assay. When subjecting A549 cells to high glucose, there was no notable difference in their proliferation (Figure 3-3); however, their metabolic activity showed a significant increase starting from day 1 (Figure 3-4). This difference became even more pronounced after three days of exposure to high glucose. Previous metabolism studies employed cellular metabolism assays as an indicator of cell proliferation (Ding et al., 2018; Meng et al., 2019). Nevertheless, our findings suggest that in the presence of a complex microenvironment, this relationship does not hold true. Thereby, we included both assays in our following studies to gain insights into both cell proliferation and general cell metabolic activity.

4.2.1 Variations in EMT, Stemness, and Metabolic Markers in A549 Cells: A Comparison Between Typical 2D System and AlgLung Hydrogel with Varying Glucose Concentrations

After obtaining a preliminary understanding of how A549 cells respond to elevated glucose levels in 2D environments in terms of proliferation and metabolic activity, we shifted our focus to investigate the differences between the 2D system and our healthy-mimetic model in relation to EMT, stemness, and metabolic markers. As predicted, significant differences were observed in the expression of EMT, stemness, and metabolic markers between A549 cells cultured in a typical 2D environment and those in our healthy-mimicking model regardless of glucose levels.

A549 cells cultured in the AlgLung environment displayed decreased expression levels of mesenchymal markers (Figure 3-5), and these expression levels were notably lower compared to cells grown on 2D. Conversely, the AlgLung groups exhibited higher

expression levels of E-Cadherin, an epithelial cell marker when compared to the 2D cultured groups. This indicates that the epithelial-mesenchymal transition of A549 cells is strongly associated with the complex nature of the environment in which the cells grow. In addition to that, we found that glucose concentration has no effect on the expression levels of EMT markers in the 2D environment. However, in the AlgLung groups, we noted significant differences in EMT marker expression levels based on glucose concentration. E-Cadherin and FN-1 were significantly upregulated in the cells cultured in AlgLung hydrogels with high glucose, and the expression of Vimentin was downregulated. Our research findings, in contrast to studies conducted on 2D, showed a distinct EMT behavior of A549 cells in response to different glucose levels (Alisson-Silva et al., 2013; X. Liu et al., 2020). Instead of increasing their mesenchymal marker expression and decreasing epithelial marker expression, A549 cells exhibited the opposite pattern in a more accurate and realistic environment, consistent with other studies conducted in a 3D model (Melissaridou et al., 2019). These results suggest that the presence of a healthy-mimetic environment influences the expression of EMT markers in A549 cells, and this influence is dependent on glucose levels. This underscores the importance of using a 3D model to gain a comprehensive understanding of cell behavior and their responses to glucose variations.

We aimed to study how A549 cell stemness responds to environmental changes, considering the influence of the ECM on cancer cell behavior (Nallanthighal et al., 2019). We observed notable differences in the stemness profile of A549 cells between the two systems, in line with previous research utilizing a 3D model (Melissaridou et al., 2019). Just as we noticed with EMT markers, the expression of stemness markers showed considerable variation between cells cultured on 2D and those in healthy-mimetic hydrogels, irrespective of glucose levels (Figure 3-6). Specifically, we found that, apart from CD44, all other stemness markers were downregulated in the healthy-mimicking conditions, regardless of glucose concentration. Besides, the response of the cells to increased glucose levels showed notable differences between the two culture systems. In 2D case, changes in glucose concentration had no impact on the expression of CD44 and KLF4; however, in 3D healthy-mimetic environment, their expression was downregulated. On the other hand, SOX2 showed upregulation when exposed to elevated glucose levels in both systems, which is consistent with findings from other studies (Agareva et al., 2022). These results collectively demonstrate that the influence of glucose

concentration on stemness markers in A549 cells is specific to each marker and may vary between the 2D and healthy-mimicking 3D environments. This indicates, as we hypothesized, that microenvironment also plays a crucial role in regulating the stemness of A549 cells.

We then investigated the influence of glucose and the AlgLung microenvironment on different metabolic markers. Similarly to EMT and stemness markers, metabolic regulators showed significant variation between 2D and AlgLung settings, regardless of glucose levels (Figure 3-7). IGFL2, IGFBP2, and IGFBP5 are regulators of IGF signaling, which is associated with proliferation and metastases of many cancer types including lung cancer (Hua et al., 2020; Velcheti & Govindan, 2006). In addition to regulating the IGF signal pathway, they have diverse roles in energy metabolism such as lipid metabolism and insulin-sensitivity. The expression level of these regulators quite differed in the presence of lung ECM when compared to conventional 2D culture. The distinct expression pattern of these metabolic markers in the presence of lung ECM can be correlated with the EMT behavior of A549 cells in the AlgLung environment. For instance, IGFBP2, known for promoting survival and migration in cancer cells (Al Qahtani et al., 2017; H. Wang et al., 2008), was found to be downregulated in A549 cells cultured in AlgLung, which also exhibited decreased expression of mesenchymal markers. These findings suggest a potential connection between the regulated metabolic pathways and the EMT-related changes observed in A549 cells when subjected to the AlgLung microenvironment.

The IGF signaling pathway was not the only one showing differences between 2D and 3D healthy lung-mimicking model. We also observed variations in the expression of ADCY5, which is involved in G protein-coupled receptor signaling; GCGR, a glucagon receptor; and PCK1, a key regulator of gluconeogenesis, in A549 cells cultured in the AlgLung environment. These markers are known for their roles in glucose and energy metabolism, but their involvement in lung cancer cell metabolism associated with the ECM has not been extensively studied. Therefore, our findings suggest a strong correlation between the presence of ECM and regulation of multiple metabolic pathways in A549 cells, and this highlights the significance of the microenvironment in influencing cancer cell metabolism. As we observed in EMT and stemness markers, the presence of lung ECM also altered the cells' response to high glucose levels regarding their metabolic profiles. Overall, our findings emphasize the significant impact of the AlgLung

microenvironment on the regulation of multiple metabolic pathways including energy metabolism in A549 cells. This further highlights the importance of the microenvironment in shaping the cellular metabolic response and underscores the complexity of the interactions between glucose levels and various metabolic processes in the AlgLung model.

As mentioned earlier, conventional 2D culture often fail to accurately represent cancer cells' epithelial-mesenchymal status and stemness (Fontoura et al., 2020; Melissaridou et al., 2019; Szot et al., 2011). Our study further confirmed the importance of the cellular microenvironment in shaping the EMT, stemness, and metabolic profiles of A549 cells. Moreover, we observed that the response of A549 cells to changes in glucose levels significantly differed between 2D and 3D healthy lung-mimicking model, indicating the crucial role of the ECM in modulating cellular responses to glucose levels. Therefore, our findings underscore the necessity of employing more accurate and representative cell culture models in cancer research studies. By using such models, we can better understand the intricate interactions between cancer cells and their microenvironment and gain insights that can be translated into more effective therapeutic strategies.

4.3 Exploring A549 Cell Behavior in 3D Tumor-Mimetic Hydrogel Models with Varying Glucose Levels

Numerous studies have highlighted the significant impact of the tumor microenvironment (TME) on cancer cells, with ECM stiffness and composition playing crucial roles in influencing cancer cell behavior, including metabolism (Burgstaller et al., 2017; Nazemi & Rainero, 2020). ECM stiffness, in particular, has been found to induce metabolic reprogramming in cancer cells, leading to more aggressive behaviors (Ge et al., 2021a). This phenomenon is evident as an increase in ECM stiffness promotes higher glycolysis and reduced oxidative phosphorylation in cancer cells (Acerbi et al., 2015; Jiang et al., 2022). Such a metabolic shift allows cancer cells to meet their energy demands and rapidly proliferate even in low oxygen conditions.

Additionally, the composition and structure of the ECM have significant roles in modulating cancer cell behavior, particularly their metabolism. Specific alterations, such as changes in the levels of sulfated glycosaminoglycan (sGAG) side chains on heparan sulfate proteoglycans (HSPGs) within the ECM, have crucial implications for the

regulation of cancer cell metabolism (Afratis et al., 2012; J. P. Li & Kusche-Gullberg, 2016; Theocharis & Karamanos, 2019). These sGAG side chains act as supportive structures for growth factors and cytokines, regulating the accessibility of these factors to neighboring cells (Kirn-Safran et al., 2009; Malavaki et al., 2011). Moreover, HSPGs on the cell surface coordinate receptor dimerization, facilitating the binding of growth factors to their receptors, thereby activating downstream signaling pathways involving fibroblast growth factor (FGF), vascular endothelial growth factor (VEGF), WNT signaling, and integrin, among others (Ornitz & Itoh, 2015; Presta et al., 2005; Vallen et al., 2014).

This interplay between sGAGs and various signaling pathways, which are well-known for their involvement in tumor initiation and progression, underscores the profound impact of ECM alterations on cancer cell metabolism. Studies have shown an abnormal increase in sGAG content within the TME in various cancer types, including lung cancer, where the elevated expression of sGAGs and their degree of sulfation can lead to overstimulation of receptor tyrosine kinases (RTKs) (Reticker-Flynn & Bhatia, 2015; Vallen et al., 2014). RTK overstimulation has been linked to lung cancer progression (Lanzi & Cassinelli, 2020; Rosenzweig, 2012). In summary, the TME, specifically ECM stiffness, and composition like sGAG level, significantly influences cancer cell behavior and metabolism, offering potential paths for understanding and targeting cancer metabolism.

Hence, after demonstrating the differences in various cellular functions between A549 cells cultured on 2D and our engineered 3D model resembling healthy tissue, we shifted our attention to observe the behavior of A549 cells within our 3D tumor-mimetic model. Specifically, we aimed to understand the influence of sulfation, as an approach to mimic the aberrant sGAGs in TME, on A549 cell behavior. Additionally, we introduced two different glucose levels in our tumor-mimetic hydrogel model to explore the impact of glucose. During our investigation, we examined multiple aspects, including cell proliferation, morphology, expression of various markers associated with different pathways, and the alterations in bioenergetics. This comprehensive approach allowed us to gain valuable insights into how A549 cells respond and adapt in our 3D tumor model under the influence of sulfation and varying glucose levels.

4.3.1 Effects of Glucose Levels and Tumor-Microenvironment on A549 Cell Proliferation and Clump Formation

In our study, we made an interesting observation regarding the growth pattern of A549 cells in tumor-mimicking hydrogels compared to healthy-mimicking ones (Figure 3-8). We noticed that clump formation occurred earlier and was more pronounced in the tumor-mimetic hydrogels compared to healthy-mimetic gels. Surprisingly, glucose levels did not seem to have a visible impact on clump formation in either type of hydrogel. These intriguing findings motivated us to conduct a more in-depth analysis, including the quantification of DNA amount, ATP levels, and the clump area analysis.

Our study reveals that the tumor-mimicking environment has a notable influence on both ATP levels (Figure 3-10) and cell proliferation (Figure 3-9), showing a substantial increase. This observation suggests that the increased presence of sulfated glycosaminoglycans (sGAGs) in the tumor microenvironment (TME) plays a critical role in regulating cancer cell proliferation and metabolism. A possible explanation for this impact is that elevated sGAG levels can lead to alterations in growth factor binding and signaling, thereby promoting cancer cell proliferation (Afratis et al., 2012). The response to glucose levels also varied depending on the specific microenvironment, highlighting the intricate interactions between cellular energy metabolism and the ECM context. These findings indicate a complex and interconnected relationship between TME and cell metabolism, and proliferation.

Moreover, the results of the clump analysis showed that tumor-mimetic environments had a higher number of clump formations compared to healthy-mimetic environments, while no significant differences were observed in their average clump areas (Figure 3-12). Besides, the influence of high glucose on clump size differed between the two models. Clumps formed in the tumor-mimetic high glucose environment exhibited notably larger areas than those formed in the tumor-mimetic low glucose environment. On the other hand, no significant differences in the clump areas were found between the low and high glucose conditions in the healthy-mimetic models. These findings suggest that while there is a correlation between increased sGAG levels and clump formation in A549 cells, this correlation does not seem to hold true when it comes to clump morphology. On the other hand, we observed a relationship between elevated sGAG levels and A549 cells' response to glucose levels, indicating a potential interplay between the microenvironment and glucose regulation in shaping cancer cell behavior.

After examining the effects of glucose levels and increased sGAG levels in the TME on A549 cell proliferation and clump formation, we turned our focus to investigating the expression of EMT, stemness, and metabolic markers in these distinct 3D models.

4.3.2 Influence of Glucose and Tumor-Microenvironment on EMT

Several studies suggest that sGAGs play a crucial role in regulating growth factor signaling, including TGF-β, which is known to promote EMT, tumor cell motility, and metastasis (Hoshiba, 2018; Kiewe et al., 2006; Ricciardelli et al., 2007). Based on these findings, we aimed to investigate the EMT process to understand how it may induce an invasive phenotype in sulfated hydrogels.

In AlgSLung hydrogels, we observed a consistent upregulation of E-Cadherin, N-Cadherin, and SNAIL markers, regardless of glucose levels (Figure 3-13). Interestingly, vimentin showed upregulation in AlgSLung hydrogels under high glucose but downregulation under low glucose conditions. The simultaneous increase in both epithelial and mesenchymal markers suggests a dynamic transition between epithelial-mesenchymal states, a phenomenon commonly observed in metastatic tumor cells (Christiansen & Rajasekaran, 2006). This dynamic shift in marker expression may reflect the complex and adaptable nature of cancer cells in response to the specific microenvironment provided by AlgSLung hydrogels.

In addition to sGAGs levels, high glucose levels have also been associated with the stimulation of EMT through the TGF-β signaling pathway in lung cancer cells (X. Kang et al., 2015; L. Wang et al., 2016). Furthermore, the effect of glucose levels on EMT markers was found to be diverse. In the healthy-mimetic environment, high glucose led to a significant increase in the expression of the epithelial marker, E-Cadherin, and a decrease in the expression of the mesenchymal marker, vimentin. On the other hand, in the tumor-mimicking environment, high glucose resulted in a significant increase in the expression of mesenchymal markers, including N-Cadherin, vimentin, and fibronectin. Additionally, EMT regulator SNAIL was upregulated in both types of hydrogels under high glucose treatment which correlates with previous findings (Xu et al., 2019).

These findings demonstrate that the impact of glucose levels on EMT markers is strongly influenced by the specific microenvironment in which the cancer cells are cultured. In the healthy-mimetic environment, high glucose levels promote a more epithelial phenotype, while in the tumor-mimicking environment, they induce a more

mesenchymal phenotype. This suggests that the tumor microenvironment plays a critical role in dictating how cancer cells respond to glucose variations and undergo EMT. Moreover, our study highlights the significant role of glucose concentration in modulating EMT, and when combined with sGAGs in the microenvironment, it may contribute to the regulation of cancer cell behavior and metastatic potential. Understanding the intricate interplay between glucose levels, sGAGs, and EMT signaling pathways can provide valuable insights into the underlying mechanisms of cancer progression and may offer potential targets for therapeutic interventions.

4.3.3 Influence of Glucose and Tumor-Microenvironment on Stemness

Interestingly, recent studies have revealed that the activation of EMT process can lead to an increase in the stemness phenotype within the tumor; however, this intriguing phenomenon has not been thoroughly investigated in a physiologically relevant lung tumor model in the context of varying glucose levels (Lin et al., 2020; Mani et al., 2008; Morel et al., 2008). Indeed, in tumor-mimetic environments, all stemness markers showed significant increases in their expression levels, regardless of glucose levels (Figure 3-14). In addition to that, high glucose impaired the expression of stemness markers in A549 cells cultured in both healthy and tumor-mimetic hydrogels. However, the impact of high glucose on stemness marker expression differed between the two hydrogel models. In healthy-mimetic gels, high glucose decreased the expression of stemness markers, whereas in tumor-mimetic gels, it increased the expression of CD44 and OCT3/4 consistent with findings from other studies (Agareva et al., 2022).

4.3.4 Influence of Glucose and Tumor-Microenvironment on Metabolic Markers

Numerous studies have highlighted the significance of alterations in the tumor microenvironment, particularly changes in the levels of sulfated glycosaminoglycans (sGAGs), in regulating cancer cell metabolism (Afratis et al., 2012; J. P. Li & Kusche-Gullberg, 2016; Theocharis & Karamanos, 2019). The interaction between HSPGs and IGF-I facilitated through β1 integrin, plays a regulatory role in the adhesion and migration of certain cancer cells (De Pasquale & Pavone, 2020b). This association triggers the phosphorylation and activation of the ERK and PI3K/AKT signaling pathways (De Pasquale et al., 2018). Moreover, emerging research suggests that metabolic reprogramming can play a role in epithelial-mesenchymal transition and stemness

behavior in cancer cells (Georgakopoulos-Soares et al., 2020; H. Kang et al., 2019). Building upon the findings of how elevated sGAGs levels in the TME led to the upregulation of EMT and stemness markers, we aimed to investigate the impact of increased sGAGs and glucose levels on different metabolic pathways in A549 cells.

In A549 cells, markers that are related to energy metabolism including glucose and lipid metabolism showed diverse responses to increased sGAGs level in the TME. The expressions of regulators in the IGF signaling pathway exhibited diverse patterns. In the tumor-mimetic hydrogels, we observed an upregulation of IGFL2 and a downregulation of IGFBP2. Interestingly, the expression of IGFBP5 was downregulated but only in the presence of elevated sGAGs levels and high glucose. On the other hand, as expected, high glucose levels increased the expression of IGFBP2 and IGFBP5 in both healthy and tumor-mimetic environments (Al Qahtani et al., 2017; Dittmer, 2022; Waters et al., 2022). These findings suggest that the sGAGs and glucose levels can independently and synergistically influence the expression of different regulators in the IGF signaling pathway.

In addition to the changes in the IGF signaling pathway, we also observed alterations in lipid metabolism. Specifically, we found that HMGCS2, which plays a crucial role in ketogenesis, and ADH1C, responsible for metabolizing various substrates, including ethanol and lipid peroxidation products, were upregulated in response to increased sGAGs levels in the tumor-mimetic environment. This upregulation of key metabolic enzymes suggests that A549 cells may have an increased energy demand in the tumor-mimetic environment, likely due to their enhanced proliferation driven by elevated sGAGs levels. Surprisingly, when we further increased glucose levels in the tumor-mimetic environment, the expression of HMGCS2 and ADH1C was further upregulated. This unexpected observation suggests that glucose availability may further enhance the metabolic activity of A549 cells in the tumor-mimetic microenvironment. The interplay between sGAG levels and glucose availability appears to have a complex and synergistic effect on lipid metabolism in A549 cells.

The expression patterns of GCGR and PCK1, both of which play important roles in maintaining glucose homeostasis in cells, also showed intriguing results. In response to elevated sGAG levels in TME, the expression of GCGR was decreased in AlgSLung hydrogels under high glucose conditions. The observed difference in the impact of high glucose levels on GCGR expression between the healthy and tumor-mimetic hydrogels is

quite interesting. In the healthy-mimetic model, high glucose led to an increase in GCGR expression, suggesting that glucose may play a stimulatory role in regulating the glucagon receptor in this specific microenvironment. On the other hand, in the tumor-mimetic model, high glucose resulted in a decrease in GCGR expression, indicating that the presence of elevated sGAG levels may modulate the response of the glucagon receptor to high glucose conditions. This suggests that the presence of elevated sGAGs in the TME may influence the regulatory mechanisms governing GCGR expression in response to glucose levels. The interaction between sGAGs and glucose signaling pathways might be influencing the expression of the glucagon receptor in a context-dependent manner.

Interestingly, PCK1, a crucial regulator of gluconeogenesis, displayed downregulation in response to elevated sGAG levels in both low and high glucose conditions. This indicates that sGAGs have a consistent suppressive effect on PCK1 expression regardless of glucose levels. On the contrary, the impact of increased glucose levels on PCK1 expression was similar in both healthy and tumor-mimetic hydrogels, leading to an increase in its expression in both microenvironments. The observed downregulation of PCK1 in the presence of elevated sGAG levels suggests that sGAGs may play a role in modulating gluconeogenesis in A549 cells. This is intriguing, as gluconeogenesis is a critical process in glucose homeostasis and cellular energy metabolism. The consistent effect of sGAGs on PCK1 expression under low and high glucose conditions suggests that the TME provided by the AlgSLung hydrogel model exerts a robust influence on this metabolic pathway. In contrast, the response of PCK1 to increased glucose levels in both healthy and tumor-mimetic hydrogels indicates that glucose itself can directly regulate the expression of this key gluconeogenic enzyme. This further emphasizes the interplay between glucose levels and the TME in shaping A549 cell metabolism.

4.3.5 Influence of Glucose and Tumor-Microenvironment on Bioenergetic Characteristics of A549 Cells

In the final stage of our investigation, we aimed to understand how A549 cells regulate their cellular metabolism in response to elevated sGAG levels with varying glucose levels. To achieve this, we utilized the Seahorse analyzer, a specialized instrument that measures the extracellular acidification rate (ECAR) and oxygen consumption rate (OCR) of the cells. The Seahorse analyzer employs specific calculations

optimized by the manufacturer to determine various bioenergetic characteristics of the cells. From the ECAR measurements, we calculated the glycolysis rate as well as the glycolytic capacity, which indicates the maximum glycolytic activity of the cells. Additionally, we assessed the glycolytic reserve, which reflects how close the glycolytic function is to its theoretical maximum in the cell. Furthermore, the OCR values allowed us to calculate basal respiration, which represents the energy demand of the cell under normal conditions. Additionally, we measured ATP production, which reflects the contribution of mitochondrial ATP to the cell's energy needs. Finally, we analyzed maximal respiration, which represents the maximum respiration rate that a cell is capable of achieving.

In the low glucose condition, we observed that increased sGAG levels in the TME had no significant effect on A549 cell glycolysis and glycolytic capacity (Figure 3-16). However, there was a noteworthy increase in the glycolytic reserve of A549 cells in response to elevated sGAG levels. Conversely, the results in high glucose conditions revealed a different picture. In this scenario, all three glycolytic parameters exhibited significant decreases in response to elevated sGAG levels. These findings indicate that the impact of sGAG levels on A549 cell glycolytic metabolism is influenced by the glucose concentration in the microenvironment. While high glucose conditions seem to suppress glycolytic activity in the presence of elevated sGAG levels, low glucose conditions show a more pronounced increase in glycolytic reserve. This suggests that sGAGs and glucose interact in a complex manner to regulate glycolysis in A549 cells.

In addition to that, the response of A549 cells to varying glucose levels was different between healthy and tumor-mimetic environments. In the presence of elevated sGAG levels, all three glycolytic parameters decreased in response to high glucose conditions. On the other hand, in healthy-mimetic environments, A549 cells' response to high glucose conditions was quite different. While their theoretical maximum level of glycolysis increased, their actual glycolysis level decreased. This suggests that in the healthy-mimetic environment, A549 cells possess the capability to enhance glycolysis theoretically, but their actual glycolytic activity is diminished when faced with elevated glucose levels and sGAGs.

While our study did not reveal a significant effect of increased sGAG levels on glycolysis in low glucose conditions, we observed notable impacts on mitochondrial metabolic parameters (Figure 3-17). Specifically, elevated sGAG levels had a significant

effect on basal respiration, ATP production, and maximal respiration, both in low and high glucose conditions. In contrast to our expectations, all mitochondrial-related metabolic parameters decreased in response to elevated sGAG levels. In addition to that, elevated glucose levels also decreased ATP production and maximal respiration in both healthy and tumor-mimetic hydrogels. These findings indicate that the interplay between sGAG levels in TME and glucose concentrations plays a crucial role in regulating mitochondrial metabolism in A549 cells. Overall, our study unraveled the complex and interconnected nature of A549 cell metabolism influenced by sGAG levels and glucose availability in the microenvironment. Besides, the distinct responses of A549 cells to varying glucose levels in healthy and tumor-mimetic environments provide valuable insight into the metabolic plasticity and potential vulnerabilities of lung cancer cells.

4.4 Exploring the Role of PIK3CA and Glucose Variations on A549 Cell Behavior in Tumor-Mimetic Hydrogel Models

It has been well known that PIK3CA is one of the key regulators having roles in multiple signaling pathways including metabolism, and as an oncogenic gene, it is regulated in multiple cancer types like lung cancer (Hemmings & Restuccia, 2012; Kerr & Martins, 2018). It can be activated due to mutations in the PI3K complex components or because of aberrant signaling from receptor tyrosine kinases (RTKs) (Cairns et al., 2011). This aberrant activation of the PI3K signaling pathway has profound effects on tumor growth and metabolism (Gonzalez & McGraw, 2009; Robey & Hay, 2009). Thereby, after investigating how A549 cells adapt their growth and metabolism when exposed to increased sGAG levels in the TME while also facing different glucose levels, we aimed to further explore the specific role of PIK3CA in these adaptive changes. Therefore, we employed short-hairpin RNA interference (shRNA) technology to create A549 cells with reduced PIK3CA expression (shPIK3CA A549 cells). Once we successfully generated the shPIK3CA A549 cell line (Figure 3-18), we proceeded to embed these cells in our tumor-mimetic model. To thoroughly examine the effects, we utilized two different glucose levels in these tumor-mimetic hydrogels. To compare results, we simultaneously examined the behavior of the A549 wild-type cell line under identical experimental conditions.

4.4.1 Unraveling the Role of PIK3CA and Glucose Levels in A549 Cell Growth and Morphology within 3D Tumor-Mimetic Hydrogels

To explore the influence of PIK3CA and glucose levels on A549 cell proliferation in a tumor-mimetic environment, we conducted DNA quantification after three weeks (Figure 3-20). Surprisingly, A549 cells did not show significant changes in their proliferation when exposed to high glucose conditions. However, shPIK3CA A549 cells, in which the PIK3CA gene was knocked down, exhibited a significant increase in cell proliferation under high glucose treatment in the tumor-mimetic environment. Our findings highlight the intricate role of PIK3CA and glucose levels in regulating A549 cell proliferation, particularly in a tumor-mimetic environment. While high glucose conditions appear to enhance the proliferative capacity of A549 cells when PIK3CA is knocked down, PIK3CA knockdown alone does not significantly impact cell proliferation in low glucose conditions. The combination of PIK3CA downregulation and high glucose seems to have a synergistic effect on promoting cell proliferation in this specific microenvironment. It is worth noting that several studies conducted in 2D cell culture have reported that cell proliferation decreases in response to PIK3CA inhibition (Tan, 2020; J. S. L. Yu & Cui, 2016). However, our findings challenge this notion and suggest that the cellular response to PIK3CA inhibition may vary depending on the environmental cues provided by the tumor-mimetic conditions.

Like A549 cells, shPIK3CA A549 cells demonstrated higher ATP levels when exposed to high glucose in tumor-mimetic environments (Figure 3-21). Conversely, PIK3CA knockdown led to reduced ATP levels in low glucose environments. Although high glucose did not fully restore the phenotype, it partially mitigated the decrease in ATP levels caused by PIK3CA inhibition. In summary, the results indicate that PIK3CA influences cell proliferation and metabolism in tumor-mimetic environments, and glucose levels can modulate this effect, particularly in shPIK3CA A549 cells. High glucose appears to enhance cell proliferation and ATP production, partially compensating for the effects of PIK3CA knockdown. These results underline the importance of studying cancer cell behavior within physiologically relevant microenvironments and highlight the need for further investigations to elucidate the complex molecular mechanisms driving the context-dependent effects of PIK3CA and glucose on cell proliferation and metabolism.

The bright-field images revealed that clump formation occurred later in shPIK3CA A549 cells compared to regular A549 cells, indicating a delay due to PIK3CA knockdown

(Figure 3-19). Interestingly, high glucose levels did not significantly affect the clump formation of shPIK3CA A549 cells in the tumor-mimetic environment although it influenced proliferation of these cells. To further validate these results, clump analysis was performed (Figure 3-23). The results suggest that PIK3CA and glucose levels have distinct effects on clump formation in A549 cells. While high glucose seems to promote clump formation in regular A549 cells, in combination with PIK3CA downregulation, this response is altered, leading to a delay in clump formation. This delay could be attributed to the specific genetic manipulation of the PIK3CA gene, which affects the signaling pathways and cellular processes involved in clump formation. Furthermore, the lack of significant variation in clump area in response to high glucose in shPIK3CA A549 cells indicates that glucose may not play a prominent role in regulating clump formation when PIK3CA activity is impaired. The absence of a strong glucose effect in shPIK3CA A549 cells indicates that other factors may dominate the regulation of clump formation in the absence of PIK3CA activity. The most intriguing finding is the synergistic increase in clump area when PIK3CA knockdown and high glucose treatment are combined. Neither factor alone had a significant effect on clump formation, but together, they resulted in a significant increase in clump size. This suggests that there is a complex interplay between PIK3CA and glucose signaling pathways in regulating clump formation. The combined effect may involve compensatory mechanisms or crosstalk between these pathways that amplify the effect on clump formation.

4.4.2 Exploring the Impact of PIK3CA and Glucose Levels on Gene Expression Profiles of A549 Cells in Tumor-Mimetic Hydrogels

After conducting a thorough analysis of the influence of PIK3CA on A549 cell proliferation and clump morphology, our research direction shifted towards exploring its effects on various markers in A549 cells cultured in a tumor-mimetic environment with different glucose levels. We aimed to understand the role of PIK3CA in regulating key markers associated with cellular processes such as EMT, stemness behavior, and cellular metabolism.

The impact of PIK3CA knockdown on A549 cells in tumor-mimetic environments showed a complex relationship with glucose levels (Figure 3-24). As expected, N-Cadherin expression decreased in response to PIK3CA knockdown, consistent with previous findings (Karimi Roshan et al., 2019; Rafael et al., 2015). However, contrary to

what was previously reported, we observed an upregulation of SNAIL expression and a downregulation of E-Cadherin expression in response to decreased PIK3CA expression in A549 cells. Previous studies have often linked PIK3CA inhibition to the suppression of EMT, suggesting that its inhibition would lead to a reduction in SNAIL expression and an increase in E-Cadherin (Hao et al., 2012; S. Lee et al., 2020). However, our findings challenge this notion and suggest a more complex regulatory relationship between PIK3CA and EMT markers in A549 cells cultured in the tumor-mimetic environment. The interplay between PIK3CA and EMT markers' expression in the context of glucose levels further adds to the complexity. It is possible that high glucose availability may influence the regulatory mechanisms governing EMT marker expression in the absence of PIK3CA activity. The tumor-mimetic microenvironment, characterized by altered nutrient and growth factor availability, likely contributes to this differential regulation. It is plausible that the interplay between PIK3CA, glucose levels, and sGAG levels in TME creates a unique context where the usual relationship between PIK3CA and EMT markers may be altered.

The influence of PIK3CA knockdown on stemness marker expression in A549 cells cultured in a tumor-mimetic environment displayed diverse outcomes (Figure 3-25). While CD44 expression decreased upon PIK3CA knockdown, there was an unexpected increase in OCT3/4 and SOX2 expression levels. These findings contrast with the conventional notion that inhibiting PIK3CA is generally associated with decreased stemness behavior in cancer cells, as suggested in previous studies (Madsen, 2020; Zi et al., 2022). The observed impact of high glucose on stemness markers was consistent in both A549 cells and shPIK3CA A549 cells. Regardless of PIK3CA knockdown, high glucose conditions resulted in the same effect on stemness marker expression. This suggests that glucose availability may play a more dominant role in regulating stemness behavior in A549 cells compared to the effect of PIK3CA expression. The divergent responses of stemness markers to PIK3CA knockdown and high glucose levels emphasize the complex interplay between PIK3CA signaling and glucose metabolism in shaping the stemness behavior of A549 cells in the tumor-mimetic environment.

Numerous studies have shown that the PIK3CA gene has diverse roles in cancer cell metabolism and its regulation (He et al., 2021; Katso et al., 2001; Martini et al., 2014). Given the significance of this gene in cancer cell metabolism, our research focused on further investigating its specific involvement in various metabolic markers (Figure 3-26).

The expression of IGFBP5 which regulates IGF signaling, lipid metabolism, and insulin sensitivity of the cells was upregulated in response to PIK3CA knockdown. There are many studies that indicate there is a relationship between IGFBP5 and PIK3CA that regulates drug and radiotherapy sensitivity (Beattie et al., 2015; Chen et al., 2020). This indicates that the interplay between PIK3CA and IGFBP5 is not only important for metabolic regulation but also has implications for the cell's response to therapeutic interventions. The upregulation of IGFBP5 in the context of PIK3CA knockdown suggests a potential feedback mechanism where alterations in PIK3CA levels may affect changes in IGFBP5 expression. Interestingly, even in the presence of PIK3CA knockdown, high glucose levels still led to the upregulation of IGFBP5. This finding indicates that glucose levels can independently influence the expression of IGFBP5, regardless of the cellular levels of the gene. This observation suggests that IGFBP5 regulation is not solely dependent on PIK3CA's expression but is subject to additional regulatory mechanisms, possibly involving glucose-dependent pathways.

We also observed an alteration in the expression of a marker that is associated with lipid metabolism. We found that HMGCS2, which plays a crucial role in ketogenesis was downregulated in response to PIK3CA knockdown. The downregulation of HMGCS2 suggests that PIK3CA may be involved in regulating lipid metabolism and, specifically, through HMGCS2. Similar to IGFBP5, high glucose resulted in upregulation of HMGCS2 regardless of PIK3CA expression. The upregulation of HMGCS2 under high glucose conditions is intriguing because glucose is the primary energy source for most cancer cells. Typically, under high glucose levels, the need for ketone bodies as an alternative energy source is reduced (Y.-H. Wang et al., 2019). However, our results suggest that glucose may also play a role in activating ketogenesis pathways by upregulating HMGCS2 expression, potentially as a response to cellular metabolic demands or stress in the tumor-mimetic model.

The expression patterns of GCGR and PCK1, both of which play important roles in maintaining glucose homeostasis in cells, also showed intriguing results. Several studies have demonstrated that under high glucose levels, insulin inhibits PCK1 expression via the PI3K-PIP3-AKT axis (Hall et al., 2000; Miyake et al., 2002; Xiang et al., 2023). Consistent with these results, our results also suggested that PIK3CA downregulation led to an increase in PCK1 expression. Besides, high glucose levels also resulted in the upregulation of the PCK1 marker regardless of the PIK3CA expression.

The observation regarding the expression of GCGR, the glucagon receptor, is intriguing and suggests a complex relationship between GCGR and PIK3CA. Surprisingly, PIK3CA knockdown did not have any significant impact on GCGR expression, indicating that GCGR regulation may occur with an alternative signaling pathway from PIK3CA signaling. However, the response to high glucose levels was distinct between A549 cells with PIK3CA knockdown and A549 cells without knockdown. In the PIK3CA knockdown A549 cells, elevated glucose levels resulted in an increase in GCGR expression. This suggests that in the absence of PIK3CA, glucose can directly influence GCGR expression, potentially through alternative signaling pathways. Conversely, in A549 cells without PIK3CA knockdown, high glucose levels led to a downregulation of GCGR expression. This implies that in normal conditions, PIK3CA may have a role in modulating GCGR expression, and glucose levels may interact with PIK3CA signaling to regulate GCGR levels.

4.4.3 The Impact of PIK3CA and Glucose Levels on Glycolytic and Mitochondrial Bioenergetics in A549 Cells

Several studies have demonstrated the crucial roles of PIK3CA in regulating cancer cell metabolism, particularly in glycolysis (Hoxhaj & Manning, 2020; Hu et al., 2016). Building on this knowledge, the final phase of our investigation focused on unraveling how PIK3CA influences the bioenergetic parameters in A549 cells within a tumor-mimetic microenvironment, with particular attention to varying glucose levels.

Our results revealed that PIK3CA downregulation and glucose levels have complex and interconnected effects on the bioenergetic characteristics of A549 cells in a tumor-mimetic environment. PIK3CA knockdown led to increased glycolysis and glycolytic capacity in A549 cells, suggesting a regulatory role of PIK3CA in glycolytic processes. Additionally, PIK3CA downregulation enhanced mitochondrial bioenergetic functions, as evidenced by increased basal respiration, ATP production, and maximal respiration. This indicates that PIK3CA not only influences glycolysis but also impacts cellular respiration and energy production through mitochondrial pathways in A549 cells.

Furthermore, the response to high glucose levels was notable, with both A549 and shPIK3CA A549 cells showing a decrease in glycolysis. However, the effect on mitochondrial bioenergetics differed between the two cell lines. A549 cells exhibited a more pronounced decrease in ATP production and maximal respiration, while basal

respiration remained relatively stable. In contrast, shPIK3CA A549 cells showed a decrease in basal respiration under high glucose conditions, suggesting that PIK3CA knockdown may influence the cellular response to glucose availability and its utilization for mitochondrial ATP production.

These findings highlight the significant role of PIK3CA in regulating cellular metabolism and bioenergetics in A549 cells within a physiologically relevant tumor-mimetic environment. Understanding the intricate interactions between PIK3CA and glucose metabolism provides valuable insights into the molecular mechanisms governing cancer cell metabolism and may have implications for the development of targeted therapeutic strategies for cancer treatment.

Chapter 5: **CONCLUSION**

Lung cancer is the second most frequent type of cancer and has the greatest mortality rate of all cancer types. Despite significant advances in drug development and therapeutic strategies targeting cancer metabolism, the insufficient understanding of the tumor microenvironment's biological complexities and dynamic properties continues to impede the development of an effective treatment approach. The experimental constraints and inconsistencies observed in two-dimensional (2D) cultures naturally brought about the convergence of cancer research and tissue engineering, consequently giving rise to the development of three-dimensional (3D) *in vitro* cancer models. In the pursuit of our research objectives, we embarked on the creation of two distinct hydrogel models for this study. The first model was designed to represent healthy lung tissue, while the second model sought to mimic tumor matrix characteristics. To achieve this, we utilized a combination of decellularized bovine lung extracellular matrix with either alginate or alginate sulfate, strategically aligning our experimental approach with the aims of the thesis.

In the initial segment of our study, we presented a comprehensive analysis of gene profiles related to various cellular processes in A549 cells. We focused on comparing these profiles between conventional 2D culture and our novel healthy-mimetic model. Our results demonstrated that the 3D healthy-mimetic environment influenced the expression of EMT markers in A549 cells in a glucose-dependent manner. Additionally, we found that the microenvironment played a crucial role in regulating the stemness of A549 cells, providing valuable insights into their behavior. Moreover, both the AlgLung environment and high glucose treatment significantly impacted the expression of metabolic markers, highlighting their role in regulating cellular metabolism.

In the second phase of this research, our aim was to explore the impact of elevated sGAG levels within the tumor microenvironment and varying glucose levels on the behavior of A549 cells. We conducted specific investigations into how these factors influenced cell growth, morphology, and metabolism. By delving into these crucial aspects, we obtained deeper insights into the complex interplay between sGAG level, glucose availability, and cellular responses, thereby making significant contributions to the advancement of our study's overarching objectives. Our study provided valuable insights into the complex interactions between A549 cells and their microenvironment

within our 3D hydrogel models. The increased sGAG level in the tumor-mimetic environment significantly impacted cell proliferation and metabolic activity, while the effect of glucose levels on cell behavior varied depending on the hydrogel model. Furthermore, we observed a complex interplay between glucose levels and the expression of EMT markers in different microenvironments, with the tumor-mimetic environment combined with high glucose showing a striking influence, leading to significant upregulation of mesenchymal markers in A549 cells. Additionally, gene expression profiles of metabolic markers in A549 cells changed significantly in tumor-mimetic environments, and unexpected outcomes challenged our predictions regarding certain markers under elevated glucose conditions. Our investigation into A549 cells' bioenergetic characteristics in tumor-mimetic environments with varying glucose levels revealed a context-dependent response, highlighting the complexity of metabolic regulation in the tumor microenvironment. Overall, this research emphasized the importance of accurately modeling microenvironments to investigate cellular behavior and provided valuable insights into the metabolic plasticity and potential vulnerabilities of cancer cells.

In the last phase of our study, we specifically investigated the role of the PIK3CA gene, a key cellular signaling regulator. Our goal was to better understand the molecular mechanisms driving the observed cellular changes in our novel hydrogel models under varying microenvironmental conditions. By delving into the role of this gene, we gained valuable insights into the complex processes influencing cellular responses within our experimental setup. These findings contribute significantly to our overall research and the understanding of microenvironmental effects on cell behavior and metabolism. Our study highlighted the significant role of PIK3CA in regulating cell proliferation in tumor-mimetic environments, with glucose levels modulating this effect. High glucose exposure enhanced cell proliferation and ATP production, partially compensating for the effects of PIK3CA knockdown. Furthermore, PIK3CA knockdown influenced EMT marker expression, stemness markers, and various metabolic pathways in A549 cells. High glucose exposure also exerted distinct effects on certain markers in the presence or absence of PIK3CA, emphasizing the complex interplay between glucose availability and PIK3CA signaling. These findings deepened our understanding of cellular metabolism, and PIK3CA's impact, and offered potential therapeutic targets for PIK3CA-associated cancers.

BIBLIOGRAPHY

Acerbi, I., Cassereau, L., Dean, I., Shi, Q., Au, A., Park, C., Chen, Y. Y., Liphardt, J., Hwang, E. S., & Weaver, V. M. (2015). Human breast cancer invasion and aggression correlates with ECM stiffening and immune cell infiltration. *Integrative Biology : Quantitative Biosciences from Nano to Macro*, *7*(10), 1120–1134. https://doi.org/10.1039/c5ib00040h

Afratis, N., Gialeli, C., Nikitovic, D., Tsegenidis, T., Karousou, E., Theocharis, A. D., Pavão, M. S., Tzanakakis, G. N., & Karamanos, N. K. (2012). Glycosaminoglycans: Key players in cancer cell biology and treatment. *FEBS Journal*, *279*(7), 1177–1197. https://doi.org/10.1111/j.1742-4658.2012.08529.x

Agareva, M., Stafeev, I., Michurina, S., Sklyanik, I., Shestakova, E., Ratner, E., Hu, X., Menshikov, M., Shestakova, M., & Parfyonova, Y. (2022). Type 2 Diabetes Mellitus Facilitates Shift of Adipose-Derived Stem Cells Ex Vivo Differentiation toward Osteogenesis among Patients with Obesity. *Life (Basel, Switzerland)*, *12*(5). https://doi.org/10.3390/life12050688

Ahmad Raus, R., Wan Nawawi, W. M. F., & Nasaruddin, R. R. (2021). Alginate and alginate composites for biomedical applications. *Asian Journal of Pharmaceutical Sciences*, *16*(3), 280–306. https://doi.org/10.1016/J.AJPS.2020.10.001

Al Qahtani, A., Holly, J., & Perks, C. (2017). Hypoxia negates hyperglycaemia-induced chemo-resistance in breast cancer cells: the role of insulin-like growth factor binding protein 2. *Oncotarget*, *8*(43), 74635–74648. https://doi.org/10.18632/oncotarget.20287

Alemany-Ribes, M., & Semino, C. E. (2014). Bioengineering 3D environments for cancer models. *Advanced Drug Delivery Reviews*, *79*, 40–49. https://doi.org/10.1016/j.addr.2014.06.004

Alisson-Silva, F., Freire-de-Lima, L., Donadio, J. L., Lucena, M. C., Penha, L., Sá-Diniz, J. N., Dias, W. B., & Todeschini, A. R. (2013). Increase of O-glycosylated oncofetal fibronectin in high glucose-induced epithelial-mesenchymal transition of cultured human epithelial cells. *PloS One*, *8*(4), e60471.

https://doi.org/10.1371/journal.pone.0060471

An, S.-J., Lin, Q.-X., Chen, Z.-H., Su, J., Cheng, H., Xie, Z., Zhang, X.-C., Zhou, H.-Y., Huang, Y., Chen, S.-L., Guo, W.-B., & Wu, Y.-L. (2012). Combinations of laminin 5 with PTEN, p-EGFR and p-Akt define a group of distinct molecular subsets indicative of poor prognosis in patients with non-small cell lung cancer. *Experimental and Therapeutic Medicine*, *4*(2), 226–230. https://doi.org/10.3892/etm.2012.577

Andersen, T., Auk-Emblem, P., & Dornish, M. (2015). 3D Cell Culture in Alginate Hydrogels. *Microarrays (Basel, Switzerland)*, *4*(2), 133–161. https://doi.org/10.3390/microarrays4020133

Anderson, N. M., & Simon, M. C. (2020). The tumor microenvironment. *Current Biology*, *30*(16), R921–R925. https://doi.org/10.1016/j.cub.2020.06.081

Arlov, Ø., Rütsche, D., Korayem, M. A., Öztürk, E., & Zenobi-wong, M. (2021). *Engineered Sulfated Polysaccharides for Biomedical Applications*. *2010732*, 1–52. https://doi.org/10.1002/adfm.202010732

Arlov, Ø., & Skjåk-Bræk, G. (2017). Sulfated alginates as heparin analogues: A review of chemical and functional properties. *Molecules*, *22*(5), 1–16. https://doi.org/10.3390/molecules22050778

Arneth, B. (2020). Tumor microenvironment. In *Medicina (Lithuania)* (Vol. 56, Issue 1). https://doi.org/10.3390/medicina56010015

Balestrini, J. L., Gard, A. L., Liu, A., Leiby, K. L., Schwan, J., Kunkemoeller, B., Calle, E. A., Sivarapatna, A., Lin, T., Dimitrievska, S., Cambpell, S. G., & Niklason, L. E. (2015). Production of decellularized porcine lung scaffolds for use in tissue engineering. *Integrative Biology : Quantitative Biosciences from Nano to Macro*, *7*(12), 1598–1610. https://doi.org/10.1039/c5ib00063g

Barbouri, D., Afratis, N., Gialeli, C., Vynios, D. H., Theocharis, A. D., & Karamanos, N. K. (2014). Syndecans as modulators and potential pharmacological targets in cancer progression. *Frontiers in Oncology*, *4*, 4. https://doi.org/10.3389/fonc.2014.00004

Beattie, J., Hawsawi, Y., Alkharobi, H., & El-Gendy, R. (2015). IGFBP-2 and -5: important regulators of normal and neoplastic mammary gland physiology. *Journal of Cell Communication and Signaling*, *9*(2), 151–158. https://doi.org/10.1007/s12079-015-0260-3

Billings, P. C., & Pacifici, M. (2015). Interactions of signaling proteins, growth factors and other proteins with heparan sulfate: mechanisms and mysteries. *Connective Tissue Research*, *56*(4), 272–280. https://doi.org/10.3109/03008207.2015.1045066

Bond, P. (2016). Regulation of mTORC1 by growth factors, energy status, amino acids and mechanical stimuli at a glance. *Journal of the International Society of Sports Nutrition*, *13*(1), 1–11. https://doi.org/10.1186/s12970-016-0118-y

Burgstaller, G., Oehrle, B., Gerckens, M., White, E. S., Schiller, H. B., & Eickelberg, O. (2017). The instructive extracellular matrix of the lung: Basic composition and alterations in chronic lung disease. *European Respiratory Journal*, *50*(1). https://doi.org/10.1183/13993003.01805-2016

Cai, X., Wang, K.-C., & Meng, Z. (2021). Mechanoregulation of YAP and TAZ in Cellular Homeostasis and Disease Progression. *Frontiers in Cell and Developmental Biology*, *9*, 673599. https://doi.org/10.3389/fcell.2021.673599

Cairns, R. A., Harris, I. S., & Mak, T. W. (2011). Regulation of cancer cell metabolism. *Nature Reviews Cancer*, *11*(2), 85–95. https://doi.org/10.1038/nrc2981

Caliari, S. R., & Burdick, J. A. (2016). A practical guide to hydrogels for cell culture. *Nature Methods*, *13*(5), 405–414. https://doi.org/10.1038/nmeth.3839

Charbonier, F., Indana, D., & Chaudhuri, O. (2021a). Tuning Viscoelasticity in Alginate Hydrogels for 3D Cell Culture Studies. *Current Protocols*, *1*(5), 1–28. https://doi.org/10.1002/cpz1.124

Charbonier, F., Indana, D., & Chaudhuri, O. (2021b). Tuning Viscoelasticity in Alginate Hydrogels for 3D Cell Culture Studies. *Current Protocols*, *1*(5), e124. https://doi.org/10.1002/cpz1.124

Chaudhuri, O., Koshy, S. T., Branco da Cunha, C., Shin, J.-W., Verbeke, C. S., Allison, K. H., & Mooney, D. J. (2014). Extracellular matrix stiffness and composition

jointly regulate the induction of malignant phenotypes in mammary epithelium. *Nature Materials*, *13*(10), 970–978. https://doi.org/10.1038/nmat4009

Chen, X., Yu, Q., Pan, H., Li, P., Wang, X., & Fu, S. (2020). Overexpression of IGFBP5 Enhances Radiosensitivity Through PI3K-AKT Pathway in Prostate Cancer. *Cancer Management and Research*, *12*, 5409–5418. https://doi.org/10.2147/CMAR.S257701

Chin, L., Xia, Y., Discher, D. E., & Janmey, P. A. (2016). Mechanotransduction in cancer. *Current Opinion in Chemical Engineering*, *11*, 77–84. https://doi.org/10.1016/j.coche.2016.01.011

Christiansen, J. J., & Rajasekaran, A. K. (2006). Reassessing epithelial to mesenchymal transition as a prerequisite for carcinoma invasion and metastasis. *Cancer Research*, *66*(17), 8319–8326. https://doi.org/10.1158/0008-5472.CAN-06-0410

De Berardinis, R. J., & Chandel, N. S. (2016). Fundamentals of cancer metabolism. *Science Advances*, *2*(5). https://doi.org/10.1126/sciadv.1600200

De Pasquale, V., & Pavone, L. M. (2020a). Heparan sulfate proteoglycan signaling in tumor microenvironment. *International Journal of Molecular Sciences*, *21*(18), 1–29. https://doi.org/10.3390/ijms21186588

De Pasquale, V., & Pavone, L. M. (2020b). Heparan Sulfate Proteoglycan Signaling in Tumor Microenvironment. *International Journal of Molecular Sciences*, *21*(18). https://doi.org/10.3390/ijms21186588

De Pasquale, V., Pezone, A., Sarogni, P., Tramontano, A., Schiattarella, G. G., Avvedimento, V. E., Paladino, S., & Pavone, L. M. (2018). EGFR activation triggers cellular hypertrophy and lysosomal disease in NAGLU-depleted cardiomyoblasts, mimicking the hallmarks of mucopolysaccharidosis IIIB. *Cell Death & Disease*, *9*(2), 40. https://doi.org/10.1038/s41419-017-0187-0

Deberardinis, R. J., & Chandel, N. S. (2016). *Fundamentals of cancer metabolism*. *May*.

DeBerardinis, R. J., Lum, J. J., Hatzivassiliou, G., & Thompson, C. B. (2008). The Biology of Cancer: Metabolic Reprogramming Fuels Cell Growth and Proliferation. *Cell Metabolism*, *7*(1), 11–20.

https://doi.org/10.1016/j.cmet.2007.10.002

Ding, C. Z., Guo, X. F., Wang, G. L., Wang, H. T., Xu, G. H., Liu, Y. Y., Wu, Z. J., Chen, Y. H., Wang, J., & Wang, W. G. (2018). High glucose contributes to the proliferation and migration of non-small-cell lung cancer cells via GAS5-TRIB3 axis. *Bioscience Reports*, *38*(2). https://doi.org/10.1042/BSR20171014

Dittmer, J. (2022). Biological effects and regulation of IGFBP5 in breast cancer. *Frontiers in Endocrinology*, *13*, 983793. https://doi.org/10.3389/fendo.2022.983793

Fernández-Pérez, J., & Ahearne, M. (2019). The impact of decellularization methods on extracellular matrix derived hydrogels. *Scientific Reports*, *9*(1), 14933. https://doi.org/10.1038/s41598-019-49575-2

Filmus, J., & Capurro, M. (2014). The role of glypicans in Hedgehog signaling. *Matrix Biology : Journal of the International Society for Matrix Biology*, *35*, 248–252. https://doi.org/10.1016/j.matbio.2013.12.007

Fontoura, J. C., Viezzer, C., Dos Santos, F. G., Ligabue, R. A., Weinlich, R., Puga, R. D., Antonow, D., Severino, P., & Bonorino, C. (2020). Comparison of 2D and 3D cell culture models for cell growth, gene expression and drug resistance. *Materials Science & Engineering. C, Materials for Biological Applications*, *107*, 110264. https://doi.org/10.1016/j.msec.2019.110264

Frantz, C., Stewart, K. M., & Weaver, V. M. (2010). The extracellular matrix at a glance. *Journal of Cell Science*, *123*(24), 4195–4200. https://doi.org/10.1242/jcs.023820

Fruman, D. A., Chiu, H., Hopkins, B. D., Bagrodia, S., Cantley, L. C., & Abraham, R. T. (2017). The PI3K Pathway in Human Disease. *Cell*, *170*(4), 605–635. https://doi.org/10.1016/j.cell.2017.07.029

Fuster, M. M., & Esko, J. D. (2005). The sweet and sour of cancer: Glycans as novel therapeutic targets. *Nature Reviews Cancer*, *5*(7), 526–542. https://doi.org/10.1038/nrc1649

Ge, H., Tian, M., Pei, Q., Tan, F., & Pei, H. (2021a). Extracellular Matrix Stiffness:

New Areas Affecting Cell Metabolism. *Frontiers in Oncology*, *11*, 631991. https://doi.org/10.3389/fonc.2021.631991

Ge, H., Tian, M., Pei, Q., Tan, F., & Pei, H. (2021b). Extracellular Matrix Stiffness: New Areas Affecting Cell Metabolism. *Frontiers in Oncology*, *11*(February), 1–12. https://doi.org/10.3389/fonc.2021.631991

Georgakopoulos-Soares, I., Chartoumpekis, D. V, Kyriazopoulou, V., & Zaravinos, A. (2020). EMT Factors and Metabolic Pathways in Cancer. *Frontiers in Oncology*, *10*, 499. https://doi.org/10.3389/fonc.2020.00499

Giaccone, G. (2005). Journal of Clinical Oncology. *JCO*, *23*(14), 3235–3242. https://doi.org/10.1200/jco.2005.08.409

Godfrey, J., Riscal, R., Skuli, N., & Simon, M. C. (2022). Glucagon signaling via supraphysiologic GCGR can reduce cell viability without stimulating gluconeogenic gene expression in liver cancer cells. *Cancer & Metabolism*, *10*(1), 4. https://doi.org/10.1186/s40170-022-00280-1

Gonzalez, E., & McGraw, T. E. (2009). The Akt kinases: Isoform specificity in metabolism and cancer. *Cell Cycle*, *8*(16), 2502–2508. https://doi.org/10.4161/cc.8.16.9335

Götte, M., & Kovalszky, I. (2018). Extracellular matrix functions in lung cancer. *Matrix Biology*, *73*, 105–121. https://doi.org/10.1016/j.matbio.2018.02.018

Gridelli, C., Rossi, A., Carbone, D. P., Guarize, J., Karachaliou, N., Mok, T., Petrella, F., Spaggiari, L., & Rosell, R. (2015). Non-small-cell lung cancer. *Nature Reviews Disease Primers*, *1*, 1–16. https://doi.org/10.1038/nrdp.2015.9

Hall, R. K., Yamasaki, T., Kucera, T., Waltner-Law, M., O'Brien, R., & Granner, D. K. (2000). Regulation of phosphoenolpyruvate carboxykinase and insulin-like growth factor-binding protein-1 gene expression by insulin. The role of winged helix/forkhead proteins. *The Journal of Biological Chemistry*, *275*(39), 30169–30175. https://doi.org/10.1074/jbc.M004898200

Hanahan, D., & Weinberg, R. A. (2011). Hallmarks of cancer: The next generation. In *Cell* (Vol. 144, Issue 5, pp. 646–674). https://doi.org/10.1016/j.cell.2011.02.013

Hao, L., Ha, J. R., Kuzel, P., Garcia, E., & Persad, S. (2012). Cadherin switch from E- to N-cadherin in melanoma progression is regulated by the PI3K/PTEN pathway through Twist and Snail. *The British Journal of Dermatology*, *166*(6), 1184–1197. https://doi.org/10.1111/j.1365-2133.2012.10824.x

Harachi, M., Masui, K., Okamura, Y., Tsukui, R., Mischel, P. S., & Shibata, N. (2018). mTOR complexes as a nutrient sensor for driving cancer progression. *International Journal of Molecular Sciences*, *19*(10). https://doi.org/10.3390/ijms19103267

Hassan, N., Greve, B., Espinoza-Sánchez, N. A., & Götte, M. (2021). Cell-surface heparan sulfate proteoglycans as multifunctional integrators of signaling in cancer. *Cellular Signalling*, *77*(October 2020). https://doi.org/10.1016/j.cellsig.2020.109822

He, Y., Sun, M. M., Zhang, G. G., Yang, J., Chen, K. S., Xu, W. W., & Li, B. (2021). Targeting PI3K/Akt signal transduction for cancer therapy. *Signal Transduction and Targeted Therapy*, *6*(1), 425. https://doi.org/10.1038/s41392-021-00828-5

Hemmings, B. A., & Restuccia, D. F. (2012). PI3K-PKB / Akt Pathway. *Cold Spring Harbor Perspectives in Medicine*, *4*(9), 1–4.

Henke, E., Nandigama, R., & Ergün, S. (2019). Extracellular Matrix in the Tumor Microenvironment and Its Impact on Cancer Therapy. *Frontiers in Molecular Biosciences*, *6*, 160. https://doi.org/10.3389/fmolb.2019.00160

Hoshiba, T. (2018). An extracellular matrix (ECM) model at high malignant colorectal tumor increases chondroitin sulfate chains to promote epithelial-mesenchymal transition and chemoresistance acquisition. *Experimental Cell Research*, *370*(2), 571–578. https://doi.org/10.1016/j.yexcr.2018.07.022

Hoxhaj, G., & Manning, B. D. (2020). The PI3K-AKT network at the interface of oncogenic signalling and cancer metabolism. *Nature Reviews. Cancer*, *20*(2), 74–88. https://doi.org/10.1038/s41568-019-0216-7

Hu, H., Juvekar, A., Lyssiotis, C. A., Lien, E. C., Albeck, J. G., Oh, D., Varma, G., Hung, Y. P., Ullas, S., Lauring, J., Seth, P., Lundquist, M. R., Tolan, D. R., Grant, A. K., Needleman, D. J., Asara, J. M., Cantley, L. C., & Wulf, G. M. (2016).

Phosphoinositide 3-Kinase Regulates Glycolysis through Mobilization of Aldolase from the Actin Cytoskeleton. *Cell*, *164*(3), 433–446. https://doi.org/10.1016/j.cell.2015.12.042

Hua, H., Kong, Q., Yin, J., Zhang, J., & Jiang, Y. (2020). Insulin-like growth factor receptor signaling in tumorigenesis and drug resistance: a challenge for cancer therapy. *Journal of Hematology & Oncology*, *13*(1), 64. https://doi.org/10.1186/s13045-020-00904-3

Huh, D., Matthews, B. D., Mammoto, A., Montoya-Zavala, M., Hsin, H. Y., & Ingber, D. E. (2010). Reconstituting organ-level lung functions on a chip. *Science (New York, N.Y.)*, *328*(5986), 1662–1668. https://doi.org/10.1126/science.1188302

Hull, E. E., Montgomery, M. R., & Leyva, K. J. (2017). Epigenetic Regulation of the Biosynthesis & Enzymatic Modification of Heparan Sulfate Proteoglycans: Implications for Tumorigenesis and Cancer Biomarkers. *International Journal of Molecular Sciences*, *18*(7). https://doi.org/10.3390/ijms18071361

Humphrey, J. D., Dufresne, E. R., & Schwartz, M. A. (2014). Mechanotransduction and extracellular matrix homeostasis. *Nature Reviews Molecular Cell Biology*, *15*(12), 802–812. https://doi.org/10.1038/nrm3896

Jensen, C., & Teng, Y. (2020). Is It Time to Start Transitioning From 2D to 3D Cell Culture? *Frontiers in Molecular Biosciences*, *7*, 33. https://doi.org/10.3389/fmolb.2020.00033

Jiang, Y., Zhang, H., Wang, J., Liu, Y., Luo, T., & Hua, H. (2022). Targeting extracellular matrix stiffness and mechanotransducers to improve cancer therapy. *Journal of Hematology & Oncology*, *15*(1), 34. https://doi.org/10.1186/s13045-022-01252-0

Kang, H., Kim, H., Lee, S., Youn, H., & Youn, B. (2019). Role of Metabolic Reprogramming in Epithelial¯Mesenchymal Transition (EMT). *International Journal of Molecular Sciences*, *20*(8). https://doi.org/10.3390/ijms20082042

Kang, X., Kong, F., Wu, X., Ren, Y., Wu, S., Wu, K., Jiang, Z., & Zhang, W. (2015). High glucose promotes tumor invasion and increases metastasis-associated protein

expression in human lung epithelial cells by upregulating heme oxygenase-1 via reactive oxygen species or the TGF-β1/PI3K/Akt signaling pathway. *Cellular Physiology and Biochemistry : International Journal of Experimental Cellular Physiology, Biochemistry, and Pharmacology*, *35*(3), 1008–1022. https://doi.org/10.1159/000373928

Kapałczyńska, M., Kolenda, T., Przybyła, W., Zajączkowska, M., Teresiak, A., Filas, V., Ibbs, M., Bliźniak, R., Łuczewski, Ł., & Lamperska, K. (2018). 2D and 3D cell cultures - a comparison of different types of cancer cell cultures. *Archives of Medical Science : AMS*, *14*(4), 910–919. https://doi.org/10.5114/aoms.2016.63743

Karimi Roshan, M., Soltani, A., Soleimani, A., Rezaie Kahkhaie, K., Afshari, A. R., & Soukhtanloo, M. (2019). Role of AKT and mTOR signaling pathways in the induction of epithelial-mesenchymal transition (EMT) process. *Biochimie*, *165*, 229–234. https://doi.org/https://doi.org/10.1016/j.biochi.2019.08.003

Katso, R., Okkenhaug, K., Ahmadi, K., White, S., Timms, J., & Waterfield, M. D. (2001). Cellular Function of Phosphoinositide 3-Kinases: Implications for Development, Immunity, Homeostasis, and Cancer. *Annual Review of Cell and Developmental Biology*, *17*(1), 615–675. https://doi.org/10.1146/annurev.cellbio.17.1.615

Kerr, E. M., & Martins, C. P. (2018). Metabolic rewiring in mutant Kras lung cancer. *FEBS Journal*, *285*(1), 28–41. https://doi.org/10.1111/febs.14125

Kiewe, P., Bechrakis, N. E., Schmittel, A., Ruf, P., Lindhofer, H., Thiel, E., & Nagorsen, D. (2006). Increased chondroitin sulphate proteoglycan expression (B5 immunoreactivity) in metastases of uveal melanoma. *Annals of Oncology : Official Journal of the European Society for Medical Oncology*, *17*(12), 1830–1834. https://doi.org/10.1093/annonc/mdl305

Kim, S. H., Turnbull, J., & Guimond, S. (2011). Extracellular matrix and cell signalling: The dynamic cooperation of integrin, proteoglycan and growth factor receptor. *Journal of Endocrinology*, *209*(2), 139–151. https://doi.org/10.1530/JOE-10-0377

Kind, S., Merenkow, C., Büscheck, F., Möller, K., Dum, D., Chirico, V., Luebke, A. M., Höflmayer, D., Hinsch, A., Jacobsen, F., Göbel, C., Weidemann, S., Fraune,

C., Möller-Koop, C., Hube-Magg, C., Clauditz, T. S., Simon, R., Sauter, G., Wilczak, W., … Marx, A. (2019). Prevalence of Syndecan-1 (CD138) Expression in Different Kinds of Human Tumors and Normal Tissues. *Disease Markers*, *2019*, 4928315. https://doi.org/10.1155/2019/4928315

Kirn-Safran, C., Farach-Carson, M. C., & Carson, D. D. (2009). Multifunctionality of extracellular and cell surface heparan sulfate proteoglycans. *Cellular and Molecular Life Sciences : CMLS*, *66*(21), 3421–3434. https://doi.org/10.1007/s00018-009-0096-1

Knelson, E. H., Nee, J. C., & Blobe, G. C. (2014). Heparan sulfate signaling in cancer. *Trends in Biochemical Sciences*, *39*(6), 277–288. https://doi.org/10.1016/j.tibs.2014.03.001

Kuşoğlu, A., Yangın, K., Özkan, S. N., Sarıca, S., Örnek, D., Solcan, N., Karaoğlu, İ. C., Kızılel, S., Bulutay, P., Fırat, P., Erus, S., Tanju, S., Dilege, Ş., & Öztürk, E. (2022). Different Decellularization Methods in Bovine Lung Tissue Reveals Distinct Biochemical Composition, Stiffness, and Viscoelasticity in Reconstituted Hydrogels. *ACS Applied Bio Materials*. https://doi.org/10.1021/acsabm.2c00968

Lanzi, C., & Cassinelli, G. (2020). Receptor tyrosine kinases and heparan sulfate proteoglycans: Interplay providing anticancer targeting strategies and new therapeutic opportunities. *Biochemical Pharmacology*, *178*(June), 114084. https://doi.org/10.1016/j.bcp.2020.114084

Lee, K. Y., & Mooney, D. J. (2012). Alginate: Properties and biomedical applications. In *Progress in Polymer Science (Oxford)* (Vol. 37, Issue 1, pp. 106–126). https://doi.org/10.1016/j.progpolymsci.2011.06.003

Lee, S., Choi, E. J., Cho, E. J., Lee, Y. Bin, Lee, J.-H., Yu, S. J., Yoon, J.-H., & Kim, Y. J. (2020). Inhibition of PI3K/Akt signaling suppresses epithelial-to-mesenchymal transition in hepatocellular carcinoma through the Snail/GSK-3/beta-catenin pathway. *Clinical and Molecular Hepatology*, *26*(4), 529–539. https://doi.org/10.3350/cmh.2019.0056n

Li, H., Raghunathan, V., Stamer, W. D., Ganapathy, P. S., & Herberg, S. (2022). Extracellular Matrix Stiffness and TGFβ2 Regulate YAP/TAZ Activity in Human

Trabecular Meshwork Cells. *Frontiers in Cell and Developmental Biology*, *10*, 844342. https://doi.org/10.3389/fcell.2022.844342

Li, J. P., & Kusche-Gullberg, M. (2016). Heparan Sulfate: Biosynthesis, Structure, and Function. *International Review of Cell and Molecular Biology*, *325*, 215–273. https://doi.org/10.1016/bs.ircmb.2016.02.009

Lin, X., Xiao, Z., Chen, T., Liang, S. H., & Guo, H. (2020). Glucose Metabolism on Tumor Plasticity, Diagnosis, and Treatment. *Frontiers in Oncology*, *10*(March), 1–10. https://doi.org/10.3389/fonc.2020.00317

Liu, X., Feng, C., Wei, G., Kong, W., Meng, H., Du, Y., & Li, J. (2020). Mitofusin1 Is a Major Mediator in Glucose-Induced Epithelial-to-Mesenchymal Transition in Lung Adenocarcinoma Cells. *OncoTargets and Therapy*, *13*, 3511–3523. https://doi.org/10.2147/OTT.S238714

Liu, Z.-L., Chen, H.-H., Zheng, L.-L., Sun, L.-P., & Shi, L. (2023). Angiogenic signaling pathways and anti-angiogenic therapy for cancer. *Signal Transduction and Targeted Therapy*, *8*(1), 198. https://doi.org/10.1038/s41392-023-01460-1

Loessner, D., Stok, K. S., Lutolf, M. P., Hutmacher, D. W., Clements, J. A., & Rizzi, S. C. (2010). Bioengineered 3D platform to explore cell-ECM interactions and drug resistance of epithelial ovarian cancer cells. *Biomaterials*, *31*(32), 8494–8506. https://doi.org/10.1016/j.biomaterials.2010.07.064

Lyssiotis, C. A., & Kimmelman, A. C. (2017). Metabolic Interactions in the Tumor Microenvironment. *Trends in Cell Biology*, *27*(11), 863–875. https://doi.org/10.1016/j.tcb.2017.06.003

Madsen, R. R. (2020). PI3K in stemness regulation: from development to cancer. *Biochemical Society Transactions*, *48*(1), 301–315. https://doi.org/10.1042/BST20190778

Malavaki, C. J., Theocharis, A. D., Lamari, F. N., Kanakis, I., Tsegenidis, T., Tzanakakis, G. N., & Karamanos, N. K. (2011). Heparan sulfate: biological significance, tools for biochemical analysis and structural characterization. *Biomedical Chromatography : BMC*, *25*(1–2), 11–20.

https://doi.org/10.1002/bmc.1536

Mani, S. A., Guo, W., Liao, M.-J., Eaton, E. N., Ayyanan, A., Zhou, A. Y., Brooks, M., Reinhard, F., Zhang, C. C., Shipitsin, M., Campbell, L. L., Polyak, K., Brisken, C., Yang, J., & Weinberg, R. A. (2008). The epithelial-mesenchymal transition generates cells with properties of stem cells. *Cell*, *133*(4), 704–715. https://doi.org/10.1016/j.cell.2008.03.027

Manning, B. D., & Cantley, L. C. (2007). AKT/PKB Signaling: Navigating Downstream. *Cell*, *129*(7), 1261–1274. https://doi.org/10.1016/j.cell.2007.06.009

Martini, M., De Santis, M. C., Braccini, L., Gulluni, F., & Hirsch, E. (2014). PI3K/AKT signaling pathway and cancer: an updated review. *Annals of Medicine*, *46*(6), 372–383. https://doi.org/10.3109/07853890.2014.912836

Melissaridou, S., Wiechec, E., Magan, M., Jain, M. V., Chung, M. K., Farnebo, L., & Roberg, K. (2019). The effect of 2D and 3D cell cultures on treatment response, EMT profile and stem cell features in head and neck cancer. *Cancer Cell International*, *19*, 16. https://doi.org/10.1186/s12935-019-0733-1

Meng, X., Li, Z., Zhou, S., Xiao, S., & Yu, P. (2019). miR-194 suppresses high glucose-induced non-small cell lung cancer cell progression by targeting NFAT5. In *Thoracic Cancer* (Vol. 10, Issue 5, pp. 1051–1059). https://doi.org/10.1111/1759-7714.13038

Merivaara, A., Koivunotko, E., Manninen, K., Kaseva, T., Monola, J., Salli, E., Koivuniemi, R., Savolainen, S., Valkonen, S., & Yliperttula, M. (2022). Stiffness-Controlled Hydrogels for 3D Cell Culture Models. *Polymers*, *14*(24). https://doi.org/10.3390/polym14245530

Miyake, K., Ogawa, W., Matsumoto, M., Nakamura, T., Sakaue, H., & Kasuga, M. (2002). Hyperinsulinemia, glucose intolerance, and dyslipidemia induced by acute inhibition of phosphoinositide 3-kinase signaling in the liver. *The Journal of Clinical Investigation*, *110*(10), 1483–1491. https://doi.org/10.1172/JCI15880

Morel, A.-P., Lièvre, M., Thomas, C., Hinkal, G., Ansieau, S., & Puisieux, A. (2008). Generation of breast cancer stem cells through epithelial-mesenchymal transition.

PloS One, *3*(8), e2888. https://doi.org/10.1371/journal.pone.0002888

Muguruma, M., Teraoka, S., Miyahara, K., Ueda, A., Asaoka, M., Okazaki, M., Kawate, T., Kuroda, M., Miyagi, Y., & Ishikawa, T. (2020). Differences in drug sensitivity between two-dimensional and three-dimensional culture systems in triple-negative breast cancer cell lines. *Biochemical and Biophysical Research Communications*, *533*(3), 268–274. https://doi.org/10.1016/j.bbrc.2020.08.075

Mytilinaiou, M., Nikitovic, D., Berdiaki, A., Kostouras, A., Papoutsidakis, A., Tsatsakis, A. M., & Tzanakakis, G. N. (2017). Emerging roles of syndecan 2 in epithelial and mesenchymal cancer progression. *IUBMB Life*, *69*(11), 824–833. https://doi.org/10.1002/iub.1678

Nallanthighal, S., Heiserman, J. P., & Cheon, D.-J. (2019). The Role of the Extracellular Matrix in Cancer Stemness. *Frontiers in Cell and Developmental Biology*, *7*, 86. https://doi.org/10.3389/fcell.2019.00086

Nazemi, M., & Rainero, E. (2020). Cross-Talk Between the Tumor Microenvironment, Extracellular Matrix, and Cell Metabolism in Cancer. *Frontiers in Oncology*, *10*(February), 1–7. https://doi.org/10.3389/fonc.2020.00239

Newsholme, E. A., Crabtree, B., & Ardawi, M. S. (1985). The role of high rates of glycolysis and glutamine utilization in rapidly dividing cells. *Bioscience Reports*, *5*(5), 393–400. https://doi.org/10.1007/BF01116556

Ng, M. R., & Brugge, J. S. (2009). A stiff blow from the stroma: collagen crosslinking drives tumor progression. *Cancer Cell*, *16*(6), 455–457. https://doi.org/10.1016/j.ccr.2009.11.013

Nikitovic, D., Assouti, M., Sifaki, M., Katonis, P., Krasagakis, K., Karamanos, N. K., & Tzanakakis, G. N. (2008). Chondroitin sulfate and heparan sulfate-containing proteoglycans are both partners and targets of basic fibroblast growth factor-mediated proliferation in human metastatic melanoma cell lines. *The International Journal of Biochemistry & Cell Biology*, *40*(1), 72–83. https://doi.org/10.1016/j.biocel.2007.06.019

Niu, F.-Y., Zhou, Q., Yang, J.-J., Zhong, W.-Z., Chen, Z.-H., Deng, W., He, Y.-Y.,

Chen, H.-J., Zeng, Z., Ke, E.-E., Zhao, N., Zhang, N., Sun, H.-W., Zhang, Q.-Y., Xie, Z., Zhang, X.-C., & Wu, Y.-L. (2016). Distribution and prognosis of uncommon metastases from non-small cell lung cancer. *BMC Cancer*, *16*(1), 149. https://doi.org/10.1186/s12885-016-2169-5

O'Neill, J. D., Anfang, R., Anandappa, A., Costa, J., Javidfar, J., Wobma, H. M., Singh, G., Freytes, D. O., Bacchetta, M. D., Sonett, J. R., & Vunjak-Novakovic, G. (2013). Decellularization of human and porcine lung tissues for pulmonary tissue engineering. *The Annals of Thoracic Surgery*, *96*(3), 1046. https://doi.org/10.1016/j.athoracsur.2013.04.022

Ornitz, D. M., & Itoh, N. (2015). The fibroblast growth factor signaling pathway. *Wiley Interdisciplinary Reviews: Developmental Biology*, *4*(3), 215–266. https://doi.org/10.1002/wdev.176

Öztürk, E., Arlov, Ø., Aksel, S., Li, L., Ornitz, D. M., Skjåk-bræk, G., & Zenobi-wong, M. (2016). *Sulfated Hydrogel Matrices Direct Mitogenicity and Maintenance of Chondrocyte Phenotype through Activation of FGF Signaling*. 3649–3662. https://doi.org/10.1002/adfm.201600092

Öztürk, E., Stauber, T., Levinson, C., Cavalli, E., Arlov, Ø., & Zenobi-wong, M. (2020). *Tyrosinase-crosslinked , tissue adhesive and biomimetic alginate sulfate hydrogels for cartilage repair Tyrosinase-crosslinked , tissue adhesive and biomimetic alginate sulfate hydrogels for cartilage repair*.

Pavlova, N. N., & Thompson, C. B. (2016). The Emerging Hallmarks of Cancer Metabolism. *Cell Metabolism*, *23*(1), 27–47. https://doi.org/10.1016/j.cmet.2015.12.006

Petersen, T. H., Calle, E. A., Colehour, M. B., & Niklason, L. E. (2012). Matrix composition and mechanics of decellularized lung scaffolds. *Cells, Tissues, Organs*, *195*(3), 222–231. https://doi.org/10.1159/000324896

Potter, E. &. (2008). Proteoglycans and Sulfated Glycosaminoglycans. *Bone*, *23*(1), 1–7. https://doi.org/10.1016/j.cellsig.2009.05.001.Proteoglycan

Presta, M., Dell'Era, P., Mitola, S., Moroni, E., Ronca, R., & Rusnati, M. (2005).

Fibroblast growth factor/fibroblast growth factor receptor system in angiogenesis. *Cytokine & Growth Factor Reviews*, *16*(2), 159–178. https://doi.org/10.1016/j.cytogfr.2005.01.004

Pupo, E., Avanzato, D., Middonti, E., Bussolino, F., & Lanzetti, L. (2019). KRAS-driven metabolic rewiring reveals novel actionable targets in cancer. *Frontiers in Oncology*, *9*(AUG), 1–9. https://doi.org/10.3389/fonc.2019.00848

Rafael, D., Doktorovová, S., Florindo, H. F., Gener, P., Abasolo, I., Schwartz, S. J., & Videira, M. A. (2015). EMT blockage strategies: Targeting Akt dependent mechanisms for breast cancer metastatic behaviour modulation. *Current Gene Therapy*, *15*(3), 300–312. https://doi.org/10.2174/1566523215666150126123642

Reticker-Flynn, N. E., & Bhatia, S. N. (2015). Aberrant glycosylation promotes lung cancer metastasis through adhesion to galectins in the metastatic niche. *Cancer Discovery*, *5*(2), 168–181. https://doi.org/10.1158/2159-8290.CD-13-0760

Rianna, C., Kumar, P., & Radmacher, M. (2018). The role of the microenvironment in the biophysics of cancer. *Seminars in Cell and Developmental Biology*, *73*, 107–114. https://doi.org/10.1016/j.semcdb.2017.07.022

Ricciardelli, C., Russell, D. L., Ween, M. P., Mayne, K., Suwiwat, S., Byers, S., Marshall, V. R., Tilley, W. D., & Horsfall, D. J. (2007). Formation of hyaluronan- and versican-rich pericellular matrix by prostate cancer cells promotes cell motility. *The Journal of Biological Chemistry*, *282*(14), 10814–10825. https://doi.org/10.1074/jbc.M606991200

Robey, R. B., & Hay, N. (2009). Is Akt the "Warburg kinase"?-Akt-energy metabolism interactions and oncogenesis. *Seminars in Cancer Biology*, *19*(1), 25–31. https://doi.org/10.1016/j.semcancer.2008.11.010

Romani, P., Valcarcel-Jimenez, L., Frezza, C., & Dupont, S. (2021). Crosstalk between mechanotransduction and metabolism. *Nature Reviews Molecular Cell Biology*, *22*(1), 22–38. https://doi.org/10.1038/s41580-020-00306-w

Rosenzweig, S. A. (2012). Acquired resistance to drugs targeting receptor tyrosine kinases. *Biochemical Pharmacology*, *83*(8), 1041–1048.

https://doi.org/10.1016/J.BCP.2011.12.025

Rosiak, P., Latanska, I., Paul, P., Sujka, W., & Kolesinska, B. (2021). Modification of Alginates to Modulate Their Physic-Chemical Properties and Obtain Biomaterials with Different Functional Properties. *Molecules (Basel, Switzerland)*, *26*(23). https://doi.org/10.3390/molecules26237264

Rudin, C. M., Brambilla, E., Faivre-Finn, C., & Sage, J. (2021). Small-cell lung cancer. *Nature Reviews Disease Primers*, *7*(1). https://doi.org/10.1038/s41572-020-00235-0

Sahlberg, S. H., Mortensen, A. C., Haglöf, J., Engskog, M. K. R., Arvidsson, T., Pettersson, C., Glimelius, B., Stenerlöw, B., & Nestor, M. (2017). Different functions of AKT1 and AKT2 in molecular pathways, cell migration and metabolism in colon cancer cells. *International Journal of Oncology*, *50*(1), 5–14. https://doi.org/10.3892/ijo.2016.3771

Sahoo, D. R., & Biswal, T. (2021). Alginate and its application to tissue engineering. *SN Applied Sciences*, *3*(1), 30. https://doi.org/10.1007/s42452-020-04096-w

Samuel, M. S., Lopez, J. I., McGhee, E. J., Croft, D. R., Strachan, D., Timpson, P., Munro, J., Schröder, E., Zhou, J., Brunton, V. G., Barker, N., Clevers, H., Sansom, O. J., Anderson, K. I., Weaver, V. M., & Olson, M. F. (2011). Actomyosin-mediated cellular tension drives increased tissue stiffness and β-catenin activation to induce epidermal hyperplasia and tumor growth. *Cancer Cell*, *19*(6), 776–791. https://doi.org/10.1016/j.ccr.2011.05.008

Sangüesa, G., Roglans, N., Baena, M., Velázquez, A. M., Laguna, J. C., & Alegret, M. (2019). mTOR is a key protein involved in the metabolic effects of simple sugars. *International Journal of Molecular Sciences*, *20*(5). https://doi.org/10.3390/ijms20051117

Sarrazin, S., Lamanna, W. C., & Esko, J. D. (2011). Heparan sulfate proteoglycans. *Cold Spring Harbor Perspectives in Biology*, *3*(7), 1–33. https://doi.org/10.1101/cshperspect.a004952

Sengyoku, H., Tsuchiya, T., Obata, T., Doi, R., Hashimoto, Y., Ishii, M., Sakai, H.,

Matsuo, N., Taniguchi, D., Suematsu, T., Lawn, M., Matsumoto, K., Miyazaki, T., & Nagayasu, T. (2018). Sodium hydroxide based non-detergent decellularizing solution for rat lung. *Organogenesis*, *14*(2), 94–106. https://doi.org/10.1080/15476278.2018.1462432

Souza, A. G., Silva, I. B. B., Campos-Fernandez, E., Barcelos, L. S., Souza, J. B., Marangoni, K., Goulart, L. R., & Alonso-Goulart, V. (2018). Comparative Assay of 2D and 3D Cell Culture Models: Proliferation, Gene Expression and Anticancer Drug Response. *Current Pharmaceutical Design*, *24*(15), 1689–1694. https://doi.org/10.2174/1381612824666180404152304

Stowers, R. S., Shcherbina, A., Israeli, J., Gruber, J. J., Chang, J., Nam, S., Rabiee, A., Teruel, M. N., Snyder, M. P., Kundaje, A., & Chaudhuri, O. (2019). Matrix stiffness induces a tumorigenic phenotype in mammary epithelium through changes in chromatin accessibility. *Nature Biomedical Engineering*, *3*(12), 1009–1019. https://doi.org/10.1038/s41551-019-0420-5

Sun, S., Schiller, J. H., & Gazdar, A. F. (2007). Lung cancer in never smokers - A different disease. *Nature Reviews Cancer*, *7*(10), 778–790. https://doi.org/10.1038/nrc2190

Szot, C. S., Buchanan, C. F., Gatenholm, P., Rylander, M. N., & Freeman, J. W. (2011). Investigation of cancer cell behavior on nanofibrous scaffolds. *Materials Science and Engineering: C*, *31*(1), 37–42. https://doi.org/10.1016/J.MSEC.2009.12.005

Tan, A. C. (2020). Targeting the PI3K/Akt/mTOR pathway in non-small cell lung cancer (NSCLC). *Thoracic Cancer*, *11*(3), 511–518. https://doi.org/10.1111/1759-7714.13328

Teng, Y., Wang, Z., Ma, L., Zhang, L., Guo, Y., Gu, M., Wang, Z., Wang, Y., & Yue, W. (2016). Prognostic significance of circulating laminin gamma2 for early-stage non-small-cell lung cancer. *OncoTargets and Therapy*, *9*, 4151–4162. https://doi.org/10.2147/OTT.S105732

Theocharis, A. D., & Karamanos, N. K. (2019). Proteoglycans remodeling in cancer: Underlying molecular mechanisms. *Matrix Biology : Journal of the International Society for Matrix Biology*, *75–76*, 220–259.

https://doi.org/10.1016/j.matbio.2017.10.008

Theocharis, A. D., Skandalis, S. S., Tzanakakis, G. N., & Karamanos, N. K. (2010). Proteoglycans in health and disease: novel roles for proteoglycans in malignancy and their pharmacological targeting. *The FEBS Journal*, *277*(19), 3904–3923. https://doi.org/10.1111/j.1742-4658.2010.07800.x

Tibbitt, M. W., & Anseth, K. S. (2009). Hydrogels as extracellular matrix mimics for 3D cell culture. *Biotechnology and Bioengineering*, *103*(4), 655–663. https://doi.org/10.1002/bit.22361

Vallen, M. J. E., Schmidt, S., Oosterhof, A., Bulten, J., Massuger, L. F. A. G., & van Kuppevelt, T. H. (2014). Primary ovarian carcinomas and abdominal metastasis contain 4,6-disulfated chondroitin sulfate rich regions, which provide adhesive properties to tumour cells. *PloS One*, *9*(11), e111806. https://doi.org/10.1371/journal.pone.0111806

Vander Heiden, M. G., Cantley, L. C., & Thompson, C. B. (2009). Understanding the Warburg effect: the metabolic requirements of cell proliferation. *Science (New York, N.Y.)*, *324*(5930), 1029–1033. https://doi.org/10.1126/science.1160809

Velcheti, V., & Govindan, R. (2006). Insulin-Like Growth Factor and Lung Cancer. *Journal of Thoracic Oncology*, *1*(7), 607–610. https://doi.org/https://doi.org/10.1016/S1556-0864(15)30370-1

Voiles, L., Lewis, D. E., Han, L., Lupov, I. P., Lin, T.-L., Robertson, M. J., Petrache, I., & Chang, H.-C. (2014). Overexpression of type VI collagen in neoplastic lung tissues. *Oncology Reports*, *32*(5), 1897–1904. https://doi.org/10.3892/or.2014.3438

Walimbe, T., & Panitch, A. (2020). Proteoglycans in biomedicine: Resurgence of an underexploited class of ECM molecules. *Frontiers in Pharmacology*, *10*(January), 1–13. https://doi.org/10.3389/fphar.2019.01661

Wang, C., Sinha, S., Jiang, X., Murphy, L., Fitch, S., Wilson, C., Grant, G., & Yang, F. (2021). Matrix Stiffness Modulates Patient-Derived Glioblastoma Cell Fates in Three-Dimensional Hydrogels. *Tissue Engineering. Part A*, *27*(5–6), 390–401. https://doi.org/10.1089/ten.TEA.2020.0110

Wang, H., Arun, B. K., Wang, H., Fuller, G. N., Zhang, W., Middleton, L. P., & Sahin, A. A. (2008). IGFBP2 and IGFBP5 overexpression correlates with the lymph node metastasis in T1 breast carcinomas. *The Breast Journal*, *14*(3), 261–267. https://doi.org/10.1111/j.1524-4741.2008.00572.x

Wang, L., Bai, Y.-Y., Yang, Y., Hu, F., Wang, Y., Yu, Z., Cheng, Z., & Zhou, J. (2016). Diabetes mellitus stimulates pancreatic cancer growth and epithelial-mesenchymal transition-mediated metastasis via a p38 MAPK pathway. *Oncotarget*, *7*(25), 38539–38550. https://doi.org/10.18632/oncotarget.9533

Wang, Y.-H., Liu, C.-L., Chiu, W.-C., Twu, Y.-C., & Liao, Y.-J. (2019). HMGCS2 Mediates Ketone Production and Regulates the Proliferation and Metastasis of Hepatocellular Carcinoma. *Cancers*, *11*(12). https://doi.org/10.3390/cancers11121876

Warburg, O. (1956a). On the origin of cancer cells. *Science (New York, N.Y.)*, *123*(3191), 309–314. https://doi.org/10.1126/science.123.3191.309

Warburg, O. (1956b). On respiratory impairment in cancer cells. *Science (New York, N.Y.)*, *124*(3215), 269–270.

Waters, J. A., Urbano, I., Robinson, M., & House, C. D. (2022). Insulin-like growth factor binding protein 5: Diverse roles in cancer. *Frontiers in Oncology*, *12*, 1052457. https://doi.org/10.3389/fonc.2022.1052457

Wei, J., Yao, J., Yan, M., Xie, Y., Liu, P., Mao, Y., & Li, X. (2022). The role of matrix stiffness in cancer stromal cell fate and targeting therapeutic strategies. *Acta Biomaterialia*, *150*, 34–47. https://doi.org/10.1016/j.actbio.2022.08.005

Weinhouse, S. (1956). On respiratory impairment in cancer cells. *Science (New York, N.Y.)*, *124*(3215), 267–269. https://doi.org/10.1126/science.124.3215.267

Xiang, J., Wang, K., & Tang, N. (2023). PCK1 dysregulation in cancer: Metabolic reprogramming, oncogenic activation, and therapeutic opportunities. *Genes & Diseases*, *10*(1), 101–112. https://doi.org/https://doi.org/10.1016/j.gendis.2022.02.010

Xu, X., Chen, B., Zhu, S., Zhang, J., He, X., Cao, G., & Chen, B. (2019).

Hyperglycemia promotes Snail-induced epithelial–mesenchymal transition of gastric cancer via activating ENO1 expression. *Cancer Cell International*, *19*(1), 344. https://doi.org/10.1186/s12935-019-1075-8

Yagi, T., Kubota, E., Koyama, H., Tanaka, T., Kataoka, H., Imaeda, K., & Joh, T. (2018). Glucagon promotes colon cancer cell growth via regulating AMPK and MAPK pathways. *Oncotarget*, *9*(12), 10650–10664. https://doi.org/10.18632/oncotarget.24367

Yamada, K. M., & Cukierman, E. (2007). Modeling tissue morphogenesis and cancer in 3D. *Cell*, *130*(4), 601–610. https://doi.org/10.1016/j.cell.2007.08.006

Yu, J. S. L., & Cui, W. (2016). Proliferation, survival and metabolism: the role of PI3K/AKT/mTOR signalling in pluripotency and cell fate determination. *Development (Cambridge, England)*, *143*(17), 3050–3060. https://doi.org/10.1242/dev.137075

Yu, L., Chen, X., Sun, X., Wang, L., & Chen, S. (2017). The glycolytic switch in tumors: How many players are involved? *Journal of Cancer*, *8*(17), 3430–3440. https://doi.org/10.7150/jca.21125

Zhu, J., & Thompson, C. B. (2019). Metabolic regulation of cell growth and proliferation. *Nature Reviews Molecular Cell Biology*, *20*(7), 436–450. https://doi.org/10.1038/s41580-019-0123-5

Zhu, X., Li, Y., Yang, Y., He, Y., Gao, M., Peng, W., Wu, Q., Zhang, G., Zhou, Y., Chen, F., Bao, J., & Li, W. (2022). Ordered micropattern arrays fabricated by lung-derived dECM hydrogels for chemotherapeutic drug screening. *Materials Today. Bio*, *15*, 100274. https://doi.org/10.1016/j.mtbio.2022.100274

Zi, D., Li, Q., Xu, C.-X., Zhou, Z.-W., Song, G.-B., Hu, C.-B., Wen, F., Yang, H.-L., Nie, L., Zhao, X., Tan, J., Zhou, S.-F., & He, Z.-X. (2022). CXCR4 knockdown enhances sensitivity of paclitaxel via the PI3K/Akt/mTOR pathway in ovarian carcinoma. *Aging*, *14*(11), 4673–4698. https://doi.org/10.18632/aging.203241